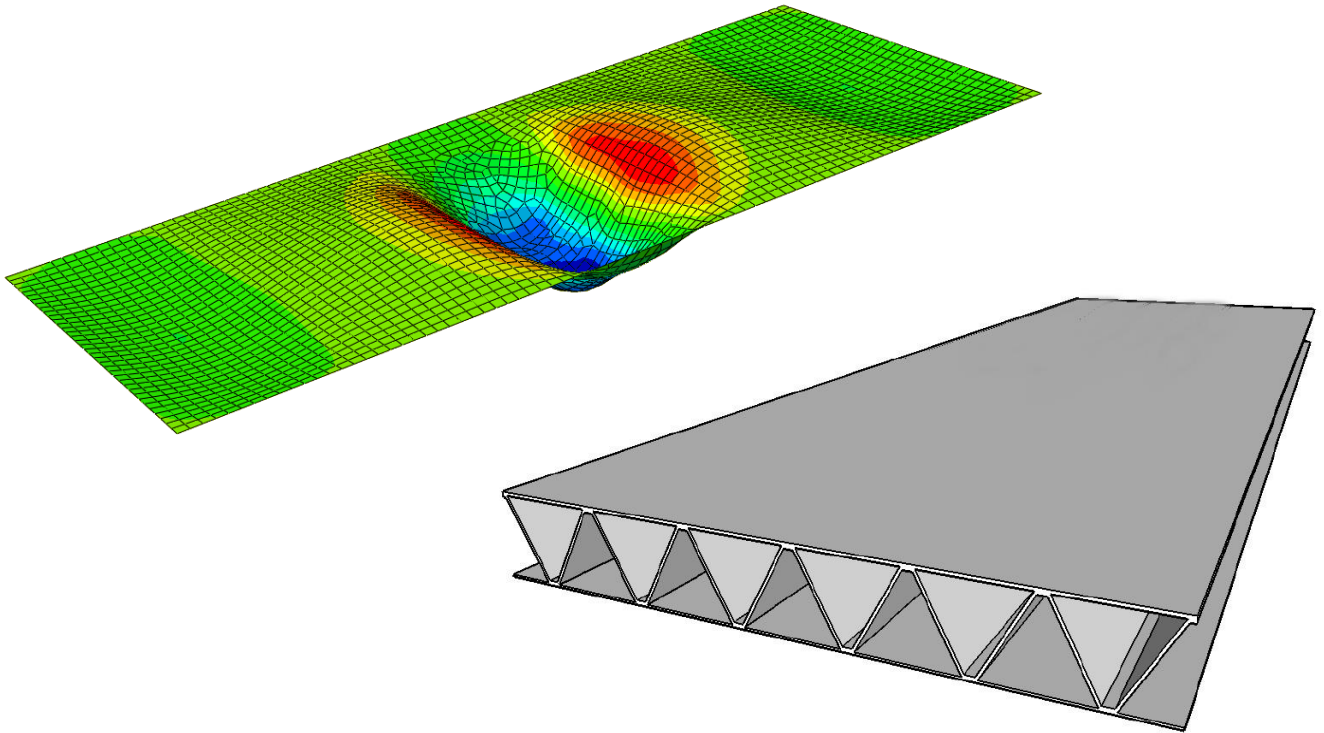![CHALMERS UNIVERSITY OF TECHNOLOGY]

Steel-Sandwich Elements in Long-Span Bridge Applications

Master's Thesis in the Master's Programme Structural Engineering and Building Technology

EMMANOUIL ARVANITIS
EVGENIOS PAPADOPOULOS

Steel-Sandwich Elements in Long-Span Bridge Applications

Master's Thesis in the Master's Programme Structural Engineering and Building Technology
EMMANOUIL ARVANITIS
EVGENIOS PAPADOPOULOS

Department of Civil and Environmental Engineering
Division of Structural Engineering
Steel and Timber Structures
CHALMERS UNIVERSITY OF TECHNOLOGY
Göteborg, Sweden 2016

Steel-Sandwich Elements in Long-Span Bridge Applications

Master's Thesis in the Master's Programme Structural Engineering and Building Technology

EMMANOUIL ARVANITIS

EVGENIOS PAPADOPOULOS

Department of Civil and Environmental Engineering
Division of Structural Engineering
Steel and Timber Structures
Chalmers University of Technology
SE-412 96 Göteborg
Sweden
Telephone: + 46 (0)31-772 1000

Cover:
Configuration of steel sandwich element as well as FE-model for the deflection analysis
Department of Civil and Environmental Engineering
Göteborg, Sweden, 2016

I

Steel-Sandwich Elements in Long-Span Bridge Applications

Master's thesis in the Master's Programme Structural Engineering and Building Technology

EMMANOUIL ARVANITIS
EVGENIOS PAPADOPOULOS
Department of Civil and Environmental Engineering
Division of Structural Engineering
Steel and Timber Structures
Chalmers University of Technology

ABSTRACT

The aim of this Master Thesis project was to investigate and identify the quantity of steel which could be saved if steel sandwich elements could be utilized in long span bridge decks instead of conventional orthotropic plates. Therefore, after a literature study about long span bridges and bridge decks, an optimization routine was created which could optimize a steel sandwich element cross-section according to the desired results. The scenarios studied in this Master Thesis project were the maximization of the moment of inertia in the longitudinal direction, the minimization of the steel used in the cross-section and the maximization of the length of the steel sandwich element between two transverse stiffeners. As a reference bridge, Höga Kusten bridge was chosen in order to compare the results. The scenarios had been studied in the serviceability limit state taking into account the maximum global deflection that the existing orthotropic deck of Höga Kusten bridge.

The results showed that steel sandwich elements could be provide a much lighter bridge deck for long span bridges as far as the SLS is concerned. The plate behaviour of a steel sandwich element enabled a better stress distribution in all directions that allowed less material in the cross-sectional compared with the conventional orthotropic deck of Höga Kusten bridge.

Key words: steel sandwich, orthotropic, plates, bridge deck

Stålsandwichelement i lång-span broapplikationer

EMMANOUIL ARVANITIS
EVGENIOS PAPADOPOULOS
Institutionen för bygg- och miljöteknik
Avdelningen för Avdelningsnamn
Forskargruppsnamn
Chalmers tekniska högskola

SAMMANFATTNING

Syftet för detta examensarbete var att undersöka och identifiera huruvida stålsandwichelement kan nyttjas som brobaneplattor istället för konventionella ortotropiska plattor för broar med stora spännviddar. Efter litteraturstudie skapades en optimeringsrutin för stålsandwichelements tvärsnitt med avseende på tvärsnittsarea eller ytträghetsmoment. Scenarierna som studerats i detta examensarbete var maximeringen av tröghetsmomentet i längdriktningen, minimeringen av tvärsnittsarea och maximeringen av längden av stålsandwichelement mellan två tväravstyvningar. Som referensbro valdes Högakustenbron. Studierna utfördes med avseende på brukgränstillståndet.

Resultaten visade att tillämpning av stålsandwichelement ger ett lättare brodäck för broar med stora spinnviddar. Dessutom påvisades att viktreducering kan utnyttjas som reducerad tvärsnittsarea eller ökat avstånd mellan tvärskott.

Nyckelord: stålsandwich, ortotropisk, plattor, brodäck

Contents

Preface

This Master Thesis was performed in order to investigate the possibility of using steel sandwich bridge decks in long-span bridge applications. The study took place from January to June 2015 and it was performed in collaboration with WSP. The project was carried out at the Department of Structural Engineering, Steel and Timber Structures, Chalmers University of Technology, Sweden.

The authors would like to thank their supervisor Peter Nilsson, as well as their examiner Mohammad Al-Emrani for their guidance and support. They would also like to thank Amanda Palmkvist and Linda Sandberg for the excellent opposition.

Göteborg June 2016

Emmanouil Arvanitis & Evgenios Papadopoulos

Notations

Roman upper case letters

CSC	Cross section class
FEM	Finite Element Method
HLAW	Hybrid laser arc welding
OSD	Orthotropic steel deck
SLS	Serviceability limit state
SS	Steel sandwich
SSE	Steel sandwich element

Roman lower case letters

f	Closest distance between the stiffeners of the core
h	Height of the steel sandwich element
h_c	Height of the core of the steel sandwich element
p	Half length of the core repetition
$t_{f.top}$	Thickness of the top plate
$t_{f.bot}$	Thickness of the bottom plate
t_c	Thickness of the corrugated core

Greek lower case letters

α	Angle of the core stiffeners with the horizontal axis

1 Introduction

1.1 Background

In the summer of 2010, the Norwegian Public Road Administration (NPRA) decided to initiate a project for a coastal trunk road that will start from Trondheim, in the middle of Norway, pass along the western corridor (E39) and end in Kristiansand, in the south part of the country. The purpose for the update of this 1330 km highway is to facilitate the trade and industry transportation in the south-western Norway, which is still hampered by the wide and deep fjord crossings. At the present time, the traffic connection in many points is accomplished by ferry boats. This increases the travel time needed between the cities in the area. The NPRA want to create an effective transportation system in the whole western region as it interconnects areas with large populations and substantial trade and industry; E39 is the most crucial route of this vision. For the construction of E39, various technological alternatives are examined for bridging the fjord crossings still being operated by ferry boats. The proposals include new innovative concepts for structural systems, construction methods and materials.

Many of the fjord crossings in Norway are difficult and expensive to be bridged. Particularly Sognefjord, possessing a width of 4km and a depth that reaches 1500m in some locations, is an extremely challenging passing. In the attempt of bridging longer spans with cable bridges, the construction of lighter and stiffer bridge decks is a necessary parameter. Nowadays, the most common deck structure is the orthotropic steel deck, consist of a steel plate stiffened by longitudinal open or closed ribs. However, orthotropic decks suffer from many disadvantages, such as poor fatigue performance and high production costs.

To counteract these problems steel sandwich elements (SSE) has been proposed to replace the conventional orthotropic bridge deck. SSE are light-weight construction elements consist of two thin face sheets connected by a core, which can be manufactured with different configurations (Beneus & Koc 2014). Their high stiffness to weight ratio has made them a considered solution in the shipbuilding and aerospace industry and some implementations have been performed (Roland & Reinert 2000). Moreover, new innovative technics, concerning laser welding, increased their fatigue performance and enabled industrialized manufacture. Today more and more efforts and research are made for the integration of these elements in bridge engineering in order to exploit all their advantages.

A box girder cross section is typically a rectangular or trapezoidal box, which is used for large scale structures and can be constructed with various materials and techniques. The box girders are a quite popular choice in the bridge engineering industry, mainly due to their high torsional stiffness (Xanthakos 1993). Moreover, this kind of cross-section enables much longer spans, while it also possesses other advantages like uncomplicated maintenance and visual aesthetics. Box girder cross-sections are mostly used in beam bridges and suspension bridges.

By combining SSE with box girder sections and exploiting their assets, new light-weight box-girders could be created. These box girder cross sections could be used to enable longer bridge spans in a more cost-efficient way.

1.2 Scope of study

The scope of this study is to investigate if it is possible to achieve an essential goal of the bridge industry; to decrease the self-weight of the structural elements of the bridge. Nowadays, researchers are examining the use of light-weight materials and structural elements, which would minimize the construction cost and reduce our CO_2 footprint. As welding technology advances, SSEs have shown great potential for bridge deck applications. Furthermore, although there is a broad bibliography on SSEs, there is no similar study done, where the SSEs have been combined with the box girder cross-section.

1.3 Aim and Objectives

The purpose of the Master Thesis project is the development of a cross-section that would utilize the advantages of the two mentioned systems, the box girder cross section and the SSE. This can make it possible to create lighter and more efficient stiffening girders for long-span bridge applications. The structural behaviour of the steel deck, for instance strength and stiffness parameters, was decided in accordance with the Eurocode 3 using numerical analysis. The specific objectives of the project are:

• Evaluation of the application of SSE in long-span bridges
• Design of SSE which are optimum for different cases with respect to SLS
• Design comparison in a case study

1.4 Methodology

To accomplish the objectives, the steps below were followed:

• Literature study on suspension bridges
• Literature study on box girder section
• Literature study on structural behaviour of steel sandwich bridge decks
• Calculation of load-carrying capacities of the compressive flange of an existing box girder section (Höga Kusten Bridge)
• Calculation of load-carrying capacities of an optimized SSE
• Comparison between the conventional section and SSE cross-section

1.5 Limitations

The Master Thesis project will be focused on the investigation of the structural behaviour and design of SSE for suspension bridge applications. Although, fatigue has been shown to be a crucial aspect in such constructions, it is not examined in the specific project. The centre of attraction of this project will be the structural behaviour of the stiffening girder and not the behaviour of the entire bridge.

Although there are many different core configurations when using SSE, for the needs of the specific project, corrugated core SSE will be used. With respect to manufacturing and structural performance this core type has been shown to be a suitable option for bridge deck applications (Beneus & Koc 2014).

The comparison between the orthotropic section and the one utilizing SSE will be based on the existing bridge geometry. In other words, the positions of the stiffeners will be the same with those of the existing bridge.

1.6 Outline

The Master Thesis project will be focused on the investigation of the structural behaviour and design of SSE for suspension bridge applications. Although, fatigue has been proven to be a crucial aspect in such constructions, it is not examined in the specific project. The centre of attraction of this project will be the structural behaviour of the stiffening girder and not the behaviour of the entire bridge.

Although there are many different core configurations when using SSE, for the needs of the specific project, corrugated SSE will be used. This is due to the fact that the specific configuration can result in light elements, with high bending and shear stiffness in both directions, i.e. a low level of orthotropy. Furthermore, the production of this element type is feasible.

The comparison between the orthotropic section and the one utilizing SSE will be based on the existing bridge geometry. In other words, the positions of the stiffeners will be the same with those of the existing bridge.

2 Literature Study

2.1 Suspension bridges

2.1.1 History

Suspension bridges have been used to overcome large spans for almost two hundred years. Since new technologies were adapted and construction processes improved, the covered main span lengths were continuously increased over the years, to reach a maximum distance of approximately 2.000 meters nowadays (Gimsing & Georgakis 2012).

The main principle behind the function of suspension bridges, and suspension systems in general, is the utilization of tensile elements for the load transfer. This principle has been used since ancient times, when the ancient Chinese used ropes and iron chains to overcome river spans 2.000 years ago (Xu & Xia 2011).

The first suspension bridge in the United States was built in the state of Pennsylvania in 1796 by James Finley and it was named Jacob's Creek Bridge (Xanthakos 1993). Jacob's Creek Bridge used wrought iron chains and a level deck to connect Uniontown to Greensburg, see Figure 2.1. Its main span was 21 m long and 3.81 m wide (Finley 1810). In Europe, the first permanent suspension bridge was built in 1823 in Geneva by Marc Seguin and Guillaume-Henri Dufour. It was the Saint Antoine Bridge, which had two equal spans of 42 m (Peters 1980). In the 19th century many suspension bridges were constructed, with pin-connected eye-bars forming huge chains, being the main load-carrying elements (Gimsing & Georgakis 2012). A characteristic example of this bridge type is the Clifton Suspension Bridge in Bristol, United Kingdom, which was designed by Isambard Kingdom Brunel and opened in 1864.
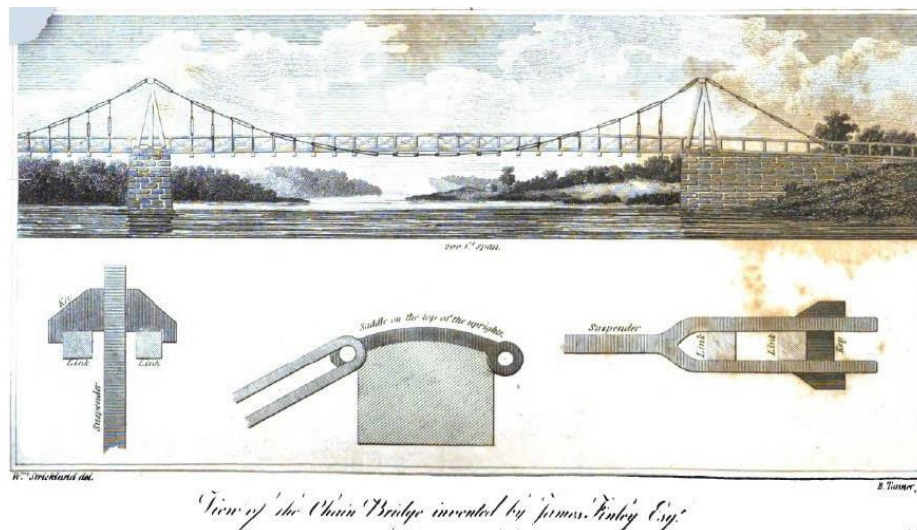
Figure 2.1   Jacob's Creek Bridge, the first suspension bridge in the United States (Finley 1810).

The first modern suspension bridge is considered to be the Brooklyn Bridge across the East river between Manhattan and Long Island in the New York, United States. The construction of Brooklyn Bridge started in 1867 under the supervision of John Roebling, who was the main designer, and it opened to traffic in 1883. In the meanwhile, John Roebling died and the construction was taken over by his son Washington. The Brooklyn Bridge had a main span of 486 m and two side spans of 286

m and at the time that it opened, it was 50% longer than the previously built bridges (Gimsing & Georgakis 2012).

2.1.2   Structural system

The typical configuration of a suspension bridge is shown in Figure 2.2. The bridge is mainly composed by the stiffening girder with the bridge deck, the cable system, the pylons and the anchor blocks. The pylons support the cable system, which in turn supports the stiffening girder. The anchor blocks stabilize the cable system vertically and horizontally.
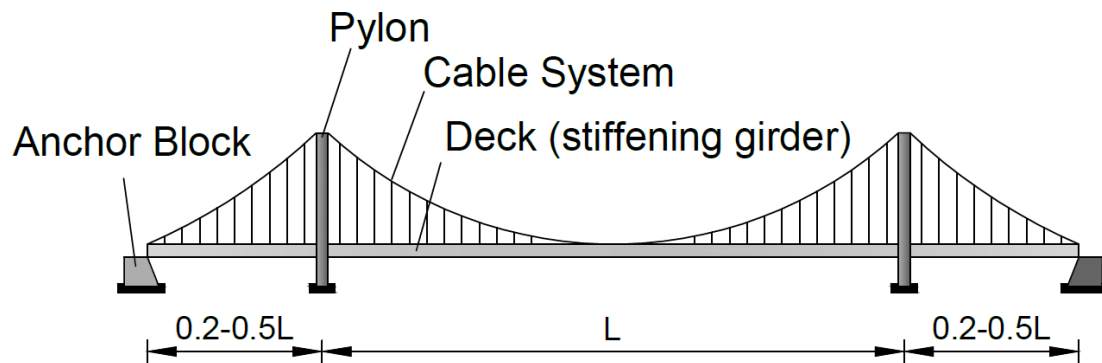
Figure 2.2   Suspension bridge with its main components (Gimsing & Georgakis 2012).

The side span lengths are usually between 0.2-0.5 times the main span, as shown in Figure 2.2 (Gimsing & Georgakis 2012). However, depending on the on-site conditions of the bridge, the length of the side spans may differ. For instance, if the side spans of the bridge have to be placed over deep water, long side spans are usually preferred, to avoid complicated support systems of the pylons in the water. On the other hand, if the supporting pylons are placed on land or in shallow water, short side spans can be chosen.

Cable bridges can be characterized depending by the way the cable system is anchored. There are two anchorage systems; the earth and the self-anchored. In the former both the vertical and the horizontal components of the cable force are transferred to the anchor block, whereas in the latter the horizontal component is transferred to the stiffening girder, see Figures 2.3 and 2.4. Although both anchorage systems can be used, earth anchorage system is mostly used. This is due to the fact that self-anchoring suffers from low structural efficiency and construct-ability, resulting in uneconomical configurations (Gimsing & Georgakis 2012).
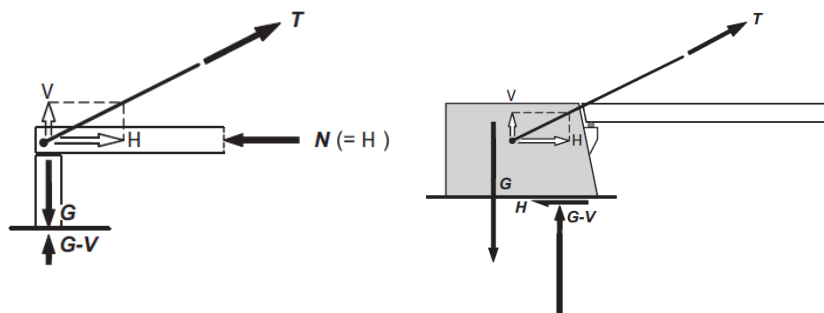
Figure 2.3   Self-anchorage system (left) and earth anchorage system (right) (Gimsing & Georgakis 2012).
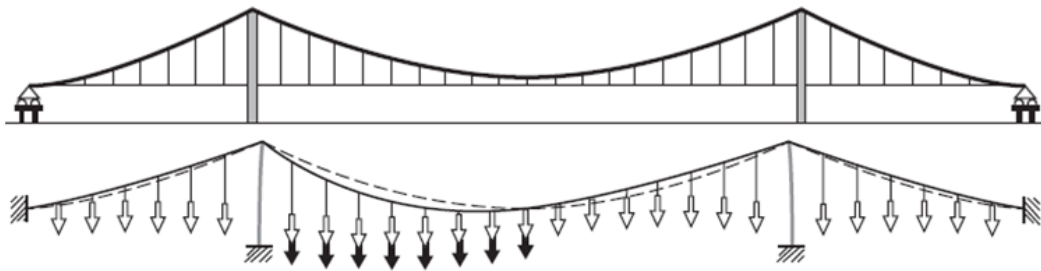
Figure 2.4   Self anchorage system (top) and earth anchorage system (bottom) (Gimsing & Georgakis 2012).

As far as the cable arrangement in the transverse direction is concerned, there are plenty of solutions; the most common is the one shown in the Figure 2.5, where the cables support the deck in the two edges. This arrangement provides adequate vertical stability, as well as additional torsional stiffness. Depending on the expected loading conditions and the design of the bridge, other configurations are also possible, see Figure 2.6.
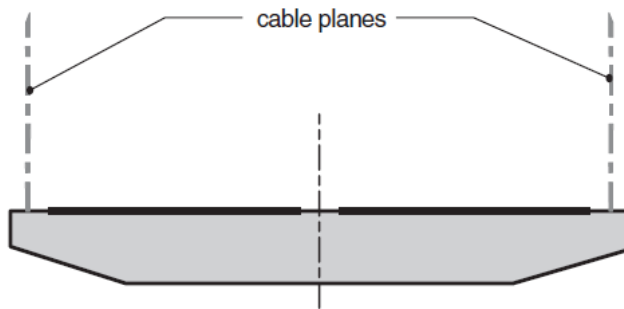
Figure 2.5   Vertical cable planes attached along the edges of the deck (Gimsing & Georgakis 2012).
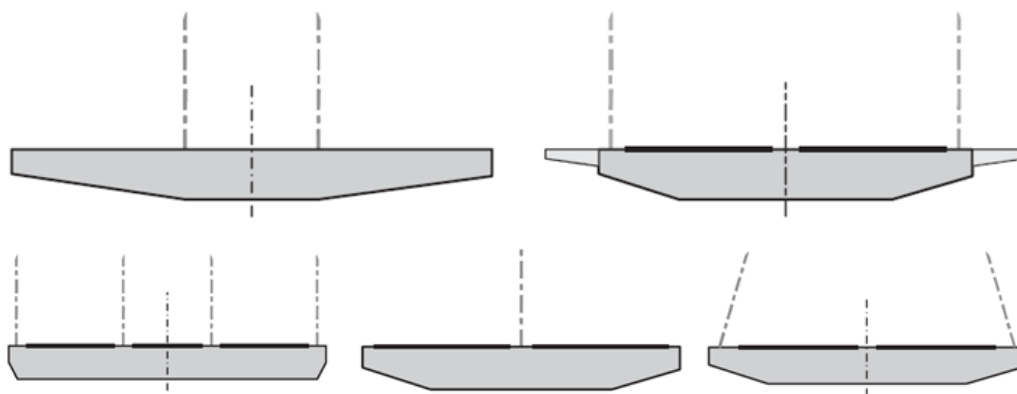
Figure 2.6   Various cable configurations in the transverse direction (Gimsing & Georgakis 2012).

The choice of the support conditions is the most significant factor regarding the structural behaviour of the stiffening girder. For the most simple and frequently used three-span suspension bridge, the stiffening girder often consists of three girders, simply supported at the pylons and longitudinally fixed at the anchor blocks (Figure 2.7).
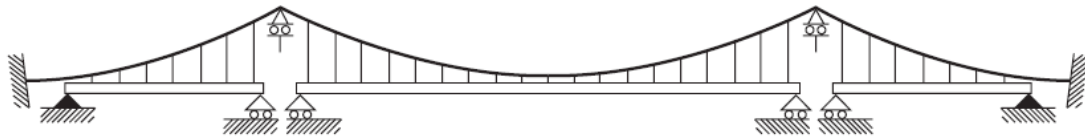
Figure 2.7   Supporting conditions in three-span suspension bridge (Gimsing & Georgakis 2012)

It should be noted that in this case, the support conditions are favourable regarding deformations caused by temperature changes, because the maximum longitudinal displacements will occur next to the pylons, where the hangers have their maximum length. Consequently, the change of the inclination of the hangers will be as low as possible (Gimsing & Georgakis 2012).

Another configuration for the stiffening girder is to be continuous all over the length of the bridge. A continuous girder will result in a lower value of the maximum moments compared with the simply supported option. However, special treatment is needed because the bottom flange of the deck will be in compression close to the pylons. An example of a configuration with continuous girder is shown in Figure 2.8. In this case, special treatment would be needed because the maximum longitudinal displacement due to temperature changes is longer than the three-span suspension bridge. In addition, the maximum longitudinal displacement due to temperature changes and asymmetric traffic loads will occur near the ends of the side spans. In this position the vertical hangers have their minimum length and consequently their inclination will be the maximum.
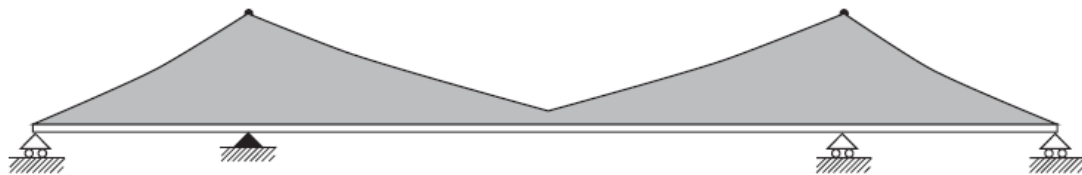
Figure 2.8   Continuous bridge deck longitudinally fixed at one pylon (Gimsing & Georgakis 2012).

2.1.3   Orthotropic steel decks

Modern steel bridges use the orthotropic deck system, in order to distribute traffic loads over the structure, as well as to strengthen the slender plate elements under compression. Compared with reinforced concrete decks, the Orthotropic Steel Decks (OSDs) are lighter and therefore they can cover larger spans. The most common configuration of an OSD consists of a flat, thin steel plate, stiffened by transverse floor beams or diaphragms and longitudinal ribs, which can be either of closed or open type, see Figure 2.9. The selection of the rib type affects the torsional rigidity of the section. The closed are advantageous compared to the open ones. Due to this configuration, the properties of an OSD vary in longitudinal and transverse direction. The longitudinal direction is much stiffer, i.e. the level of orthotropy is high. A typical configuration of an OSD, utilized in a box section girder, is shown in Figure 2.10.
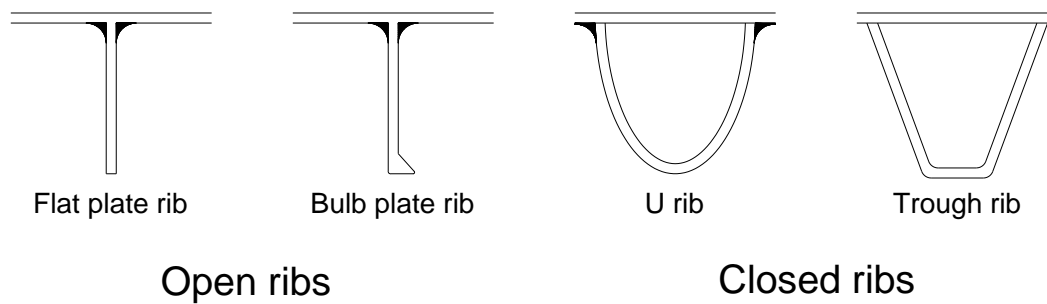
Figure 2.9   Types of longitudinal ribs(Chen & Duan 2014).
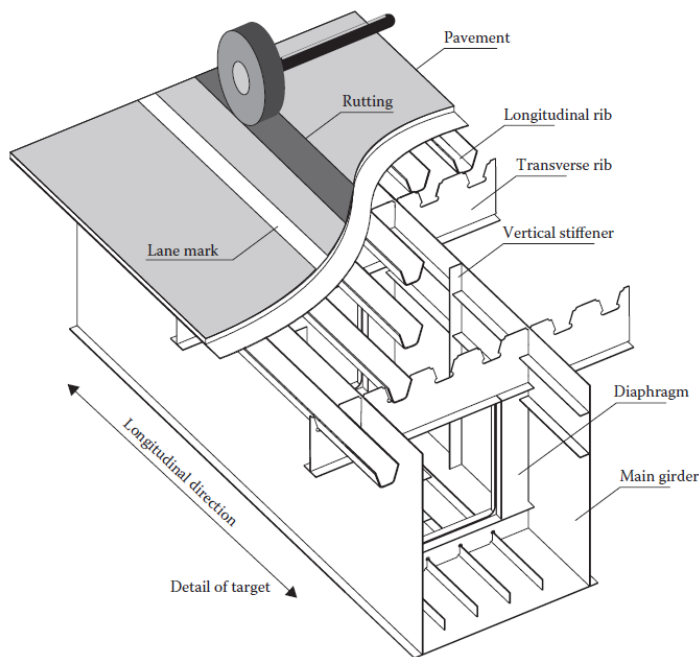
Figure 2.10   General structure of box section girder with orthotropic steel bridge deck (Chen & Duan 2014).

The main reason for utilization of OSD bridges is that they have high stiffness to weight ratio. Moreover, the application of OSD solutions results in structures made wholly of steel with high degree of standardization in the design. On the other hand, the behaviour of OSD with regard to fatigue is considered to be problematic, since fatigue cracking is a common problem in such decks due to the complicated welded details (Lebet & Hirt 2013).

2.1.4   Box girder section

The box girder section is often used in steel-bridge structures due to the high performance regarding torsional stiffness. Moreover, using box girders can result in improved durability compared to open sections, due to the fact that a large proportion of the steel is not exposed. In addition, box girder sections are advantageous regarding the erection of bridges, as they are more suitable for the cantilevering method and they present smaller deformations during the erection. On the other hand, the main

disadvantage when choosing box girder sections is the increased cost (Xanthakos 1993).

The distortion of a box girder under the effect of eccentric loading is shown in Figure 2.11a. Figure 2.11b shows the transverse bending moments due to out-of-plane flexure of the plates and Figure 2.11c shows the longitudinal stresses due to in-plane bending (Hambly 1991).
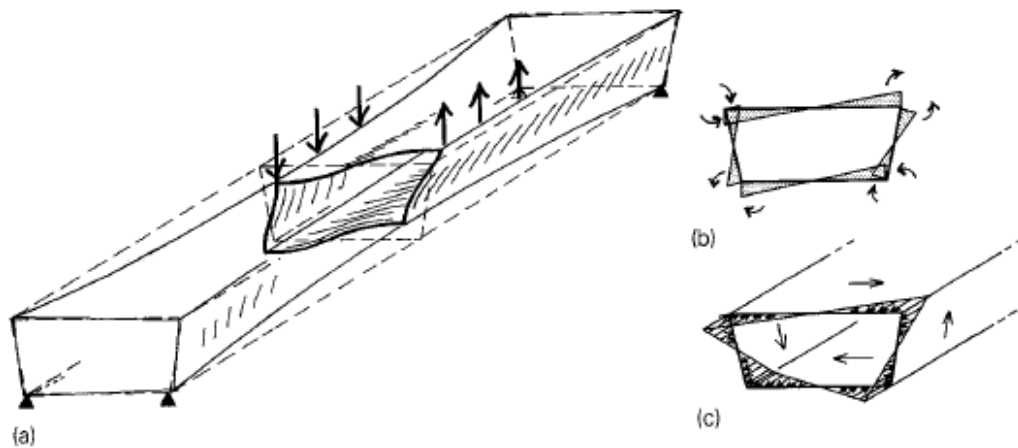
Figure 2.11   (a) Distortion of box girder; (b) out-of-plane bending moments; (c) in-plane bending (warping) stresses (Hambly 1991).

Figure 2.12 shows how distortion forces develop in box girders. The warping constant is assumed to be zero and consequently the stresses based on the thin walled beam theory response are very small. As a result, the distortion of the box girder leads to important plate bending and normal stresses.
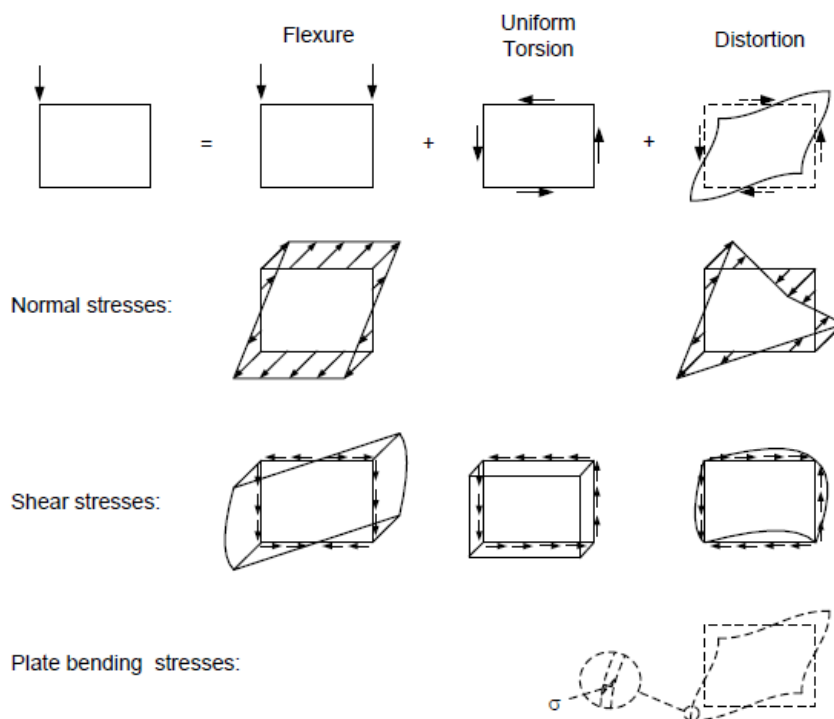
Figure 2.12   Stresses in box-section under eccentric load (US Department of Transportation 2012b).

To show analytically the development of the distortion forces in a box girder, the eccentric load in Figure 2.13 can be divided in two loads, a symmetric and an antisymmetric. The symmetric component results to vertical bending of the box-girder. The antisymmetric load cannot be directly linked with torsion on the box, since pure torsion includes a system of shear flows round the cell as shown in Figure 2.13e, so it is redrawn and it results in the combination of pure torsion shear flows and distortion shear flows as shown in Figure 2.13d. The torque involved in the pure torsion (Figure 2.13e) is equal to the torque of the antisymmetric loading (Figure 2.13d). The distortion shear flows in Figure 2.13f are self-balanced and have no net resultant but at the same time they cause distortion of the cell as shown in Figure 2.13c. The box girder section is very stiff in pure torsion and most of the twist is due to distortion. Therefore, cross bracing is needed to reduce the distortion effects and this is why vertical beams are used in box girders (Hambly 1991).
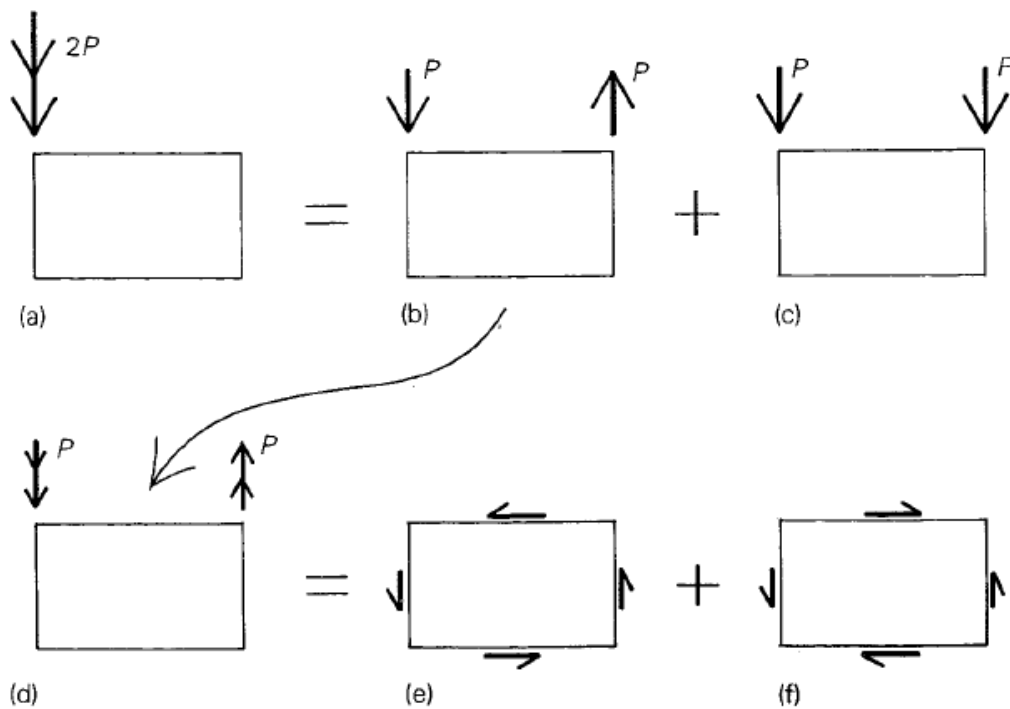
Figure 2.13   Distortion forces in box girders (Hambly 1991).

In some cases, a box girder element underlain to torque is going to present also warping stresses. Moreover, every wall element will obtain some shear deformation to establish the continuity of axial displacements in the perimeter. The warping distribution does not remain the same in every section of the beam, due to the varying torsional moment and the different form along the span.
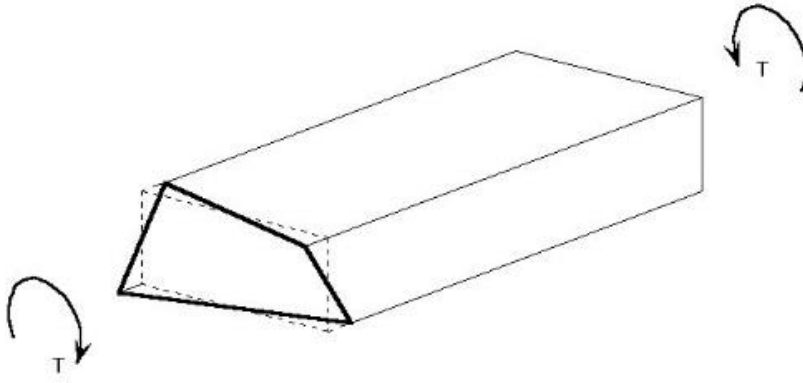
Figure 2.14   Warping Torsion in box girder element.

The structural analysis of a box girder bridge, which is subjected to external load, can be simplified by studying a beam located at the centre of gravity of the box girder (Figure 2.15). For this simplification to be valid, the following conditions must be satisfied:

•   The length of the beam must be considerably greater than the cross section dimensions
•   The cross section must not distort because of beam deflections
•   Shear deflections are negligible
•   Stresses are proportional to deformations
In order to satisfy the 2nd condition, cross bracing is needed as already mentioned.

(a) Spatial structure

(b) Modelling as a bar element
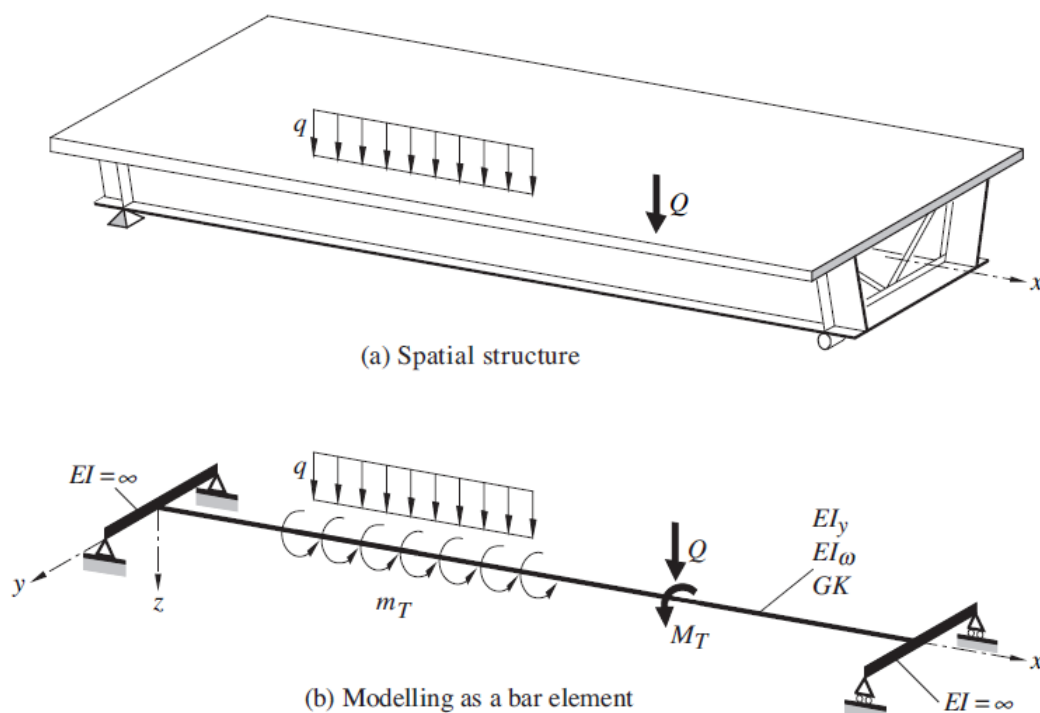
Figure 2.15   Modelling of the bridge (Lebet & Hirt 2013).

The structural analysis of a bridge includes the calculation of its internal section forces due to the external load. To show analytically how the internal moments are calculated, an example of a bridge with box girder cross section will be used. As shown in the Figure 2.16, the bridge is subjected to the vertical load qz and the horizontal load qy.

With the assumption of linear elastic behaviour, the internal moments and forces are resolved about the shear centre CT and bending is caused. Moreover, if the loads do pass through the shear centre CT, a torque mT will develop on the beam, as shown in the Figure 2.17. This torque causes torsional moments Mx about the x axis.

Then the structural analysis can be carried out, with the calculation of the bending moments and shear forces, as well as the torsional moments. It should be noted that the choice of the restraints depends on the type of bearings, as well as on the type of piers. The calculation of the internal moments and forces through the above steps is shown in the Figure 2.18.

The simplified analysis is valid only if the required conditions are satisfied. In case that these conditions are not fulfilled, the three dimensional behaviour of the bridge should be considered; for instance when the local effects are of the same magnitude with the global effects, more complex analyses are required.
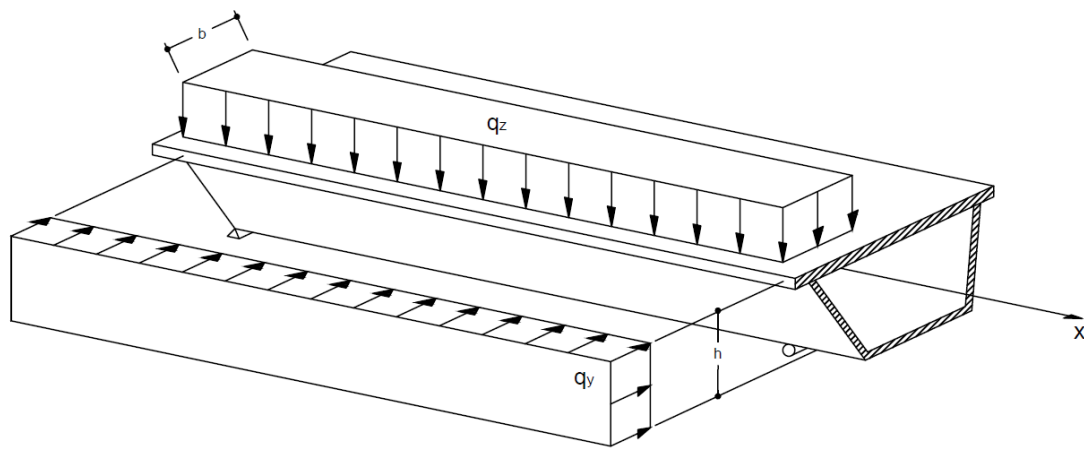
Figure 2.16   Actions on the bridge.
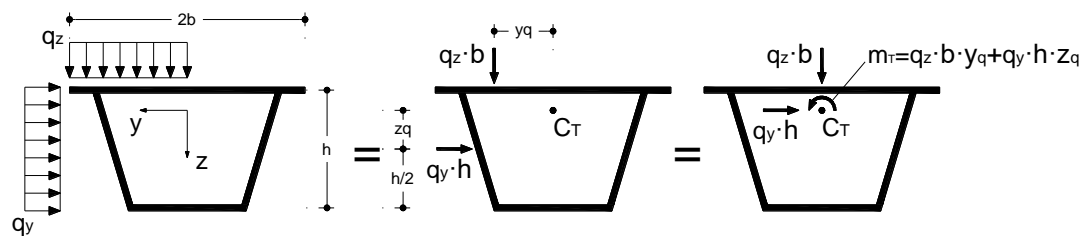
Figure 2.17   Analysis of the forces acting on the cross-section.
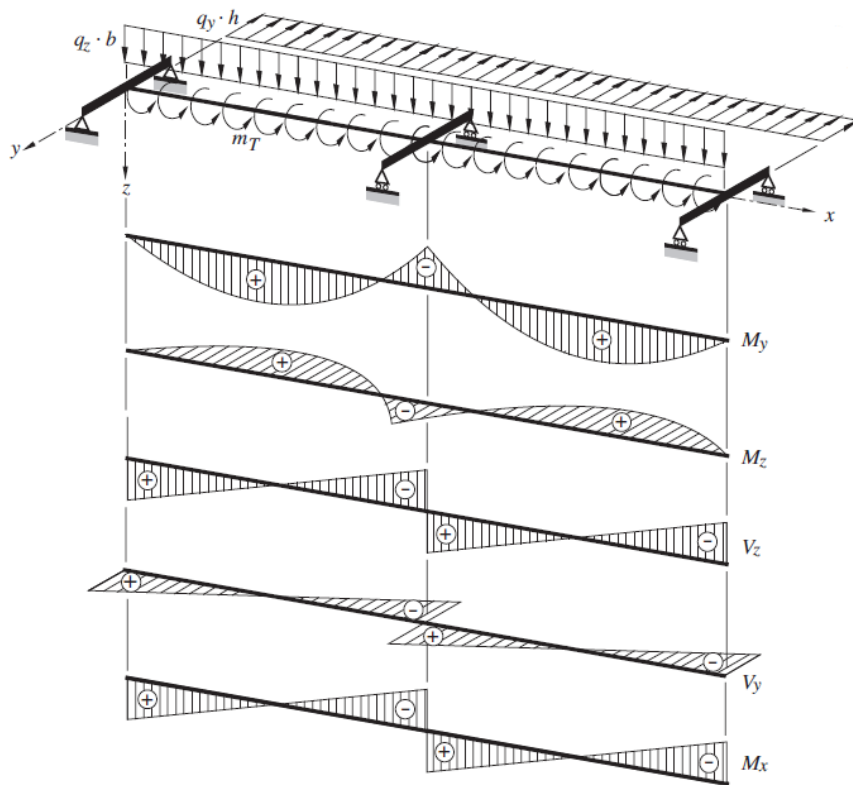
Figure 2.18   Internal moments and forces along the x axis (Lebet & Hirt 2013).

2.1.5   Stiffening girder

The stiffening girder of a suspension bridge is the structural component which is subjected to the largest proportion of the external load. This is due to the fact that the traffic load is applied directly to it. Moreover, the self-weight and the wind loads are usually larger for the stiffening girder than for the cable system. Therefore, the stiffening girder must be able to withstand all the global stresses created by its self-weight and the variable loads, redistribute them and transfer them to the cables. In addition, it should have sufficient flexural rigidity to resist the local stresses between the hangers. It should also possess enough torsional stiffness to resist the torsional stresses induced by eccentric loading and wind. The axial stiffness is normally not of importance for suspension bridges, because the hangers are vertical. Thus, there is no horizontal component induced.

Regarding the stiffness against vertical loads, the stiffening girder should at least be able to resist the loads between the hangers. This is the local scale of the loading. For the global resistance, the stiffening girder will be assisted by the cable system to carry the load and transfer it at the supports.

The stiffening girder should also have sufficient resistance against lateral loads. In this direction there is no assistance from the cable system. Therefore, it is preferable to have a continuous bridge stiffening girder, so that the total moment would be distributed between the positive moment in the span and the negative moment at the pylons, see Figure 2.19.
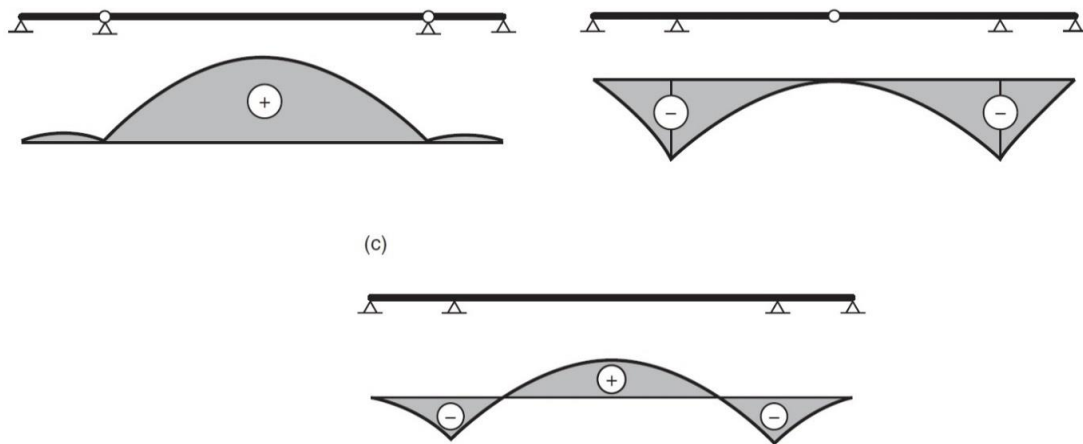
Figure 2.19   Transverse moment distribution with different approaches in the bridge stiffening girder (Gimsing & Georgakis 2012)

When lateral or transverse load acting on the stiffening girder is not passing through the shear centre of the beam - shear centre is defined as the point which shear loads do not cause twist - apart from bending, twisting will occur as well. When an element is symmetrical to all three directions, then the shear centre is located in the centre of the element. Likewise, if the element has a cross section symmetrical to two directions, then the shear centre is on the centre of the cross section, while if it is has just a symmetry axis then the shear centre is moving on that symmetry axis.

The result of a load, eccentric to the shear centre acting on the element, is double; apart from twisting, warping will take place as well. Warping is the phenomenon of torsion that does not permit a twisting plane section to remain plane while rotating. Warping can be considered as the second effect of torsional loading. If a cross-section can elongate freely, then warping does not induce stresses. This is known as free warping. Otherwise, the warping torsion is added to the uniform torsion to counterbalance the torque and is referred as non-uniform torsion. In this case, apart from shear stresses, axial stresses are induced, as shown in the Figure 2.20.
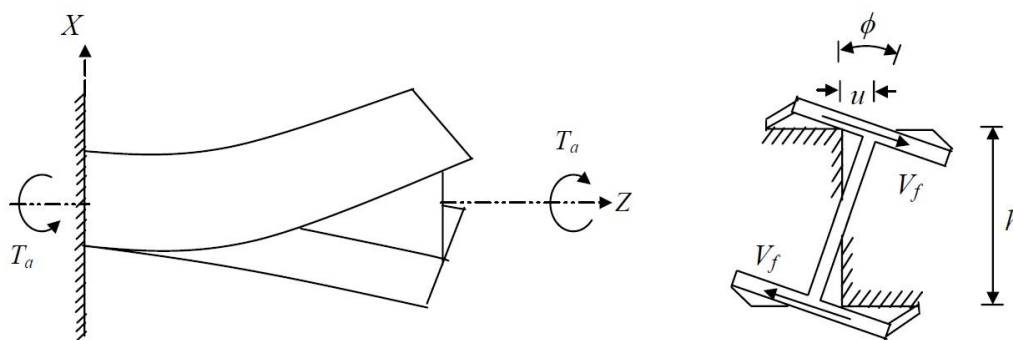
Figure 2.20   Non uniform torsion: Prevented end warping deters free twisting (Institute for Steel Development & Growth 1999).

Non-uniform torsional resistance is generally the sum of two phenomena; St. Venant's torsion (also referred as pure torsion) and warping torsion. The major parameters affecting the non-uniform torsional rigidity are the properties of the material, the length

of the member, the dimensions of the cross sections and the supporting conditions. Some examples are presented in the Figure 2.21 below.
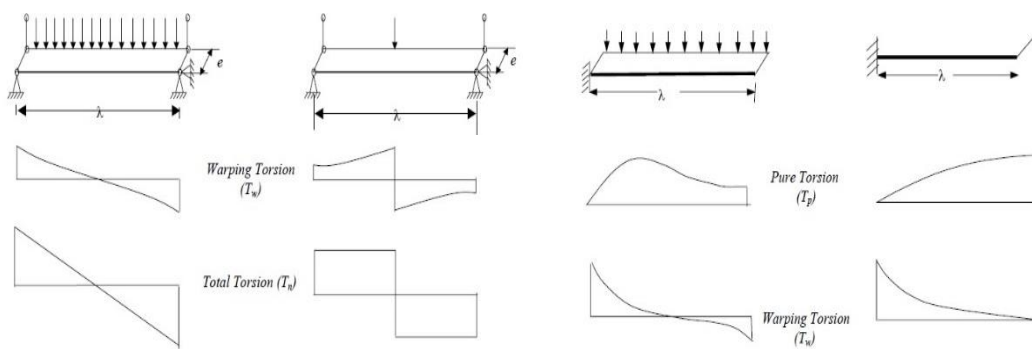
Figure 2.21   Examples of pure and warping torsion in simply supported beams and cantilevers (Institute for Steel Development & Growth 1999).

In cable bridges, the required torsional stiffness of the stiffening girder is highly dependent on the choice of the cable system. A suspension bridge with a cable system centrally placed in the transverse direction requires a more torsional rigid stiffening girder, in relation to a bridge with two cable planes on the edges. Generally, the torsion is governed by the number and the configuration of the cable planes.

The torsional moment of a vertical eccentric load can be sustained either by the stiffening girder or by the cables or a combination of them, as show in the Figure 2.22. The torsion taken from the stiffening girder is imported in the section by the parallel action of two components, see Figure 2.23. In the first one a linear distribution of the shear stresses along the thickness is noticed, while in the second the shear distribution remains constant along the thickness of different components. However, most of the times the former is small compared to the latter and therefore is neglected. Similar behaviour is also expected for loads parallel to the bridge stiffening girder such as wind, earthquake, etc.
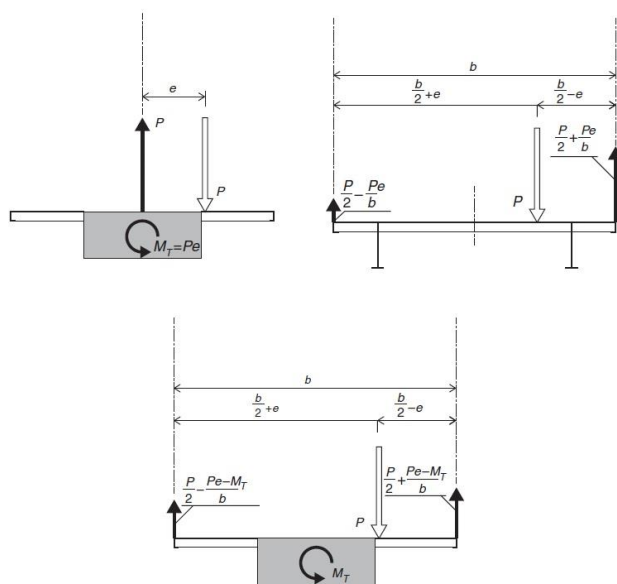
Figure 2.22   Various ways of carrying an eccentric load depending on the torsional stiffness and the cable system (Gimsing & Georgakis 2012).
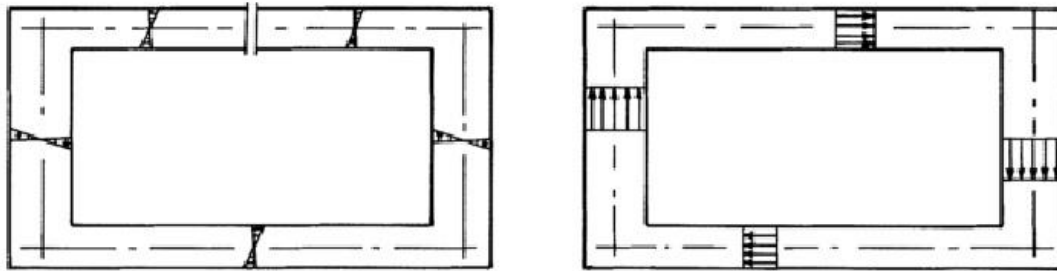
Figure 2.23   *The combined action of the two components to resist pure torsion* (Waldron 1988).

The designers' purpose, when studying the buckling response of a bridge stiffening girder is to improve the cross-section. With the term improve meaning that the cross-section will become more effective in terms of bending stiffness, while providing adequate web support to secure post-buckling strength. As in common plate girders, linear distribution of stresses is used and failure occurs when the compression flange reaches the ultimate stress or the tension flange the yield stress, if no buckling occurs.

In most cases the flanges of the box girder are reinforced with stiffeners to achieve high utilization of thin plates. When stiffeners are used, the upper flange is divided into subpanels with smaller dimensions.

2.1.6   Shear lag effect

Until today the design of horizontal structural elements is mainly based on the Euler-Bernoulli beam theory. Euler-Bernoulli Beam Theory is based on a number of assumptions. One of the main assumptions is that the cross section of the element remains plane during bending. In addition to that, shear deformation impact on deflection is neglected. Particularly, in case of beams with flanges, these two assumptions lead to lack of shear stresses and strains in the flanges, as well as to dependence of the axial displacements of the flanges only by the distance from the neutral axis and not to the distance from the webs.

However, Beam Theory does not fully correspond to reality. What actually happens in the behaviour of the beam is that the web and the flanges are interconnected and thus the longitudinal strains at the joint between them should be equal. This leads to a shear deformation in the flange that creates a non-uniform membrane stress distribution. This phenomenon, which is called "Shear Lag Effect", increases the stresses in the junction between the web and the flanges and is particularly obvious in beams with wide and short flanges.

If the "Shear Lag Effect" was neglected, it could result to the underestimation of the stress magnitude in the flanges. Consequently, to end up in a sufficient design, an effective width should be adopted for the top flange of the box girder, to be equal to the actual stresses in the flanges. The effective width b_{eff} for shear lag under elastic conditions should be determined from:

$$b_{eff} = \beta \, b_0 \tag{2.1}$$

where the effective factor β is given in (ENV 1993-1-5, Table 3.1) and the width b_0 is taken according to the Figure 2.24, depending on whether it is an outstand or an internal element.
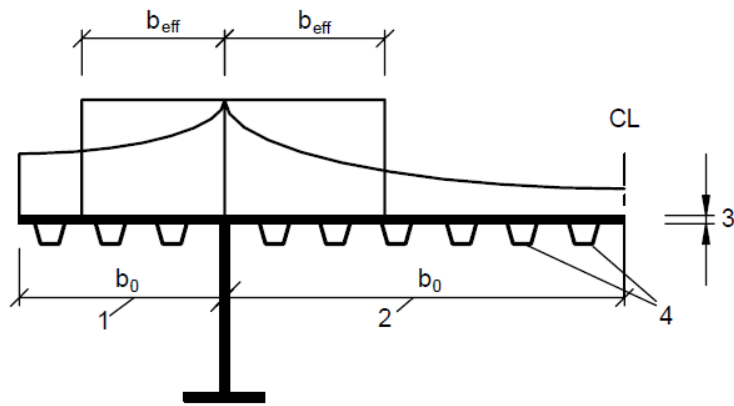
1   for flange outstand
2   for internal flange
3   plate thickness t
4   stiffeners with $A_{s\ell} = \sum A_{s\ell i}$

Figure 2.24   Notations for shear lag (ENV 1993-1-5).

b_{eff} is the effective part of the flange under uniform stress is in equilibrium with the actual non-uniform stress distribution.

2.1.7   Local distortion mechanisms in bridge deck

The action of the wheel loads in the bridge deck is responsible for a series of local deformation which are shown on Table 2.1 and discussed below.

Table 2.1   Orthotropic steel deck deformation mechanisms (US Department of
            Transportation 2012a).

System	Action	Figure
1	Local Deck Plate Deformation	
2	Panel Deformation	
3	Rib Longitudinal Flexure	
4	Floorbeam In-plane Flexure	
5	Floorbeam Distortion	
6	Rib Distortion	
7	Global	

In system 1 the wheel loads are transferred from the deck plate to the supporting ribs. The decisive factors for this response are the relative thickness of the deck plate and the ribs, as well as the spacing of the ribs. This action can cause fatigue failure in the connection between the ribs and the deck plate, but in most cases it is not crucial for strength based limit states.

System 2 represents the deformation of the deck panel under out-of-plane loading which results in transverse deck stresses due to the differential displacements of the

ribs. This system is the most complicated to analyse due to the two-way load distribution of the OSD panel. Furthermore, its behaviour is further affected by the type of the ribs.

System 3 represents the behaviour of the ribs in their longitudinal direction. After the load distribution in the transverse direction as described in system 2, the ribs transfer the load in the longitudinal direction to the transverse beams of the girder. The ribs are considered as continuous beams on discrete flexible supports which represent the transverse beams.

Systems 4 and 5 are used to show the mechanisms which are developed during the transference of the loads from the ribs to the girders through the transverse beams. The transverse beams act as beams between rigid girders and the stresses that develop are due to combination of in-plane stress (flexure and shear) and out-of-plane stress (twisting) from rib rotation. System 4 describes the former, whilst system 5 describes the latter.

System 6 corresponds to the rotation of the rib in a closed-rib system, when the wheel load is at the mid-span and acts eccentric to the axis of the rib. In such loading cases, the rib twists about its centre of rotation and results in lateral displacement at the mid-span.

Finally, the 7th system describes the behaviour of the primary girder between the global supports and the resulting axial, shear and flexural stresses due to the deformations (US Department of Transportation 2012a).

2.2 Steel sandwich elements

2.2.1 Introduction

Throughout the centuries, the constant need for bigger, lighter and more durable constructions has pushed researchers to pursue solutions for innovative materials, new structural systems and high performance elements to achieve their most ambitious visions. Structural steel was always an outstanding choice for meeting these expectations as it provides a variety of advantages; high strength to weight ratio, durability, versatility, low cost and sustainability etc. In a continuous attempt for exploiting these assets, engineers came up with new configurations; used for different applications. Steel sandwich elements are considered the state of art of this endeavour, especially after new welding techniques came to limelight. The sandwich plates considered in this Thesis consist of a corrugated plate fastened between two face plates, see Figure 2.26.

2.2.2 History

Although sandwich elements became more well-known after the second half of the 20th century, evidences show their existence since 1849, when they were mentioned in the texts of Sir William Fairbairn (Sir William Fairbairn 1849). The first proven sandwich application though, was made of wood and it was shown in the 'Mosquito' aircraft in 1940s (Vinson 1999). This is considered as the beginning of using sandwich elements in the marine and aerospace industry. Until now, a variety of difficulties connected to the manufacturing caused SSE limited utilization. Particularly, welding process was making the total procedure relatively slow and expensive. Moreover, the lack of

knowledge about their long-term behaviour was the main reason that made engineers sceptical about their field of application (Wolchuk 1990).

The last 20 years, steel sandwich panels began to enter drastically to the civil and mechanical engineering industry. The main reason why this has happened is laser welding, which has replaced the previous conventional spot-welding. Laser welding techniques, and especially the combination of laser and gas metal arc welding into a hybrid welding process, were proven to be a viable (Roland et al. 2004). HLAW minimizes the part distortion and increases the accuracy, while the welding time can be 10 times faster than common welding methods (Blomquist et al. 2004). Furthermore, it provides control of the geometric parameters of the welds and temperature variation, high connection quality and excellent surface finish reducing the fairing and fitting work in outfitting (Olsen 2009).

Figure 2.25   Production of SSE with HLAW (http://www.esab.com).

The application of SSE can result in a series of advantages but these can be summarized in the following:
- High stiffness to weight ratio
- Low level of orthotropy
- Industrialized construction process

Laser welded SSE can save approximately 30-50% of material compared with conventional steel members (Kujala & Klanac 2005); fact that enables them to be an economical solution in terms of manufacturing and transportation. The areas of their application are extremely wide, extending from the marine, aerospace and offshore industry to wind turbine blades, hoods, hatches, lift floors and bridge decks lately.

2.2.3   Corrugated core steel sandwich elements

The steel sandwich elements can be divided into two big categories: elements with steel faces bonded with an elastomeric core and elements with both faces and core made of steel welded together. The latter includes steel cores that can be manufactured in various shapes depending on the type of application. In this specific Master Thesis project, the steel sandwich element studied has a corrugated core, as shown in the Figure 2.26. A typical section of this type of elements, along with its characteristics, is shown in the Figure 2.27. The reason why this type of SSE was examined, is because it has been shown to be suitable for bridge decks(Beneus & Koc 2014).
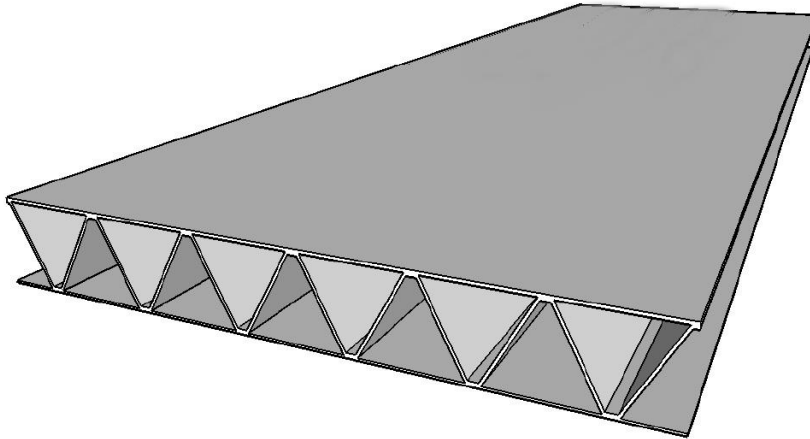
Figure 2.26   Corrugated core SSE.

Taking into account that the steel core of the sandwich has different configuration in the two main axes, it is obvious that the element possesses a strong and a weak direction. Strong is called the direction where the flexural and shear rigidity is higher; the other direction is the weak one lacking mainly in shear stiffness. In such a formation, the function of the top and bottom plates is focused on the resistance to the bending moments, while the core transmits shear forces. To model the behaviour of the SSE, the Reissner-Mindlin plate theory can be applied, in order to transform the 3D sandwich element to an equivalent 2D plate, see figure 2.27. This plate will have the elastic constants that describe the behaviour of the SSE, see chapter 4.4.
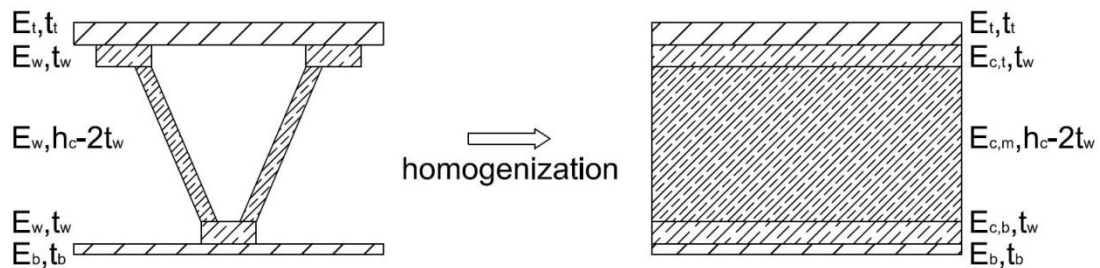
Figure 2. 27   The principle of homogenization of the core properties.
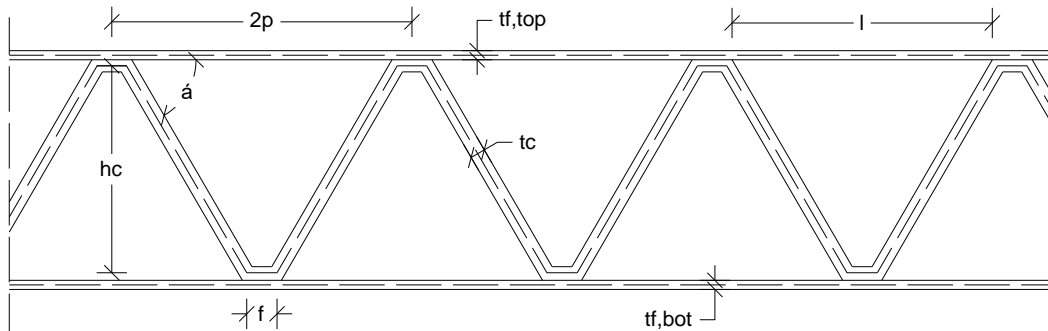
Figure 2.28   Typical section of corrugated core SSE.

The variables, which characterize such a structural system (Figure 2.28), are:
- the length between the core repetition, 2p
- the height of the core, h_c
- the thickness of the top plate, $t_{f.top}$
- the thickness of the bottom plate, $t_{f.bot}$
- the thickness of the corrugated core, t_c
- the angle of the core stiffeners with the horizontal axis, α
- the horizontal distance between two stiffeners, f

3 Höga Kusten Bridge

Höga Kusten bridge, illustrated in Figures 3.1 and 3.2, is a suspension bridge located in northern Sweden, between the municipalities of Härnösand and Kramfors. The bridge was constructed in 1997 to connect the banks of Ångerman River and replace the previously existing Sandö Bridge in the main road connection. The total length and width of the bridge comes to 1867 and 22 meters respectively, while the height of the two pylons holding the main cables extends more than 180 meters (Structurae.net, 2015). The long span of the bridge ranks it 3rd in Scandinavia and 4th in Europe among the longest suspension bridges. The construction period was almost 4 years.

Figure 3.1   Höga Kusten bridge (http://www.bridge-info.org).
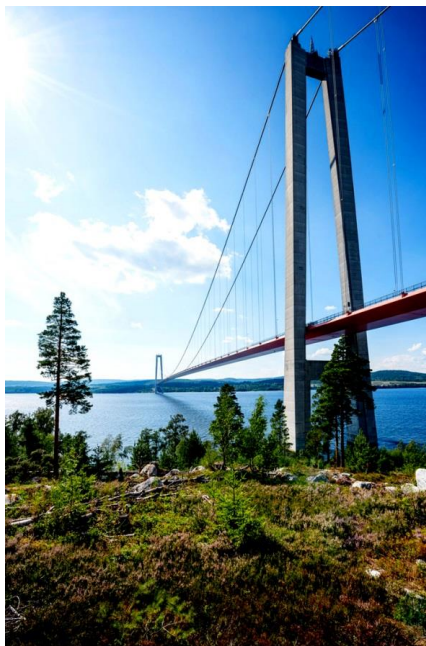
Figure 3. 2   Höga Kusten bridge (http://www.hogakustenstugor.se).

The cross section of the Höga Kusten bridge was chosen to be studied for this Master Thesis project. This is due to the fact that it is one of the two suspension bridges located in Sweden; the other one is the Älvsborg bridge. In addition to this, it is the only one combining the box girder cross-section with a suspension system.

3.1 The compression flange

The compression flange of the box girder is composed by a plate which is stiffened longitudinally by stiffeners of closed type. The stiffened compression flange is composed by several continuous beams, supported at the diaphragms. The compression flanges may be subjected to the following stresses:

i)   Longitudinal stresses caused by the global bending moment on the main girder.
ii)   In-plane shear stress in the flange plate caused by local shear forces and torsion.
iii)   Flexural stresses in the stiffeners caused by the local loads on the deck.
iv)   In-plane transverse stresses in the flange plate caused by the bending of the transverse flange stiffeners and the distortion of the box girder section.

Regardless of the stressing field mentioned above, a series of geometrical complexities have to be investigated as well. These are:

i)   The longitudinal continuity over the transverse stiffeners.
ii)   The transverse continuity between parallel stiffeners.
iii)   The different buckling modes.
iv)   Geometrical imperfections and residual stresses in the flange plate and the stiffeners.

Critical for the compression flange is the interaction between local buckling and global buckling. This phenomenon can lead to rapid loss of the load resistance. Therefore, the design codes for stiffened plate define the geometrical limitations which are not prone to buckling and have no initial imperfections.

3.2 Classification of the cross section

Initially, the orthotropic plate used for the bridge deck was checked with reference to local buckling. The cross-section is composed by four parts, each of which has been studied as individual plate. The slenderness ratio of each part has been calculated to define the rotational capacity and check the sensitivity with regards to local buckling. The clear dimensions were specified as the dimension of the middle lines minus the thicknesses of the parts, as shown in Figure 3.3. The unit studied is part of the top plate of the total box girder cross-section, which is principally subjected to uniform compression in the middle span of the bridge.
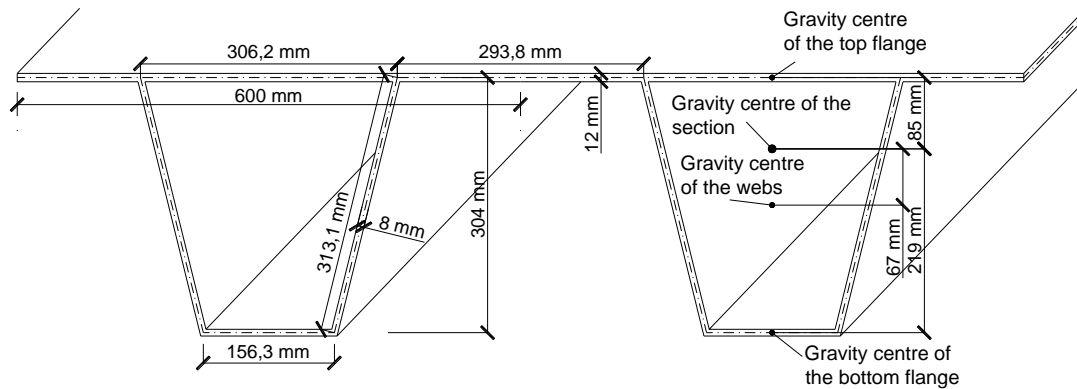
Figure 3.3   Cross-section of the two units.

After defining the width to thickness ratios for the different components of the compression flange, it was proven that the top and bottom horizontal parts belong to Class 1. Therefore, their whole cross-sectional area can be used in the design, as they can form plastic hinges in a statically indeterminate system. However, the webs of the stiffener have a high slenderness ratio and therefore local buckling can take place before yielding. These parts, which are classified in the 4th category, do not use their whole cross-section regarding the moment and load carrying resistance, i.e. an effective cross-section should be calculated. The classification and the effective area of each unit are illustrated in Figures 3.4 and 3.5 respectively. Finally, the end parts in the edges of the top plate were also classified in Class 1.
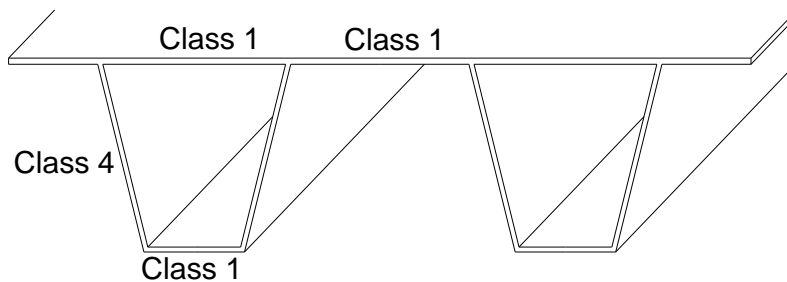
Figure 3.4   Classification of different parts.
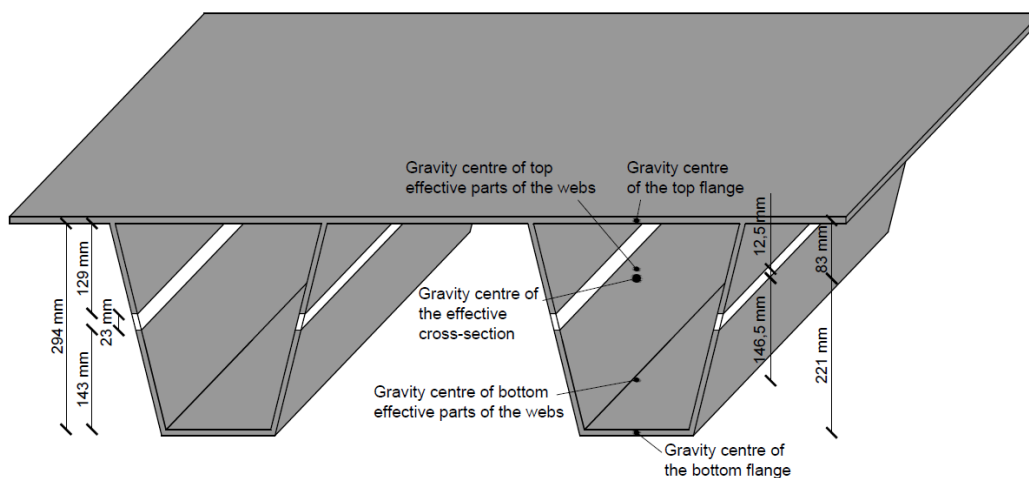
Figure 3.5   Effective areas and gravity centre of the cross-section.

3.3 Axial load-carrying capacity

For defining the moment capacity, the interaction between the column-type and the plate-type buckling of the deck has to be studied. From the individual reduction factors for each case, a final reduction factor will be obtained according to the following equation (EN 1993-1-5):

$$\rho_c = (\rho - \chi_c)\xi(2 - \xi) + \chi_c \tag{3.1}$$

where $\quad \xi = \dfrac{\sigma_{cr.p}}{\sigma_{cr.c}} - 1 \quad$ but $\quad 0 \leq \xi \leq 1$

$\sigma_{cr,p}$ is the elastic critical plate buckling stress
$\sigma_{cr,c}$ is the elastic critical column buckling stress
χ_c is the reduction factor due to column buckling
ρ is the reduction factor due to plate buckling

According to the drawings, the distance between the diaphragms was 4 m. The bridge deck is subjected to uniform compression, see Figure 3.6. The normal compressive stresses vary along the depth of each unit, as shown in Figure 3.7. To calculate the distribution of the stresses, the neutral axis of the whole section, as well as the neutral axis of the top plate has been defined. The centre of gravity was defined from the bottom flange of the bridge deck, taking into consideration the position of the neutral axis of each unit.
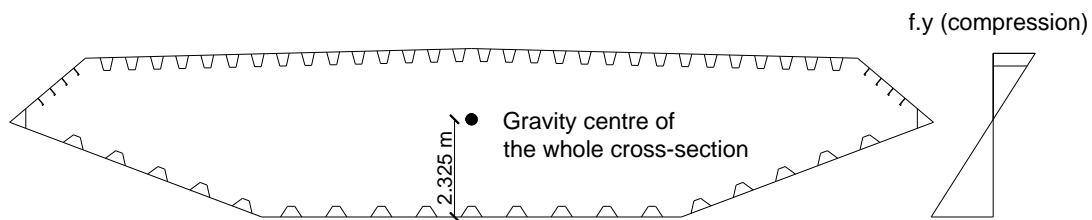
Figure 3.6   Cross section of Höga Kusten bridge.
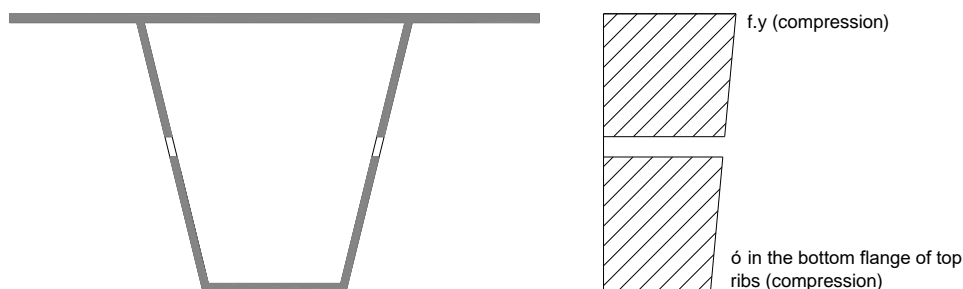
Figure 3.7   Cross-section of one longitudinal stiffener.

For the column-type behaviour, one of the repeated units has been used, as seen in Figure 3.8. The elastic critical column buckling stress was determined from the stiffener which is closest to the panel edge and had the highest compressive stress. Its value was 1.649×10^3 MPa, while the reduction factor ρ obtained was 0.862. Exact calculations can be found in the Appendix A.
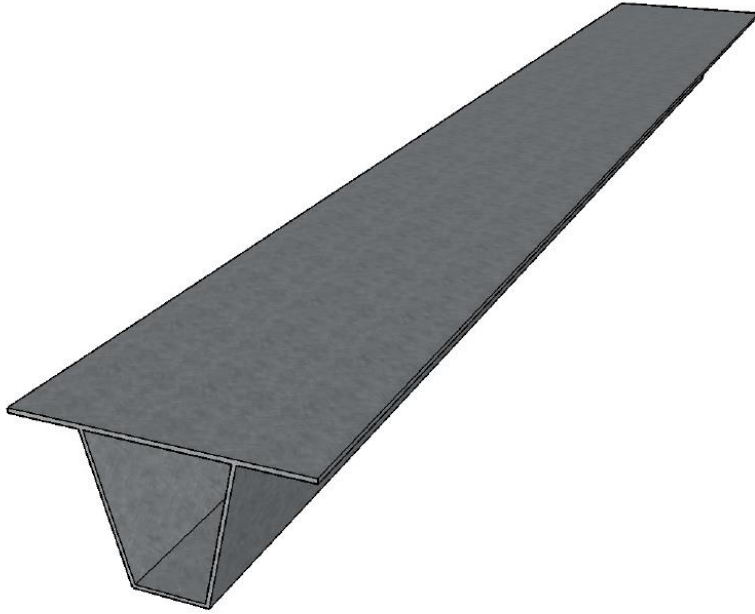
Figure 3.8   Section for calculation of column-type behaviour.

On the other hand, for the plate-type behaviour the whole cross-section was utilized, as illustrated in Figure 3.9. In the beginning, the relative plate slenderness was defined. Then, the elastic critical stress and the reduction factor for the plate-like buckling were extracted equal to 1.605×10^3 MPa and 1 respectively. Thus, the bridge deck behaves as a column and will have very little, if any, post-critical strength.
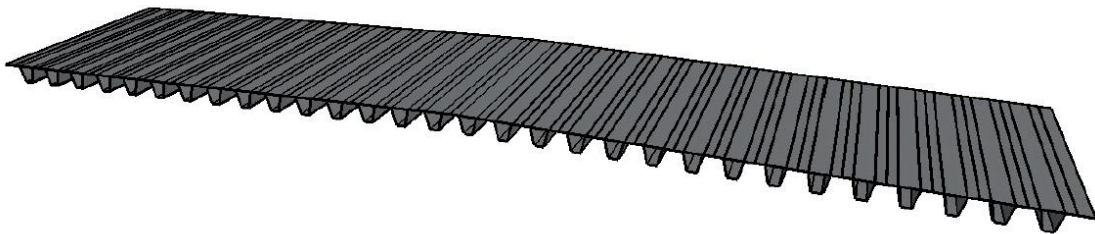
Figure 3.9   Section for calculation of plate-type behaviour.

The compressive axial load carrying capacity used in the design is affected by local and global instability. The final axial load carrying capacity of the bridge deck was 6.718×10^3 kN/m. The axial load for the current case comes mostly from the bending moment of the vertical loads, while the axial forces from the acceleration and breaking of the vehicles can be neglected.

3.4 Deflection

In order to find the local deflection between diaphragms of the bridge deck, a beam between two transverse hangers was selected. The whole length of the element extends to 20 meters. Supports have been placed every 4 meters, exactly in the positions where the diaphragms are located. Figure 3.10 portrays the model in *Abaqus/CAE*.
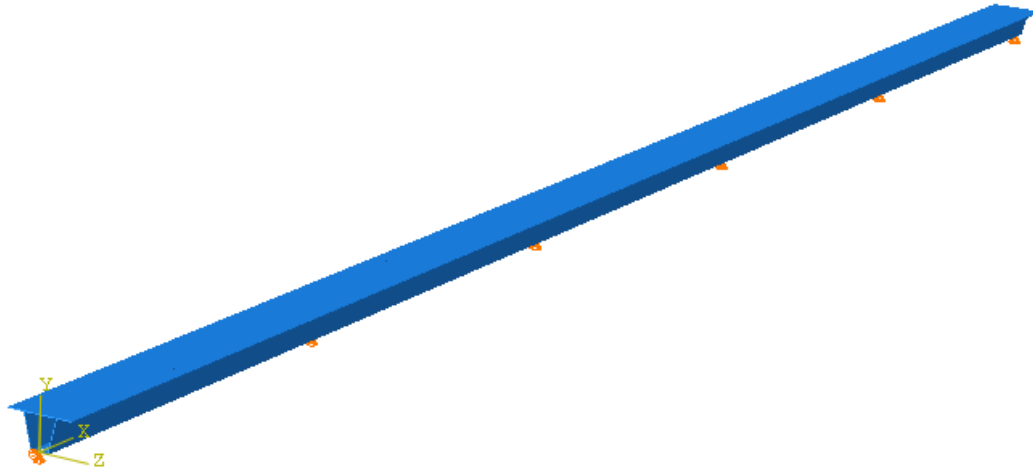
Figure 3.10   Abaqus/CAE model of the examined element.

Different load combinations were considered, according to (EN 1991-2) and the worst case was chosen; it is the one illustrated in the Figure 3.11. In this load combination, the uniform load represents the traffic flow and the self-weight, whilst the concentrated loads represent the wheel loads of Load Model 1. More analytical calculations can be found in Appendix A.
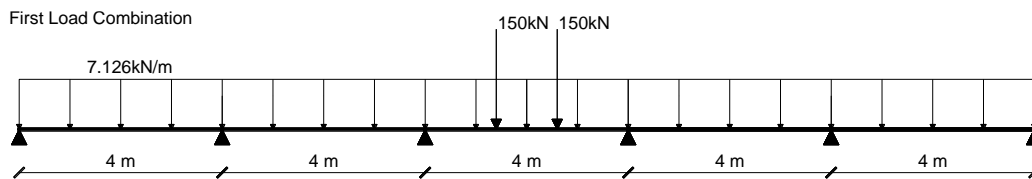
Figure 3.11   Most dominant load combination with regard to deflection.
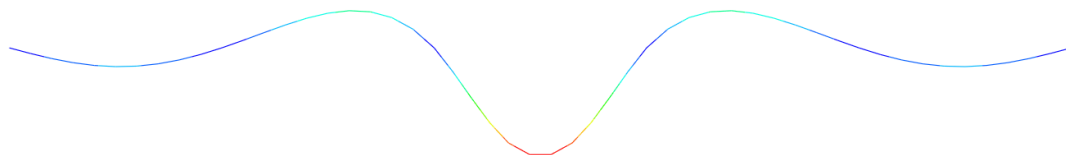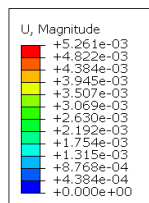
Figure 3.12   Deflection for the most dominant load combination.

The maximum allowed deflection for every span has been specified in the Swedish National Annex equal to L/400. For the studied case, the final global deflection from the worst load combination, illustrated in Figure 3.12, was calculated equal to 5.26 mm, which is smaller than L/400 = 10 mm.

4 Optimization analysis

4.1 Introduction

All indications show that the constant development of welding techniques nowadays may allow the reintroduction of SSE as a suitable solution for bridging long spans. In the specific Master Thesis project, the replacement of the OSD of Höga Kusten Bridge with corrugated core SSE was investigated to prove the previous statement.

The study was performed only with regard to deflection, which means that only the service limit state was taken into account. The optimization routine built was based on (Beneus, E., & Koc, I., 2014) but it inserts also the plate behaviour of the SSE through Chang's formula, (Chang, 2004) . Figure 4.1 shows the flow chart of the optimization routine.
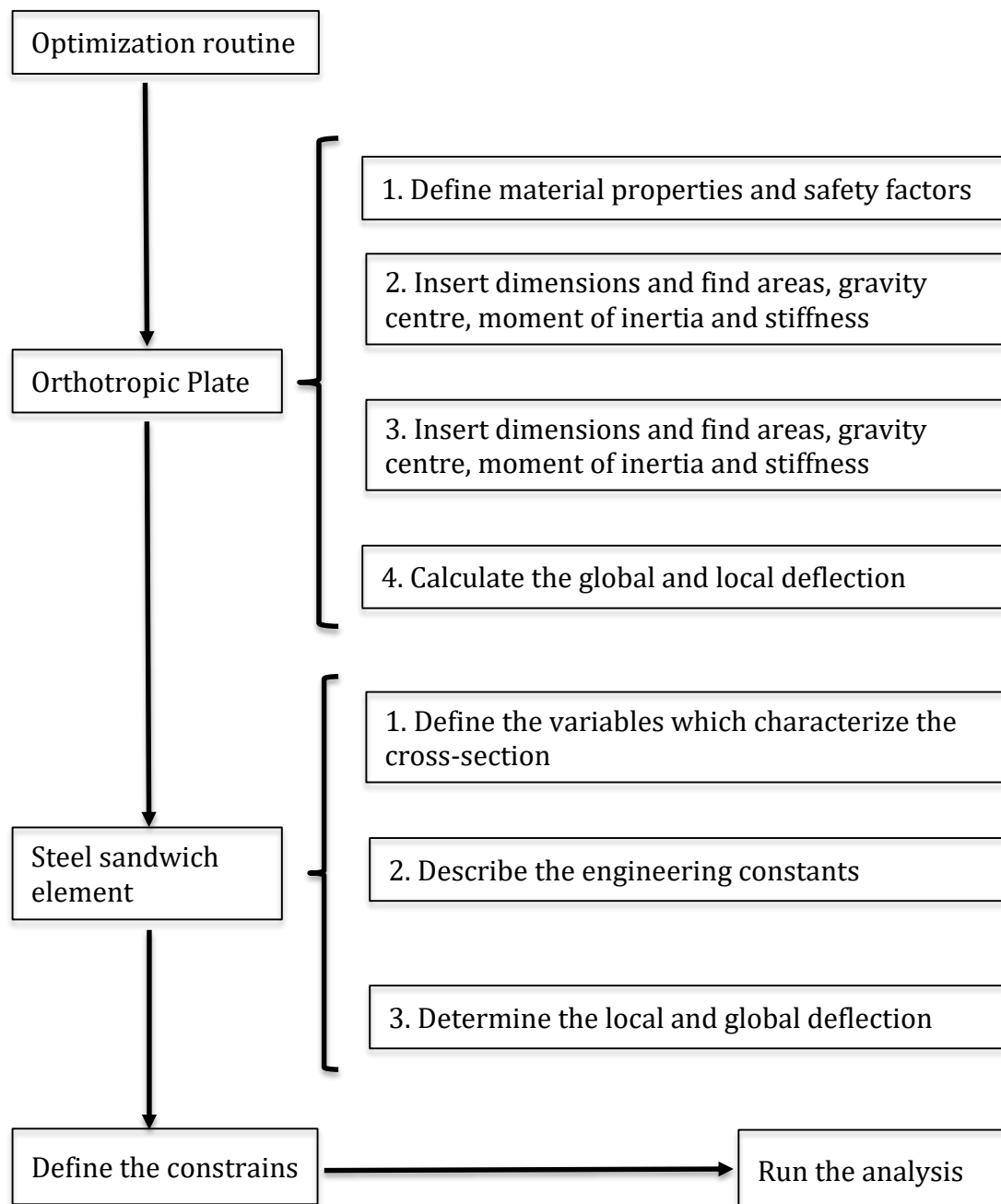
Figure 4.1   Flow chart of the optimization routine.

The rigidity and behaviour of the new SSE are affected by the geometry of the section. The geometry of the section can be defined by 6 parameters, which from this point on will be referred as the independent variables. For the needs of this specific Master thesis project, these variables set to be the following, see Figure 4.1:
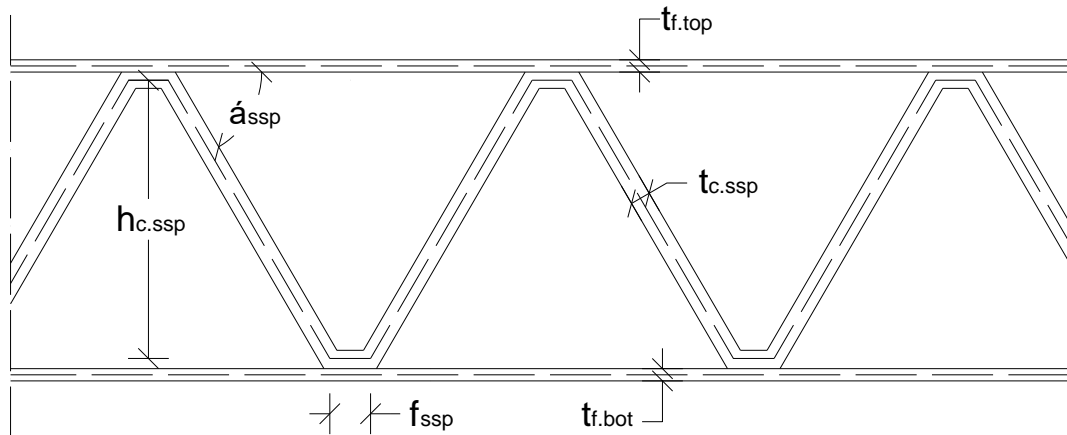
Figure 4.2   Typical section of V-type corrugated SSE.

- the height of the core, $h_{c.ssp}$
- the thickness of the top plate, $t_{f.top}$
- the thickness of the bottom plate, $t_{f.bot}$
- the thickness of the corrugated core, $t_{c.ssp}$
- the angle of the core stiffeners with the horizontal axis, α_{ssp}
- the horizontal part of the core between two stiffeners, f_{ssp}

All the parameters of the algorithm have been defined in relation to the independent variables of the SSE. Thus, setting values for the independent variables results in a fully defined SSE section; all the dimensions as well as all the stiffness parameters according to (Libove, C., & Hubka, R. E., 1951).

The optimization analysis aims at producing sections which will be optimized for a series of different cases. This was performed through a numerical method suitable to solve constraint non-linear optimization problems. This iterative method allows a property of SSE to be maximized or minimized. To execute this numerical approach, the build-in solver of the calculation program Mathcad used.

In order to obtain the desired results, a number of constraints were set. These constraints were the conditions which must be valid to create an appropriate final section. The constraints in all of the analyses, as well as the corresponding input in the routine, are shown in Table 4.1. The motives behind the selection of these constraints are analysed in detail in chapter 4.2.

Table 4.1   Constraints in the optimization routine.

Constraint	Input
The top and bottom plates should be at least in class 3.	$t_{f.top}, t_{f.bot} \leq 42\varepsilon$
The corrugated core should be at least in class 3.	$t_{c.ssp} \leq 42\varepsilon$

The global deflection of the SSE in the center of the plate should be limited to a value smaller than the smallest dimension divided by 400.	$w_{tot} \leq \dfrac{L_{ssp}}{400}$
The local deflection between the transverse beams of the SSE should be smaller than the length divided by 400.	$\delta_I \leq \dfrac{l_{ssp}}{400}$
The angle of the corrugated core should be ranging between 40 and 70°.	$40° \leq a_{ssp} \leq 70°$
The distance between the inclined stiffeners of the core should be between 20mm and 40mm.	$20\ mm \leq f_{ssp} \leq 40\ mm$

These constraints should be fulfilled in all the cases studied. The different scenarios considered were:

1) Maximization of the moment of inertia in the longitudinal direction (I_x)

2) Minimizing the material used

3) Minimizing the material used, considering an updated main girder configuration

4) Maximizing the length between the transverse stiffeners

In every scenario a specific property is chosen to be optimized. To optimize the value of a property, the user must enter the corresponding function in the program, accompanied by the independent variables by which this property is dependent from. All the independent variables should fluctuate in the margin set by the constraints. Furthermore, the user must set initial values for the independent variables for the program to start running. As explained, the optimization routine is a numerical iterative method. That means that during the execution of the routine, the program sets values for the independent variables, until the optimum solution is found depending on each scenario. The tolerance in the program is set equal to 10^{-6}.

4.2 Choice of the constraints

The theory behind the calculations of the limiting values of the constraints will be discussed in the current section. To begin with, all the individual parts of the cross section in the routine were chosen to be in class 3 or better. That means that their whole cross-sectional area could be used in the design and be loaded to the yielding point. According to (EN 1993-1-1., 2005, Table 5.2), for parts subjected to uniform compression, the maximum value of the width to thickness ratio is *42ε*,

where $\varepsilon = \sqrt{235/f_y}$

Structural steel grade S355 was chosen, with f_y = 355MPa, resulting in *ε = 0,814*. Therefore, the width to thickness ratios of the several parts of the cross section should be below *34.2*.

Furthermore, the deflection between the diaphragms was set to be smaller or equal than their distance, which is 4 meters, divided by 400, i.e. 10 millimetres. The deflection in the routine was calculated for a simply supported plate equally wide to the half of the total width (9 m) and equally long to the length between the diaphragms (4 m). The deflection was calculated using double Fourier series, based on the Mindlin–Reissner

plate theory, see (Chang, W.-S., 2004). The distributed load applied consists of the traffic load for the main and the secondary lanes which is 9 and 2,5 kN/m² respectively as well as the asphalt load and the self-weight of the construction. The asphalt load is 1,15 kN/m² for asphalt 50 mm thick. The self-weight for a section with the same amount of material as the orthotropic deck of the Höga Kusten bridge is 1,727 kN/m². In addition to this, there is also the load from two vehicles. The load according to (EN 1991-2, 2010) is 150 kN per wheel for the main lane and 100 kN per wheel for the secondary. The distance between the wheels of each truck is 1,2 m in the direction of the traffic flow and 2 m in the transverse direction. The magnitudes and the positions of the loads are shown in Figure 4.2. It should be noted that, due to the difficulty to calculate the deflection for different uniform loads in different lanes, the uniform loads were transformed in an equivalent uniform load which acts all over the plate. The value of this load was 4,67 kN/m².
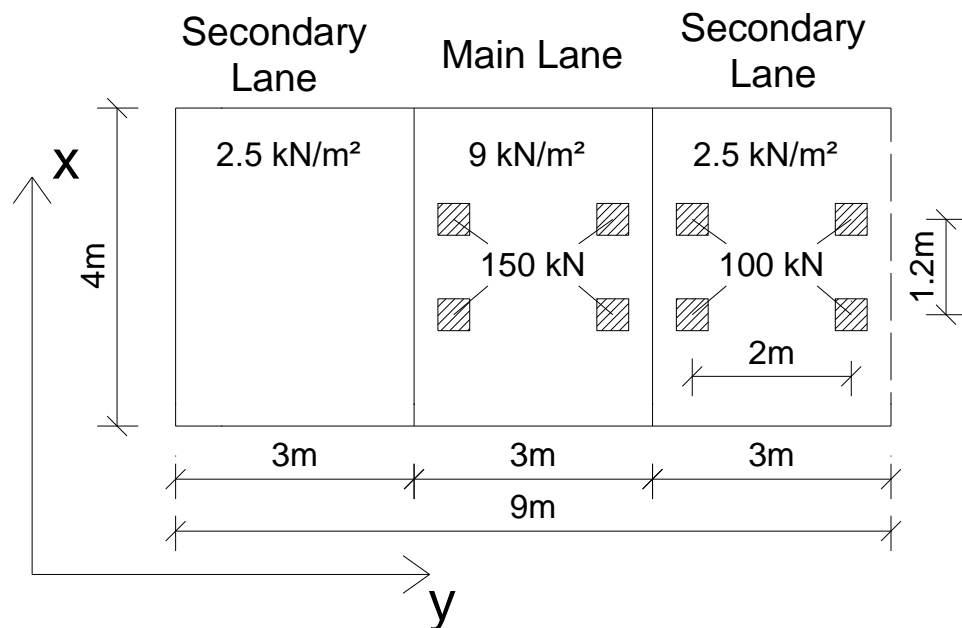
Figure 4.3   Load magnitudes and positions.

The calculation of the deflection using a simply supported plate does not represent the reality, since there is also the continuity of the plate over the supports which will result in a lower deflection value. To find a more accurate deflection between two consecutive transverse beams including the effect of the continuity, the Finite Element (FE) program Abaqus/CAE was used. Verification of the FE analysis was made, in order to ensure that there is correspondence between its results and the analytical solution. The verification can be found in chapter 5.5.

Another constraint was set due to the local deflection. According to this constraint the deflection between the core repetitions (δ_I) should be less than the repetition length (l_{ssp}) divided by 400, see Figure 4.3. The applied load is the wheel load divided by the width of the wheel increased by 100 mm, see Figure 4.4.
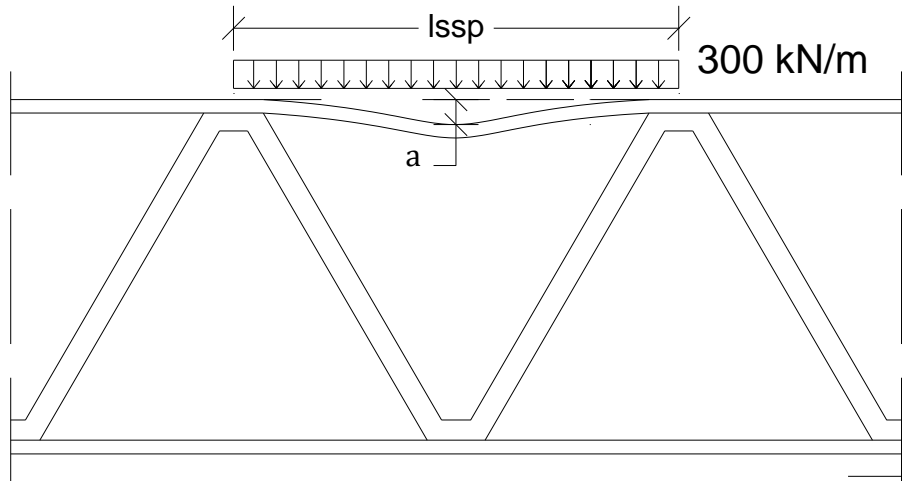
Figure 4.4   Local deflection of SSE.

Furthermore, the angle of the corrugated core (α_{ssp}), was set between 40 and 70 degrees, while the distance between the inclined stiffeners of the core (f_{ssp}) was chosen to be between 20 and 40 mm.

4.3 The studied scenarios

4.3.1 Maximization of the moment of inertia in the longitudinal direction

Following the same concept as (Beneus & Koc 2014), the initial purpose was to create a steel sandwich element for the Höga Kusten Bridge, which would have a better structural behaviour than the existing orthotropic deck. For this purpose, the first use of the optimization routine was the design of an SSE which could the same amount of material and at the same time better moment of inertia in the longitudinal direction (x-direction).

4.3.2 Minimizing the material used

From the literature study, it was underlined that the main asset of the SSE is its potential to behave as a plate and distribute the loads in both directions. Therefore, the total deflection of the plate was studied rather than the bending stiffness in the strong direction. This was achieved by adjusting the optimization routine to minimize the global deflection in the middle of the plate.

To verify the results a plate model was then created in Abaqus/CAE, where a single layer homogenous core was adopted, as described in (Romanoff & Kujala 2002). The model was generated as a lamina plate using the engineering constants from the optimization routine. The point in which the maximum global deflection appeared in the FEM approach was then compared with the point assumed to deflect more in the optimization routine; in the specific case the middle of the plate.
Provided that there should exist no point in the plate with higher deflection than the minimum value of Lssp/400 and Bssp/400, the previous optimization routine was rerun, searching the deflection in the new spot found and assuming that this point would not change due to the different cross-section obtained. The reutilization of the routine provided the right value for the maximum deflection. In the end of the procedure, it had been verified that the most deflected point stayed immovable.

However, the results obtained were reflecting the behaviour of a single supported SSE, which is not the real case in long-span decks. So, the next step was to take into account the continuity of the plates between the diaphragms that form the bridge deck. In this occasion the whole deck was modelled in Abaqus/CAE. The deflection of the equivalent plate was calculated for a continuous plate 9 m wide, which is the half of the deck width, simply supported every 4 m, which is the distance between the transverse beams, for a total length of 20 m, which was the distance between the diaphragms in the Höga Kusten case. By creating the bridge geometry in Abaqus/CAE, with the corresponding loading, the real global deflection could be extracted.

4.3.3 Minimizing the area by adding a longitudinal stiffener

In this case, the above analysis and methodology was implemented with the addition of a longitudinal stiffener in the middle of the width of the plate. The aim was the creation of two more square shaped steel sandwich plates that would grant improved structural behaviour compared with the original rectangular plate of the previous scenario. This stiffener, which was modelled as a support, resulted in panels 4 m long and 4,5 m wide. A new equivalent uniformly distributed load was calculated, as only the main vehicle could fit in the deck lane.

4.3.4 Maximizing the length between the transverse stiffeners

The final study that was performed was the investigation of the maximum length that the SSE could have between two diaphragms. In this case, the routine aimed to optimize the plate's length, while the material used on the SSE section was set equal to the OSD. The purpose of the specific study was to investigate if it is possible to reduce the number of the transverse beams, and thus, save material. The major advantage of the SSE compared to the OSD is the fact that it provides much larger stiffness in the y-direction. Therefore, the increment of its length would be beneficial by enhancing the plate behaviour of the SSE. Moreover, apart from saving material by decreasing the number of the transverse stiffeners, the implementation of longer elements would reduce significantly the production time and cost.

4.4 Finite Element Analysis

As mentioned above, in order to take into account the continuity of the plates between diaphragms, the FEM program Abaqus/CAE was used. The Simplified Finite Element Approach, as described in (Romanoff & Kujala 2002) was used. The geometry of the bridge deck between the diaphragms was modelled for all the examined cases. However, the final steel sandwich sections were not modelled in detail as that could not give more value to the aim of this Master Thesis project. Instead the elements used were 3D deformable shell elements including shear-induced vertical displacements. The elastic properties of the material were defined using lamina material model and the engineer constants for out-of-plane condition were obtained from (Lok & Cheng 2000):

$$E_x = \frac{12 \cdot D_x}{h^3}, \tag{4.1}$$

$$E_y = \frac{12 \cdot D_y}{h^3}, \tag{4.2}$$

$$G_{xy} = \frac{6 \cdot D_{xy}}{h^3}, \tag{4.3}$$

$$G_{xz} = \frac{D_{Qx}}{k \cdot h},$$ (4.4)

$$G_{yx} = \frac{D_{Qy}}{k \cdot h},$$ (4.5)

where k is the shear correction factor; chosen equal with 5/6.

Regarding the boundary conditions, the translation in the vertical direction was prevented on the outer edges of the plate, as well as in the positions of the transverse stiffeners. In addition to this, the longitudinal movement was also prevented where a longitudinal stiffener was added in one of the studies.

For the mesh, 4-node elements were used with quad-dominated shape. The approximate size of the elements was 250 mm.

Finally, the loading was set as pressure for both the uniform distributed load as well as for the wheel loads. The uniformly distributed load, which included the self-weight, the traffic and the asphalt loads, was 7,544 kN/m^2 in the cases where the area of the section was equal to the one of the orthotropic section. In the cases where this area is reduced, this load somewhat smaller. The wheel loads were set as pressure over an area of 500 x 500 mm which was defined by (EN 1991-2, 2010) increased by 100 mm, to account the height of the asphalt, see Figure 4.4.
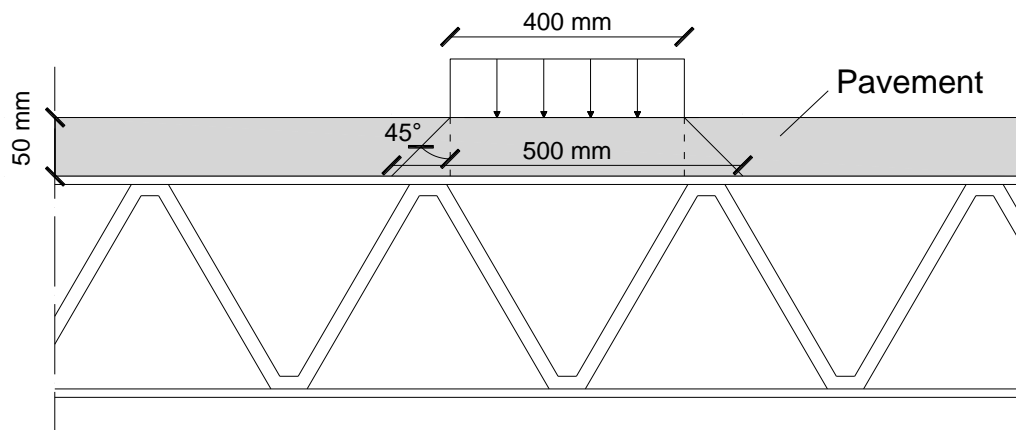
Figure 4.5   Distribution of the wheel load in the pavement.

5 Results

In this chapter the results from the different analyses are presented. For detailed calculations see Appendix A.

5.1 Study 1 - Maximization of the moment of inertia in the longitudinal direction

The first study has proven that with the specific amount of material given by the cross section of Höga Kusten deck and all the constraints considered, it was hard to create a steel sandwich element that could have larger moment of inertia in the direction of the traffic flow. The reason was that the existing bridge deck consists of quite slender parts (i.e. the webs are in class 4). On the other hand, the SSE was constrained to achieve cross-sectional properties of class 3 or lower and thus to provide a structural member with all the individual parts insensitive to local buckling.

5.2 Study 2 - Minimization of the material used

The most important conclusion of this scenario was the proof that studying the steel sandwich element as a plate did give the opportunity of reducing the area of the cross section in long span bridges.

The first phase of the analysis was the usage of the routine for the acquisition of an initial cross-section that could be used for extracting the most deformed point. An FE model was then created in Abaqus/CAE, as explained in Chapter 4.3.2. The result for the equivalent plate is illustrated in Figure 5.1.

Table 5.1 Initial cross-section for the formation of the Abaqus/CAE model in Study 2.

	Function	Minimize w_{tot}		
Optimization Results	Global deflection (for i,j=1…1) in the optimization routine	w_{tot}	mm	6,72
	Height of the core	$h_{c.ssp}$	mm	163,0
	Thickness of the upper plate	$t_{f.top}$	mm	6,5
	Thickness of the bottom plate	$t_{f.bot}$	mm	5,1
	Thickness of the core	$t_{c.ssp}$	mm	5,3
	Angle of the core	a_{ssp}	degrees	64,7
	Distance between diagonals	$f_{.sp}$	mm	21,6
	Engineering Constants	E_{xb}	N/mm^2	55730
		E_{yb}	N/mm^2	46170
		$G_{xy.1}$	N/mm^2	16020
		G_{xz}	N/mm^2	4470
		G_{yz}	N/mm^2	642,8

To ensure that the deflection values calculated from the hand calculations and Abaqus/CAE correspond well to each other, there has been a verification which may be found later in this chapter.
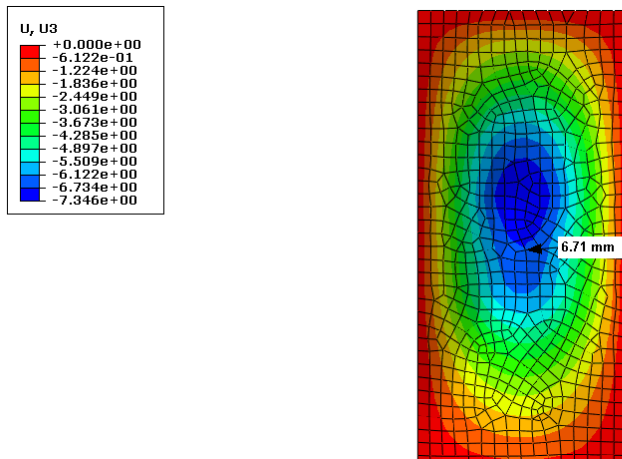
Figure 5.1   Deflection in the middle of the plate for the equivalent plate in Abaqus/CAE.

It was observed that the maximum deflection was obtained in a different point and not in the middle of the plate. That was expected due to the asymmetric traffic loading. The point of the maximum deflection had coordinates (X, Y) = (2m, 5,4m). The coordinates of this spot as well as the value of its deflection are shown in the Figures 5.1 and 5.2.
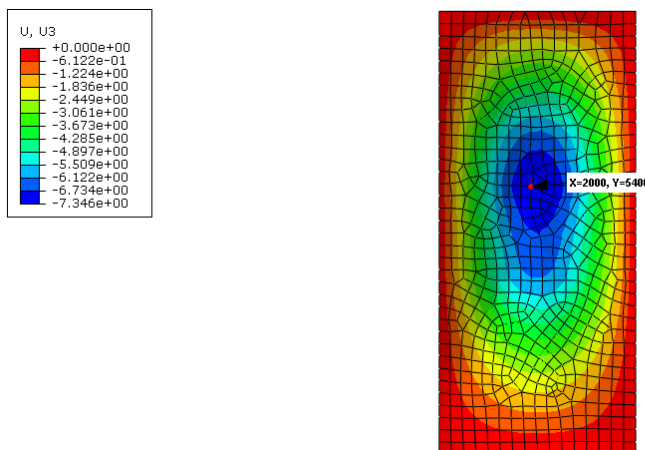
Figure 5.2   Maximum deflection point for the equivalent plate in Abaqus.

Having extracted the most the most deflected point, a new cross-section was searched out with the assistance of the optimization routine, which gave the following results (Table 5.2).

Table 5.2 Cross-section which includes the correct coordinates for the point with the maximum deflection and has been used in the continuous plates in Study 2.

	Function			Minimize w_{tot}
Optimization Results	Global deflection (for i,j=1..1) in the optimization routine	w_{tot}	mm	6,39
	Height of the core	$h_{c.ssp}$	mm	163,0
	Thickness of the upper plate	$t_{f.top}$	mm	6,5
	Thickness of the bottom plate	$t_{f.bot}$	mm	5,1
	Thickness of the core	$t_{c.ssp}$	mm	5,3
	Angle of the core	a_{ssp}	degrees	64,7
	Distance between diagonals	f_{ssp}	mm	21,6
	Engineering Constants	E_{xb}	N/mm^2	55730
		E_{yb}	N/mm^2	46170
		$G_{xy.1}$	N/mm^2	16020
		G_{xz}	N/mm^2	4470
		G_{yz}	N/mm^2	642,8
Comparison between Huga Kusten and SSE	Length between transversal beams	ΔL_{ssp}	$(L_{ssp}-L_{.HK})/L_{.HK}$	-
	Area	ΔA_{ssp}	$(A_{.ssp}-A_{.HK})/A_{.HK}$	-
	Moment of Inertia	ΔI_x	$(I_{.x.ssp}-I_{.x.HK})/I_{.x.HK}$	-59,2%
		ΔI_y	$(I_{.y.ssp}-I_{.y.HK})/I_{.y.HK}$	6,6*10^4%
	Axial Stiffness	ΔE_x	$(E_{.x.ssp}-E_{.x.HK})/E_{.x.HK}$	-
		ΔE_y	$(E_{.y.ssp}-E_{.y.HK})/E_{.y.HK}$	-2,850%
	Bending Stiffness	ΔD_x	$(D_{.x.ssp}-D_{.x.HK})/D_{.x.HK}$	-59,2%
		ΔD_y	$(D_{.y.ssp}-D_{.y.HK})/D_{.y.HK}$	6,1*10^4%
	Torsional Stiffness	ΔD_{xy}	$(D_{.xy.ssp}-D_{.xy.HK})/D_{.xy.HK}$	897,5%
	Transversal Shear Stiffness	$\Delta D_{Q.x}$	$(D_{.Q.x.ssp}-D_{.Q.x.HK})/D_{.Q.x.HK}$	409,705%

The cross-section that was created from the optimization routine was exactly the same as the previous analysis and that happened due to the fact that in none case the global deflection was exceeding the allowable limit. However, it was noticed that the maximum global deflection was smaller than the previous analysis, which happened because the analysis was run for i and j equal to 1, i.e. no iterations. Therefore an Abaqus equivalent plate was created again. The Abaqus model gave the below results.
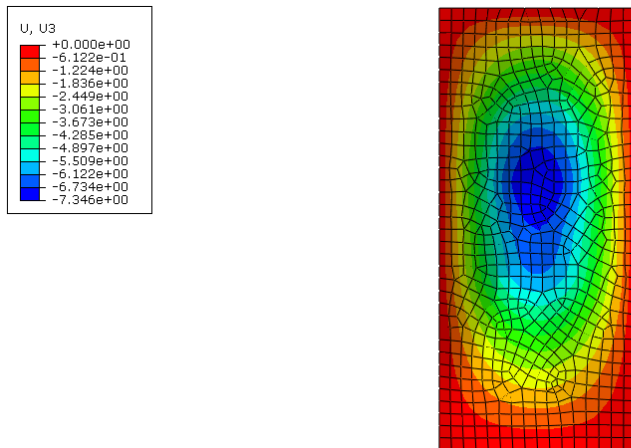
Figure 5.3   Deflection results for the analysis of the cross-section in Table 5.2.

The deflection magnitude obtained from Abaqus was 7,35mm. The difference between this value and the analytical solution had to do with the number of iterations. For an increased number of iterations the two solutions converged. The reason why in the specific study i and j were taken equal to 1 was the fact that for increased values of them the routine was becoming rather time consuming.

As described in Chapter 4.3.2, the comparison between the two decks in that point was not correct as the global deflection for the OSD was measured for a continuous beam while in the SSE was calculated for a simple supported plate. The design of a new FEM model with 5 continuous plates between the diaphragms provided the results illustrated of the Figure 5.4.
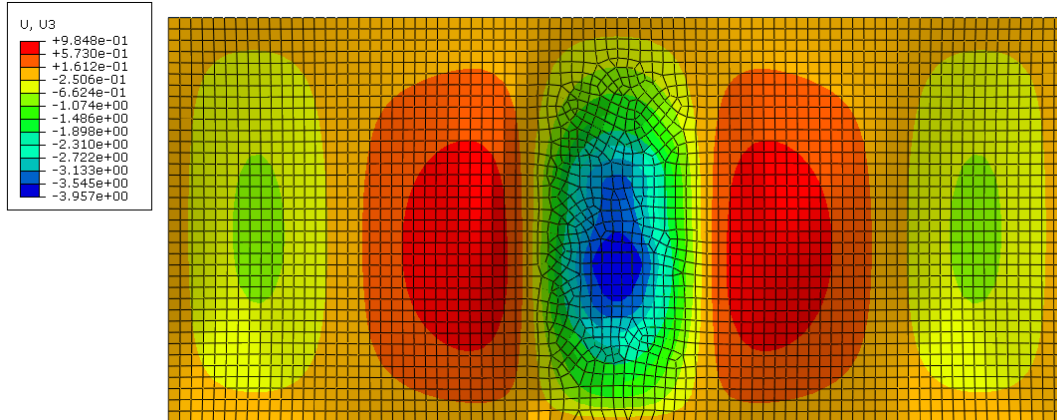
Figure 5.4   Results for deflection using the continuity of the plate in Table 5.2.

With the continuity condition, the deflection value was 3,96mm. Therefore, it was possible to construct an SSE that would have the same deflection with the orthotropic section, but less material per unit width. Another optimization routine was run in order to minimize the area of the steel sandwich element. The target of the investigation was to create a lighter element that would have the same maximum deflection with the orthotropic deck. However, to move from the simply supported plate, which was used in the optimization, to the continuous one, which was the case in reality, the ratio of the deflection for the two cases was used. Thus, the allowable deflection in the optimization was multiplied by 7,35mm/3,96mm=1,86. The results, for minimizing the total area of the steel sandwich element, were the following:

Table 5.3 Cross-section after inserting the deflection ratio due to the continuous plates in Study 2.

	Function			Minimize A_{ssp}
Optimization Results	Global deflection (for i,j=1…1) in the optimization routine	w_{tot}	mm	9,77
	Height of the core	$h_{c.ssp}$	mm	140,9
	Thickness of the upper plate	$t_{f.top}$	mm	5,7
	Thickness of the bottom plate	$t_{f.bot}$	mm	4,4
	Thickness of the core	$t_{c.ssp}$	mm	4,5
	Angle of the core	a_{ssp}	degrees	65,4
	Distance between diagonals	f_{ssp}	mm	21,5
	Engineering Constants	E_{xb}	N/mm^2	56040
		E_{yb}	N/mm^2	46660
		$G_{xy.1}$	N/mm^2	16010
		G_{xz}	N/mm^2	4353
		G_{yz}	N/mm^2	451,7
Comparison between Huga Kusten and SSE	Length between transversal beams	ΔL_{ssp}	$(L_{.ssp}-L_{.HK})/L_{.HK}$	-
	Area	ΔA_{ssp}	$(A_{.ssp}-A_{.HK})/A_{.HK}$	-13,7%
	Moment of Inertia	ΔI_x	$(I_{x.ssp}-I_{x.HK})/I_{x.HK}$	-73,5%
		ΔI_y	$(I_{y.ssp}-I_{y.HK})/I_{y.HK}$	4,3*10^4%
	Axial Stiffness	ΔE_x	$(E_{x.ssp}-E_{x.HK})/E_{x.HK}$	-13,653%
		ΔE_y	$(E_{y.ssp}-E_{y.HK})/E_{y.HK}$	-15,9%
	Bending Stiffness	ΔD_x	$(D_{x.ssp}-D_{x.HK})/D_{x.HK}$	-73,5%
		ΔD_y	$(D_{y.ssp}-D_{y.HK})/D_{y.HK}$	4,0*10^4%
	Torsional Stiffness	ΔD_{xy}	$(D_{xy.ssp}-D_{xy.HK})/D_{xy.HK}$	543,5%
	Transversal Shear Stiffness	$\Delta D_{Q.x}$	$(D_{Q.x.ssp}-D_{Q.x.HK})/D_{Q.x.HK}$	329,0%
		$\Delta D_{Q.y}$	$(D_{Q.y.ssp}-D_{Q.y.HK})/D_{Q.y.HK}$	-

The Abaqus equivalent plate from the above results had the below behaviour (Figure 5.5).
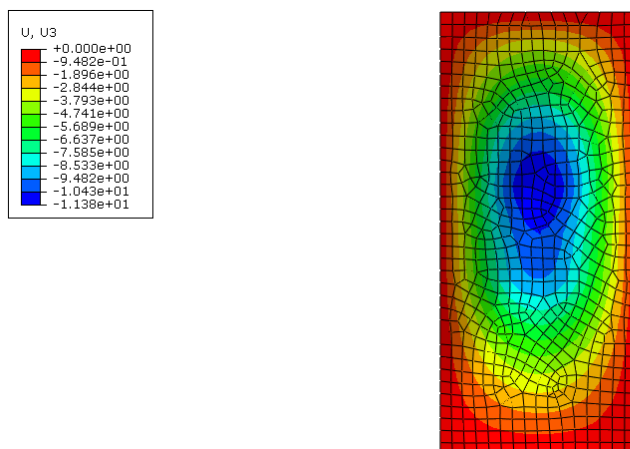
Figure 5.5   Deflection results for the cross-section presented in Table 5.3.
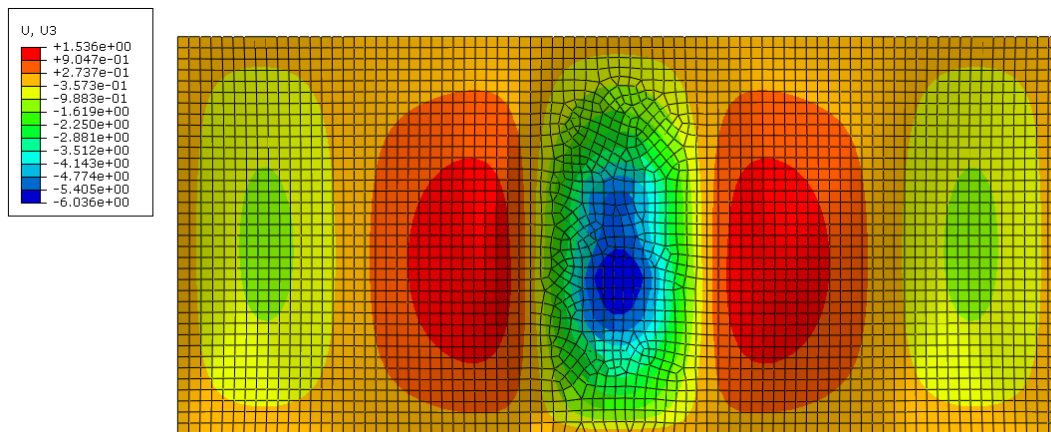
Figure 5.6   Global deflection for the SSE presented in Table 5.3 including the continuity of the plate.

The ratio between the simply supported plate and the continuous one was 11,38mm/6,04mm=1,88. This value was very similar to the obtained ratio from the previous analysis. Thus, it was assumed that the ratio remained almost the same ,independent of the different properties of the lamina plate and so it was acceptable to approve the final results.

However, the assumption that the new SSE would end up with an equal or smaller deflection than the OSD was not valid in this case, since the maximum deflection for the SSE was 6,04 mm. For that reason, a tighter constraint was set for the area per unit width and the optimization routine for minimizing the global deflection was executed again. After an iterative procedure, the below results (Table 5.4) were extracted by using the 90,55% of the initial area. The SSE was having a global deflection of 8,51mm and 5,26mm for the simply supported and the continuous plate respectively.

Table 5.4 Final cross-section after allowing a tighter constrain for the area per unit width in Study 2.

	Function			Minimize w_{tot}
Optimization Results	Global deflection (for i,j=1…1) in the optimization routine	w_{tot}	mm	8,51
	Height of the core	$h_{c.ssp}$	mm	147,7
	Thickness of the upper plate	$t_{f.top}$	mm	5,9
	Thickness of the bottom plate	$t_{f.bot}$	mm	4,6
	Thickness of the core	$t_{c.ssp}$	mm	4,8
	Angle of the core	a_{ssp}	degrees	65,2
	Distance between diagonals	f_{ssp}	mm	21,6
	Engineering Constants	E_{xb}	N/mm^2	55904
		E_{yb}	N/mm^2	46454
		$G_{xy.1}$	N/mm^2	15998
		G_{xz}	N/mm^2	4395
		G_{yz}	N/mm^2	503,4
Comparison between Huga Kusten and SSE	Length between transversal beams	ΔL_{ssp}	$(L_{.ssp}-L_{.HK})/L_{.HK}$	-
	Area	ΔA_{ssp}	$(A_{.ssp}-A_{.HK})/A_{.HK}$	-9,45%
	Moment of Inertia	ΔI_x	$(I_{x.ssp}-I_{x.HK})/I_{x.HK}$	-69,5%
		ΔI_y	$(I_{y.ssp}-I_{y.HK})/I_{y.HK}$	-9,5%
	Axial Stiffness	ΔE_x	$(E_{x.ssp}-E_{x.HK})/E_{x.HK}$	-9,45%
		ΔE_y	$(E_{y.ssp}-E_{y.HK})/E_{y.HK}$	-12,0%
	Bending Stiffness	ΔD_x	$(D_{x.ssp}-D_{x.HK})/D_{x.HK}$	-69,5%
		ΔD_y	$(D_{y.ssp}-D_{y.HK})/D_{y.HK}$	$4,6*10^4$%
	Torsional Stiffness	ΔD_{xy}	$(D_{xy.ssp}-D_{xy.HK})/D_{xy.HK}$	641,4%
	Transversal Shear Stiffness	$\Delta D_{Q.x}$	$(D_{Q.x.ssp}-D_{Q.x.HK})/D_{Q.x.HK}$	354,3%
		$\Delta D_{Q.y}$	$(D_{Q.y.ssp}-D_{Q.y.HK})/D_{Q.y.HK}$	-
Global deflection for continuous plates (Abaqus)		w_{tot}	mm	5,26
Final equivalent distributed load		q_{eq}	kPa	7,380
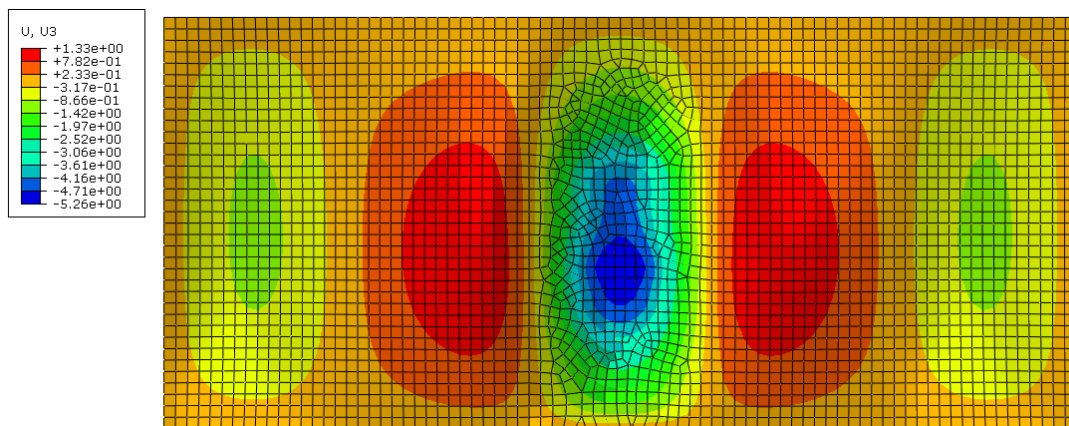
Figure 5.7   Deflection of the SSE cross-section of Table 5.4 including the continuity of the plate.

The same principle was also used in the optimization routine for minimizing the area of the SSE by setting a looser constraint for the deflection. The results were exactly the same with the above cross-section showing that the two solutions were converging to an optimum one. The Abaqus simulation for the following case is not illustrated as it is exactly the same as in the Figure 5.7. However, the table with the results is shown below.

Table 5.5 Final cross-section after allowing a looser constrain for the deflection in Study 2.

	Function			Minimize w_{tot}
Optimization Results	Global deflection (for i,j=1…1) in the optimization routine	w_{tot}	mm	8,515
	Height of the core	$h_{c.ssph.core}$	mm	147,6
	Thickness of the upper plate	$t_{f.top}$	mm	5,9
	Thickness of the bottom plate	$t_{f.bot}$	mm	4,6
	Thickness of the core	$t_{c.ssp}$	mm	4,8
	Angle of the core	a_{ssp}	degrees	65,2
	Distance between diagonals	f_{ssp}	mm	21,6
	Engineering Constants	E_{xb}	N/mm^2	55940
		E_{yb}	N/mm^2	46498
		$G_{xy.1}$	N/mm^2	16017
		G_{xz}	N/mm^2	4391
		G_{yz}	N/mm^2	505
Comparison between Huga Kusten and SSE	Length between transversal beams	ΔL_{ssp}	$(L_{.ssp}-L_{.HK})/L_{.HK}$	-
	Area	ΔA_{ssp}	$(A_{.ssp}-A_{.HK})/A_{.HK}$	-9,46%
	Moment of Inertia	ΔI_x	$(I_{x.ssp}-I_{x.HK})/I_{x.HK}$	-73,5%
		ΔI_y	$(I_{y.ssp}-I_{y.HK})/I_{y.HK}$	4,9*10^4%
	Axial Stiffness	ΔE_x	$(E_{.x.ssp}-E_{.x.HK})/E_{.x.HK}$	-9,46%
		ΔE_y	$(E_{.y.ssp}-E_{.y.HK})/E_{.y.HK}$	-11,9%
	Bending Stiffness	ΔD_x	$(D_{.x.ssp}-D_{.x.HK})/D_{.x.HK}$	-69,5%
		ΔD_y	$(D_{.y.ssp}-D_{.y.HK})/D_{.y.HK}$	4,6*10^4%
	Torsional Stiffness	ΔD_{xy}	$(D_{xy.ssp}-D_{xy.HK})/D_{xy.HK}$	641,3%
	Transversal Shear Stiffness	$\Delta D_{Q.x}$	$(D_{.Q.x.ssp}-D_{.Q.x.HK})/D_{.Q.x.HK}$	353,6%
		$\Delta D_{Q.y}$	$(D_{.Q.y.ssp}-D_{.Q.y.HK})/D_{.Q.y.HK}$	-
Global deflection for continuous plates (Abaqus)		w_{tot}	mm	5,26
Global deflection for simply supported plate (Abaqus)		w_{tot}	mm	
Final equivalent distributed load		q_{eq}	kPa	7,380

Summing up, both analyses converge to an SSE that reduces the material used by 9,45% compared with the existing bridge deck. That means that it is possible to save 2120 mm^2 of material per unit width (m). Regarding the total length of the bridge this is translated in tons of material saved. The cross-section of the new steel sandwich element is illustrated below.
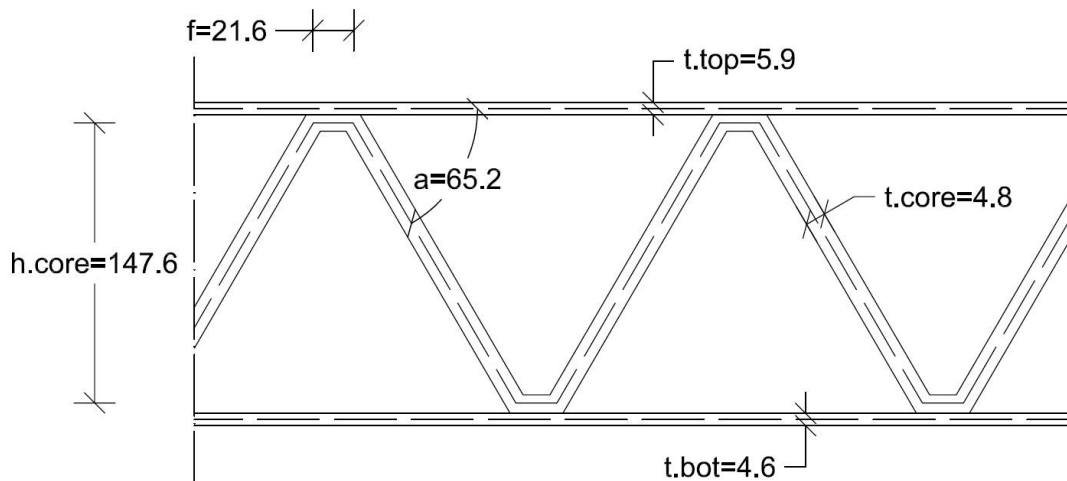
Figure 5.8 *Final cross-section of the new steel sandwich element that minimizes the material used.*

5.3 Study 3 - Minimizing the material used by adding a longitudinal stiffener

For the third scenario a longitudinal stiffener has been added under the steel sandwich element as described in chapter 4.3.3. The methodology followed was exactly the same as the previous study. The results are shown in the table and the figures below. The maximum deflection turned up in the middle of the plate, while the ratio of the simply supported plate to the continuous one was calculated equal with 4,27mm/2,40mm=1,779.

Table 5.6 Initial cross-section obtained in Study 3.

	Function			Minimize w_{tot}
Optimization Results	Global deflection (for i,j=1…1) in the optimization routine	w_{tot}	mm	6,39
	Height of the core	$h_{c.ssp}$	mm	163,0
	Thickness of the upper plate	$t_{f.top}$	mm	6,5
	Thickness of the bottom plate	$t_{f.bot}$	mm	5,1
	Thickness of the core	$t_{c.ssp}$	mm	5,3
	Angle of the core	a_{ssp}	degrees	64,7
	Distance between diagonals	f_{ssp}	mm	21,6
	Engineering Constants	E_{xb}	N/mm²	55730
		E_{yb}	N/mm²	46170
		$G_{xy.1}$	N/mm²	16020
		G_{xz}	N/mm²	4470
		G_{yz}	N/mm²	642,8
Comparison between Huga Kusten and SSE	Length between transversal beams	ΔL_{ssp}	$(L_{.ssp}-L_{.HK})/L_{.HK}$	-
	Area	ΔA_{ssp}	$(A_{.ssp}-A_{.HK})/A_{.HK}$	-
	Moment of Inertia	ΔI_x	$(I_{x.ssp}-I_{x.HK})/I_{x.HK}$	-59,2%
		ΔI_y	$(I_{y.ssp}-I_{y.HK})/I_{y.HK}$	6,6*10⁴%
	Axial Stiffness	ΔE_x	$(E_{.x.ssp}-E_{.x.HK})/E_{.x.HK}$	-
		ΔE_y	$(E_{.y.ssp}-E_{.y.HK})/E_{.y.HK}$	-2,9%
	Bending Stiffness	ΔD_x	$(D_{.x.ssp}-D_{.x.HK})/D_{.x.HK}$	-59,2%
		ΔD_y	$(D_{.y.ssp}-D_{.y.HK})/D_{.y.HK}$	6,1*10⁴%
	Torsional Stiffness	ΔD_{xy}	$(D_{xy.ssp}-D_{xy.HK})/D_{xy.HK}$	897,5%
	Transversal Shear Stiffness	$\Delta D_{Q.x}$	$(D_{.Q.x.ssp}-D_{.Q.x.HK})/D_{.Q.x.HK}$	409,7%
		$\Delta D_{Q.y}$	$(D_{.Q.y.ssp}-D_{.Q.y.HK})/D_{.Q.y.HK}$	-
Global deflection for continuous plates		w_{tot}	mm	2,40
Global deflection for simply supported plate		w_{tot}	mm	4,27
Final equivalent distributed load		q_{eq}	kPa	6,833
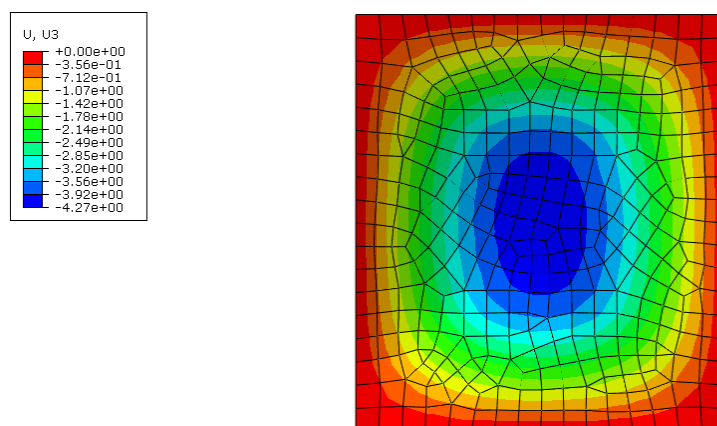
Figure 5.9   Deflection results for a simple supported SSE with the properties described in Table 5.6.
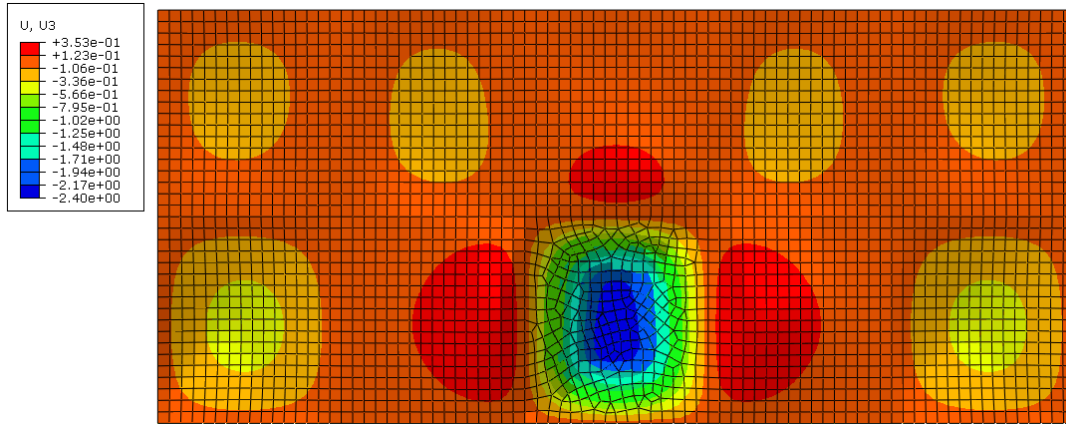
Figure 5.10   Deflection results for the continuous SS plate described in Table 5.6.

By adopting the ratio mentioned above and aiming for the same deflection as the existing orthotropic deck, which was 5,26mm, the optimization routine for minimizing the area of the material for the SSE was used.

Table 5.7 Final cross-section in Study 3.

	Function			Minimize A_{tot}
Optimization Results	Global deflection (for i,j=1..1) in the optimization routine	w_{tot}	mm	9,36
	Height of the core	$h_{c.ssp}$	mm	121,3
	Thickness of the upper plate	$t_{f.top}$	mm	5,3
	Thickness of the bottom plate	$t_{f.bot}$	mm	4,1
	Thickness of the core	$t_{c.ssp}$	mm	4,0
	Angle of the core	a_{ssp}	degrees	63,3
	Distance between diagonals	f_{ssp}	mm	20,0
	Engineering Constants	E_{xb}	N/mm²	59095
		E_{yb}	N/mm²	50292
		$G_{xy.1}$	N/mm²	17437
		G_{xz}	N/mm²	3972
		G_{yz}	N/mm²	471,8
Comparison between Huga Kusten and SSE	Length between transversal beams	ΔL_{ssp}	$(L_{ssp}-L_{.HK})/L_{.HK}$	-
	Area	ΔA_{ssp}	$(A_{ssp}-A_{.HK})/A_{.HK}$	-23,7%
	Moment of Inertia	ΔI_x	$(I_{x.ssp}-I_{x.HK})/I_{x.HK}$	-82,0 %
		ΔI_y	$(I_{y.ssp}-I_{y.HK})/I_{y.HK}$	3*10⁴%
	Axial Stiffness	ΔE_x	$(E_{x.ssp}-E_{x.HK})/E_{x.HK}$	-23,7%
		ΔE_y	$(E_{y.ssp}-E_{y.HK})/E_{y.HK}$	-21,2%
	Bending Stiffness	ΔD_x	$(D_{x.ssp}-D_{x.HK})/D_{x.HK}$	-82,0%
		ΔD_y	$(D_{y.ssp}-D_{y.HK})/D_{y.HK}$	2,8*10⁴%
	Torsional Stiffness	ΔD_{xy}	$(D_{xy.ssp}-D_{xy.HK})/D_{xy.HK}$	352,0%
	Transversal Shear Stiffness	$\Delta D_{Q.x}$	$(D_{Q.x.ssp}-D_{Q.x.HK})/D_{Q.x.HK}$	238,3%
		$\Delta D_{Q.y}$	$(D_{Q.y.ssp}-D_{Q.y.HK})/D_{Q.y.HK}$	-
Global deflection for continuous plates		w_{tot}	mm	5,22
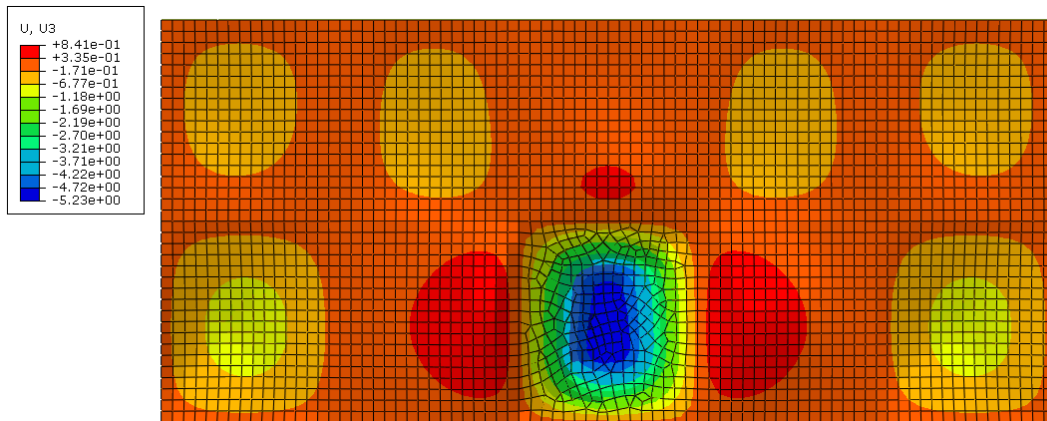
Figure 5.8   Final deflection results for the continuous SSE described in Table 5.7.

The final deflection for the continuous plate was 5,23mm, which is almost the same as the deflection of the orthotropic section. Therefore, the SSE with the above characteristics was acceptable. With the specific cross-section and configuration, about 23,7% of material could be saved. That means that a total of 5314 mm^2 of material per unit width can be saved. Of course this should be decreased by the area of the longitudinal stiffeners. To make a rough estimation, a longitudinal stiffener with profile IPE 360 was chosen as longitudinal stiffener. For details see Appendix A. This section has an area of 7270 mm^2. The total amount of material saved for the half of the width is 5314*9 = 47826 mm^2, and subtracting the area of the stiffener it end ups to 40556 mm^2 of material saved. This equals to 4506 mm^2 material per unit width or 20,1% saved material.

The final cross-section of the SSE for the 4m×4,5m plate is shown in Figure 5.12.
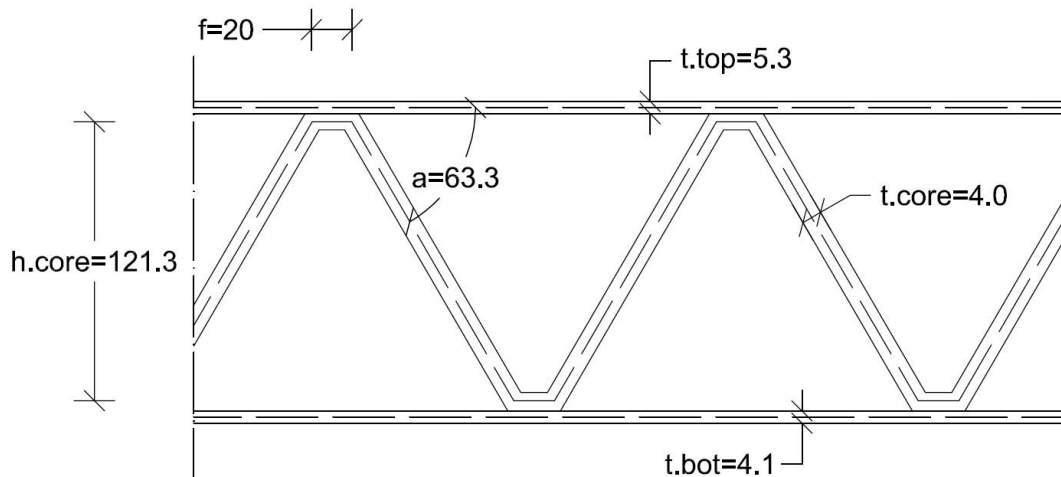
Figure 5.12   Cross-section of the new steel sandwich element.

5.4 Study 4 - Maximizing the length between the transverse stiffeners

The final study included the maximization of both the plate deflection and the length of the SSE by using again the constraints mentioned in chapters 4.1 and 4.2. The continuity of the plates was inserted again in the study with the help of Abaqus/CAE. The results from the analysis are shown below in the Table 5.8.

Table 5.8 Initial cross-section obtained in Study 4.

	Function			Max w_{tot} and L_{ssp}
Optimization Results	Length between transversal beams	L_{ssp}	m	4,64
	Height of the core	$h_{c.ssp}$	mm	162,4
	Thickness of the upper plate	$t_{f.top}$	mm	6,6
	Thickness of the bottom plate	$t_{f.bot}$	mm	5,2
	Thickness of the core	$t_{c.ssp}$	mm	5,3
	Angle of the core	a_{ssp}	degrees	64
	Distance between diagonals	f_{ssp}	mm	21,3
	Engineering constants	E_{xb}	N/mm^2	52251
		E_{yb}	N/mm^2	43718
		$G_{xy.1}$	N/mm^2	15456
		G_{xz}	N/mm^2	3984
		G_{yz}	N/mm^2	604
Comparison between Huga Kusten and SSE	Length between transversal beams	ΔL_{ssp}	$(L_{.ssp}-L_{.HK})/L_{.HK}$	16,0%
	Area	ΔA_{ssp}	$(A_{.ssp}-A_{.HK})/A_{.HK}$	-
	Moment of Inertia	ΔI_x	$(I_{x.ssp}-I_{x.HK})/I_{x.HK}$	-59,3%
		ΔI_y	$(I_{y.ssp}-I_{y.HK})/I_{y.HK}$	$6,6*10^4$%
	Axial Stiffness	ΔE_x	$(E_{.x.ssp}-E_{.x.HK})/E_{.x.HK}$	-
		ΔE_y	$(E_{.y.ssp}-E_{.y.HK})/E_{.y.HK}$	-2,0%
	Bending Stiffness	ΔD_x	$(D_{.x.ssp}-D_{.x.HK})/D_{.x.HK}$	-59,3%
		ΔD_y	$(D_{.y.ssp}-D_{.y.HK})/D_{.y.HK}$	$6,1*10^4$%
	Torsional Stiffness	ΔD_{xy}	$(D_{.xy.ssp}-D_{.xy.HK})/D_{.xy.HK}$	901,1%
	Transversal Shear Stiffness	$\Delta D_{Q.x}$	$(D_{.Q.x.ssp}-D_{.Q.x.HK})/D_{.Q.x.HK}$	402,9%
		$\Delta D_{Q.y}$	$(D_{.Q.y.ssp}-D_{.Q.y.HK})/D_{.Q.y.HK}$	-
Limit for the total deflection		L/400	mm	11,6
Global deflection for continuous plates		w_{tot}	mm	5,89

From the first analysis, it was acquired an increase in the length equal to 16%. However, the global deflection of the plate was still much smaller than the allowed limit. This happened because the optimization routine could not take into account the continuity of the plates, as mentioned before. So, a looser constraint for the global deflection was decided. Furthermore, it was observed that the maximum deflection was very close to the centre of the plate although the loading was asymmetric. The reason was that the SSE was behaving more like a plate compared with the previous studies, distributing the loads in two directions.

By setting different constraints for the simply supported case, an iterative analysis was used to get the global deflection of the continuous sandwich elements closer to the allowed limit. The final iteration gave the results presented in Table 5.9.

Table 5.9 Final cross-section from Study 4.

	Function		Max w_{tot} and,L_{ssp}	
Optimization Results	Length between transversal beams	L_{ssp}	m	7,38
	Height of the core	$h_{c.ssp}$	mm	160,3
	Thickness of the upper plate	$t_{f.top}$	mm	6,7
	Thickness of the bottom plate	$t_{f.bot}$	mm	5,4
	Thickness of the core	$t_{c.ssp}$	mm	5,3
	Angle of the core	a_{ssp}	degrees	63
	Distance between diagonals	f_{ssp}	mm	20,9
Comparison between Huga Kusten and SSE	Length between transversal beams	ΔL_{ssp}	$(L_{.ssp}-L_{.HK})/L_{.HK}$	92,9%
	Area	ΔA_{ssp}	$(A_{.ssp}-A_{.HK})/A_{.HK}$	-
	Moment of Inertia	ΔI_x	$(I_{x.ssp}-I_{x.HK})/I_{x.HK}$	-59,6%
		ΔI_y	$(I_{y.ssp}-I_{y.HK})/I_{y.HK}$	$6,6*10^4$%
	Axial Stiffness	ΔE_x	$(E_{x.ssp}-E_{x.HK})/E_{x.HK}$	-
		ΔE_y	$(E_{y.ssp}-E_{y.HK})/E_{y.HK}$	0,9%
	Bending Stiffness	ΔD_x	$(D_{x.ssp}-D_{x.HK})/D_{x.HK}$	-59,6%
		ΔD_y	$(D_{y.ssp}-D_{y.HK})/D_{y.HK}$	$6,1*10^4$%
	Torsional Stiffness	ΔD_{xy}	$(D_{xy.ssp}-D_{xy.HK})/D_{xy.HK}$	909,3%
	Transversal Shear Stiffness	$\Delta D_{Q.x}$	$(D_{Q.x.ssp}-D_{Q.x.HK})/D_{Q.x.HK}$	379,5%
		$\Delta D_{Q.y}$	$(D_{Q.y.ssp}-D_{Q.y.HK})/D_{Q.y.HK}$	-
Limit for the total deflection		L/400	mm	18,46
Global deflection for continuous plates		w_{tot}	mm	18,42
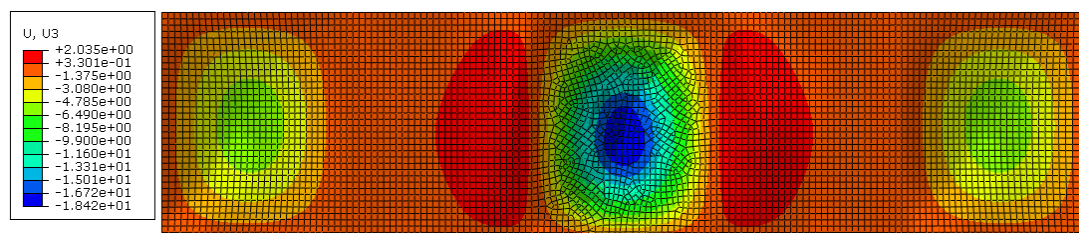
Figure 5.9   Final deflection results for the continuous SSE described in Table 5.9.

The conclusions demonstrate that the length of the bridge deck between two transversal stiffeners could be increased up to 92,9% by using steel sandwich elements for the case of the Höga Kusten bridge.

5.5 Verification of the deflection

To confirm the correspondence between the analytical calculation of deflection and the results from Abaqus/CAE, a comparison between their results was made. This was performed for a simply supported plate. For the calculation of the deflection with the analytical model the optimized section for each case is used, for 21 iterations.

Table 5.10 Difference between hand calculations and Abaqus/CAE for a bigger number of iterations.

Plate dimensions (m)	Analysis	Deflection Point X, Y	Deflection between transverse beams (mm)		Difference
			Hand calculations	Abaqus	
4x9	Part 1	2 , 4.5	6,57	6,71	2,13%
	Part 2	2 , 5.4	7,17	7,35	2,51%
	Part 3	2 , 5.4	11,00	11,24	2,21%
	Part 4	2 , 5.4	9,56	9,80	2,47%
	Part 5	2 , 5.4	9,56	9,80	2,47%

5.6 Moment and axial capacity

As mentioned, the studies performed in this work compared only by the deflection between the conventional orthotropic deck of Höga Kusten bridge and the potential steel sandwich elements in the SLS. However, any changes in the configuration of the cross-section of the bridge deck has impact on the design moment and axial load carrying capacity. Therefore, these parameters in relation with the corresponding values of the initial deck were studied. The results are summed up in the Tables 5.11 and 5.12 below, while further calculations could be found in the Appendix B. The calculations have been executed according to (EN 1993-1-1, 2005).

Table 5.11 Moment and axial capacity of the original orthotropic deck as well as the SSE created in the different studies.

Studies	Parameter	Units	Value
Orthotropic Deck of Höga Kusten Bridge	Reduction factor $x_{\rho.c}$ for column-like buckling	-	0.862
	Reduction factor $x_{\rho.pl}$ for plate-like buckling	-	1
	Total reduction factor x_ρ	-	0.886
	Moment capacity	kN×m/m	444.129
	Axial capacity	kN/m	6.718×10^3
Study 2 - Minimizing the material used	Reduction factor $x_{\rho.c}$ for column-like buckling	-	0.675
	Reduction factor $x_{\rho.pl}$ for plate-like buckling	-	0.996
	Total reduction factor x_ρ	-	0.852
	Moment capacity	kN×m/m	369.125
	Axial capacity	kN/m	6.142×10^3
Study 3 - Minimizing the material used by adding a longitudinal stiffener	Reduction factor $x_{\rho.c}$ for column-like buckling	-	0.58
	Reduction factor $x_{\rho.pl}$ for plate-like buckling	-	1
	Total reduction factor x_ρ	-	0.76
	Moment capacity	kN×m/m	263.657
	Axial capacity	kN/m	4.62×10^3
Study 4 - Maximizing the length between the transverse stiffeners	Reduction factor $x_{\rho.c}$ for column-like buckling	-	0.719
	Reduction factor $x_{\rho.pl}$ for plate-like buckling	-	0.872
	Total reduction factor x_ρ	-	0.62
	Moment capacity	kN×m/m	450.696
	Axial capacity	kN/m	4.937×10^3

Table 5.12 Comparison between the moment and axial carrying capacity between the initial orthotropic bridge deck and the SSEs.

Comparison of the moment and axial capacities of the different studies with the initial orthotropic bridge deck			
Studies	**Parameter compared**	**Formula**	**Value**
Study 2 - Minimizing the material used	Moment capacity M_{Rd}	$(M_{Rd.ssp1} - M_{Rd}) / M_{Rd}$	- 16.888%
	Axial capacity N_{Rd}	$(N_{Rd.ssp1} - N_{Rd}) / N_{Rd}$	- 8.564%
Study 3 – Minimizing the material used by adding a longitudinal stiffener	Moment capacity M_{Rd}	$(M_{Rd.ssp2} - M_{Rd}) / M_{Rd}$	-40.635%
	Axial capacity N_{Rd}	$(N_{Rd.ssp2} - N_{Rd}) / N_{Rd}$	- 31.222%
Study 4 – Maximizing the length between the transverse stiffeners	Moment capacity M_{Rd}	$(M_{Rd.ssp3} - M_{Rd}) / M_{Rd}$	1.479%
	Axial capacity N_{Rd}	$(N_{Rd.ssp3} - N_{Rd}) / N_{Rd}$	- 26.504%

However, the carrying capacity of the newly generated SSEs would only have meaning if it was directly connected to the loading of the deck. And that is due to the fact that changes in the dimensions of the plates in the different studies would affect the acting moment on the bridge deck. Therefore, in every study performed the acting moment has been extracted in order to calculate the utilization factor with the assistance of Abaqus/CAE. Figures 5.14-16 and table 5.13 show the values of the moment in every scenario, while table 5.14 demonstrate the respective utilization factors. Furthermore, the acting moment of every optimized model was compared to their bending capacity, see tables 5.13 and 5.14.

Table 5.13 Acting moment in the different scenarios.

Studies	**Parameter compared**	**Notation**	**Value (kNm/m)**
Study 2 - Minimizing the material used	Acting moment $M_{Ed.ssp1}$	$M_{Ed.ssp1}$	76.20
Study 3 – Minimizing the material used by adding a longitudinal stiffener	Acting moment $M_{Ed.ssp2}$	$M_{Ed.ssp2}$	50.20
Study 4 – Maximizing the length between the transverse stiffeners	Acting moment $M_{Ed.ssp3}$	$M_{Ed.ssp3}$	139.40
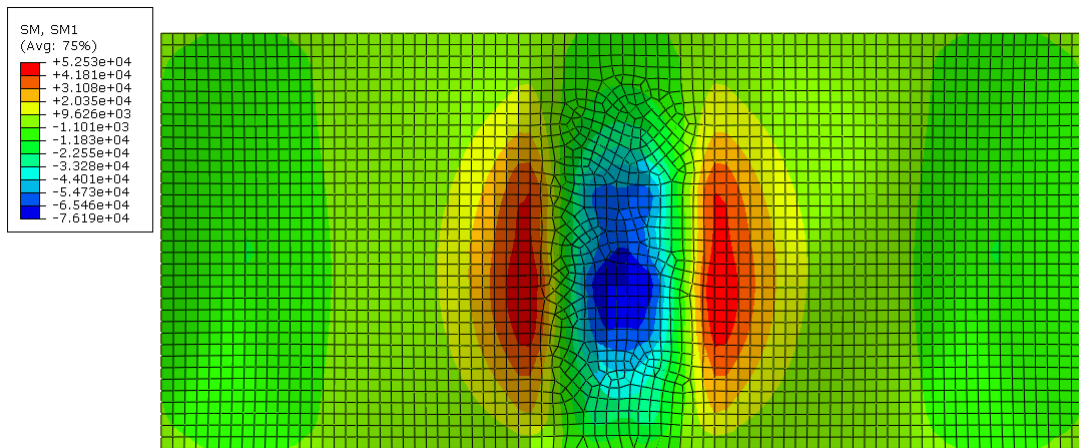
Figure 5.10   Acting moment (76.20 kNm/m) in Study 2.
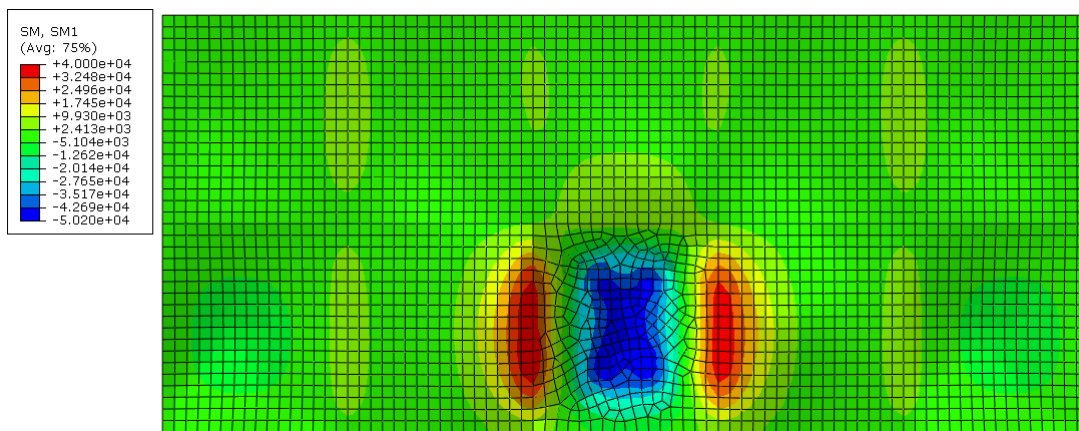
Figure 5.11   Acting moment (50.20 kNm/m) in Study 3.
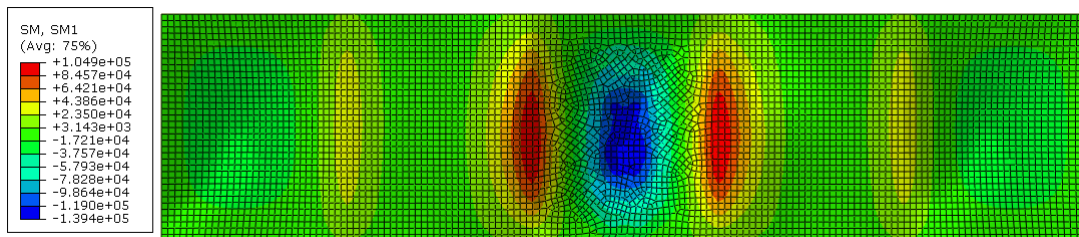
Figure 5.126   Acting moment (139.4 kNm/m) in Study 4.

Table 5.144 Utilization factor for the moment capacity in the different scenarios.

Calculation of the utilization factors for the moment capacities of the different studies with the initial orthotropic bridge deck			
Studies	**Parameter compared**	**Formula**	**Value**
Study 2 - Minimizing the material used	Utilization factor for the moment capacity $u_{M.ssp1}$	$M_{Ed.ssp1} / M_{Rd.ssp1}$	0.206
Study 3 – Minimizing the material used by adding a longitudinal stiffener	Utilization factor for the moment capacity $u_{M.ssp2}$	$M_{Ed.ssp2} / M_{Rd.ssp2}$	0.19
Study 4 – Maximizing the length between the transverse stiffeners	Utilization factor for the moment capacity $u_{M.ssp3}$	$M_{Ed.ssp3} / M_{Rd.ssp3}$	0.309

6 Discussion

The purpose of this Master thesis project was the investigation of how effective the steel sandwich elements may be, when they were utilized as part of the stiffening girder of a suspension bridge. The study was performed in the serviceability limit state. The results showed that in almost all the scenarios studied, steel sandwich decks may reduce significantly the amount of steel used for the bridging of long spans compared with convectional solutions. In the following sub-chapters there is a discussion about the results that the different optimization routines produced.

6.1 Study 1 - Maximization of the moment of inertia in the longitudinal direction

In the first case, the optimization aimed to maximize the moment of inertia in the longitudinal direction. However, the results showed a significant lower moment of inertia compared to the orthotropic steel deck. Taking into consideration the fact that the superior property of the orthotropic deck is the moment of inertia in the longitudinal direction and that the original OSD was quite slender - web in class 4 -, the result seemed to be reasonable.

6.2 Study 2 - Minimization of the material used

The second case which was examined was an attempt to minimize the material used in the cross-section by restraining the deflection of the upper flange of the box girder between the transverse beams in the optimization routine. In this scenario the fact that in the first attempt the deflection between transverse beams was smaller when using sandwich elements than with the OSD led to a sub-study to investigate the possible reduction of the area per unit width, if the original section was replaced by an SSE and the deflection remained constant. The 10% in material reduction was absolutely an amount that could not be unnoticed especially in so large scale constructions like cable bridges. The main reason for this result was the two-way plate behaviour of the SSE compared with the OSD. This could also conclude, apart from the main deck, to a chain material deduction in almost all the parts of the bridge like the hangers, the main cables and the pylons, as the self-weight of the bridge deck would be decreased.

6.3 Study 3 - Minimizing the material used by adding a longitudinal stiffener

Another study was conducted to investigate the behaviour of the sandwich section when the geometry of the bridge tended to be more square-shaped. In this scenario it was assumed that in the half of the bridge deck a longitudinal stiffener was added, resulting in smaller almost square plates. The deflection between the transverse beams was again equal to the one of the orthotropic section, whilst the area per unit width was reduced as much as possible. The results here was a reduction of the area of about 23%, and with a rough calculation for the dimensions of the longitudinal stiffener it was advantageous compared to the first investigation. However, the reader should keep in mind that this solution may increase the cost, as well as the production time, due to the increased and more complicated welding.

6.4 Study 4 - Maximizing the length between the transverse stiffeners

In this case the aim was to increase the distance between the transverse beams, in order to be able to decrease their number and save material that way. This was done by maximizing the allowable deflection between the transverse beams up to the limit value, which is the length divided by 400. The results showed that using sandwich elements could result in a significant increment of the length between transverse beams. Particularly the length could be increased by 92.9%, which resulted to plates 7.38 m long and 9 m wide in the Höga Kusten bridge case. The logic behind that was that the bridge deck was allowed to maximize itself its length keeping the width constant and thus take the most optimum shape depending on its stiffness constants.

7   Conclusions

In this master thesis project, the possibility of replacing conventional orthotropic steel decks with a steel sandwich bridge deck was investigated with respect to serviceability limit state. The results of the different studies conducted is encouraging and allow the further research of the topic.

In general, the concluding remarks from this project could be summed up the following:

- The utilization of SSE bridge decks could result in smaller deflections between the transverse beams compared to conventional orthotropic decks.

- With equal bending stiffness, the SSE utilizes less material compared to the convectional solutions. Width to length aspect ratios close to 7 was shown to increase the effectiveness of the SSE bridge deck.

- The distance between transverse beams could be increased when using SSE compared to the convectional solutions. Therefore, material could be saved from the reduction of the number of the transverse stiffeners.

- As far as the bending moment capacity of the newly created SSEs is concerned, it was proven that the SSEs had quite lower bending stiffness compared with the original OSD due to their smaller total height. However, the Abaqus/CAE analysis had proven also that the bending moment acting on the SSEs would have also a lower value as their plate behaviour distributed the stresses with a more efficient two-way action.

8   References

Allen, H. G. (1969): *Analysis and Design of Structural Sandwich Panels. Analysis and Design of Structural Sandwich Panels*. Pergamon Press. http://doi.org/10.1016/B978-0-08-012870-2.50011-0

Alwan, U., & Järve, D. (2012): *New Concept for Industrial Bridge Construction*. M.Sc. Thesis, Department of Structural Engineering, Chalmers University of Technology, Publication no. 2012:110, Göteborg, Sweden.

Banck, F., & Almberg, O. R. (2014). *Application of CFRP Cables in Super Long Span Cable Supported Bridges*. M.Sc. Thesis, Department of Structural Engineering, Chalmers University of Technology, Publication no. 2014:95, Göteborg, Sweden.

Beneus, E., & Koc, I. (2014). *Innovative road bridges with steel sandwich decks*. M.Sc. Thesis, Department of Structural Engineering, Chalmers University of Technology, Publication no. 2014:138, Göteborg, Sweden.

Billington, C. J., Chapman, J. C., Dowling, P. J., & Lim, P. T. K. (1971). *The structural behaviour of steel and concrete box girder bridges*, *49*(3), 111–120.

Chang, W. S., Ventsel, E., Krauthammer, T., & John, J. (2004). Bending behavior of corrugated-core sandwich plates. *Composite Structures*, *70*(1), 81–89. http://doi.org/10.1016/j.compstruct.2004.08.014

Chang, W.-S. (2004). *Elasto-Plastic Analysis of Corrugated Sandwich Steel Panels*. The Pennsylvania State University.

Chatterjee, S. (2003). *The Design of Modern Steel Bridges*. *Blackweel Science* (Second Edi). Blackweel Science. http://doi.org/10.1002/9780470774373

Chen, W.-F., & Duan, L. (2014). *Bridge Engineering Handbook* (2nd ed.).

Chen, Y. S., & Yen, B. T. (n.d.). *Analysis of Composite Box Girders* (Vol. 12). Fritz Engineering Laboratory.

Djubek, J., Kondar, R., & Skaloud, M. (1983). Limit State of the Plate Elements of Steel Structures (pp. 220–255).

EN 1993-2:2006. (2011). *Eurocode 3: Design of steel structures - Part 2: Steel bridges*.

EN1991-2. (2010). Eurocode 1: *Actions on structures - Part 2: Traffic loads on bridges*.

EN 1993-1-1. (2005). *Eurocode 3: Design of steel structures - Part 1-1: General rules and rules for buildings*.

Feldmann, M., Sedlacek, G., & Geßler, a. (2007). A system of steel-elastomer sandwich plates for strengthening orthotropic bridge decks. *Mechanics of Composite Materials*, *43*(2), 183–190. http://doi.org/10.1007/s11029-007-0018-y

Finley, J. (1810). The Portfolio - The Chain Bridge.

Gimsing, N., & Georgakis, C. (2012). *Cable Supported Bridges: Concept and Design*. *Wiley* (Vol. 27). Wiley. http://doi.org/10.1016/j.jfluidstructs.2011.04.006

Guohao, L. (1987). *Analysis of Box Girder and Truss Bridges*. China Academic Pubilshers. Retrieved from http://gjgcb.sirt.edu.cn/UploadFile/ZL/F1/Analysis of Box Girder and Truss Bridges.pdf

Hambly, E. C. (1991). *Bridge Deck Behaviour* (2nd ed.). E & FN SPON.

Helwig, T., Yura, J., Herman, R., Williamson, E., & Li, D. (2007). *Design Guidelines For Steel Trapezoidal Box Girder Systems* (Vol. 7).

Institute for Steel Development & Growth. (1999). *Beams subjected to torsion and bending*.

Kennedy, D. J. L., Dorton, R. A., & Alexander, S. D. B. (2002). *The Sandwich Plate System For Bridge Decks*.

Kolsters, H., & Wennhage, P. (2009). Optimisation of laser-welded sandwich panels with multiple design constraints. *Marine Structures*, *22*(2), 154–171. http://doi.org/10.1016/j.marstruc.2008.09.002

Kujala, P., & Klanac, A. (2005). Steel sandwich panels in marine applications. *Brodogradnja*, *56*, 305–314.

Lebet, J.-P., & Hirt, M. (2013). *Steel Bridges Conceptual and Structural Design of Steel and Steel-Concrete Composite Bridges Title*. EPFL Press.

Libove, C., & Hubka, R. E. (1951). Elastic Constants for Corrugated-Core Sandwich Plates. *NACA TECHNICAL NOTE 2289*.

Lok, T.-S., & Cheng, Q.-H. (2000). Analysis of Sandwich Panel as a 2-D Orthotropic Thick Plate Continuum. *International Offshore and Polar Engineering Conference*, *IV*, 110–115.

US Department of Transportation, U. S. D. (2012). Steel Bridge Design Handbook Structural Behavior of Steel.

Peter, W. (1987). The significance of warping torsion in the design of straight concrete box-girder bridges.

Peters, T. F. (1980). The first wire suspension bridge : Geneva 1823, 7.

Roman, W. (1963). Design Manual for Orthotropic Steel Plate Deck Bridges. American Institute of Steel Construction.

Romanoff, J. (2007). *Bending Response of Laser-Welded Web-Core Sandwich Plates*. Helsinki University of Technology. http://doi.org/10.1016/j.compstruct.2006.08.021

Romanoff, K., & Kujala, P. (2002). Formulation for the strength analysis of all steel sandwich panels.

Ronald, F., Manzon, L., Kujala, P., Brede, M., & Weitzenböck, J. (2004). Advanced joining techniques in European shipbuilding. *Journal of Ship Production*, *20*(3), 200–210.

Sir William Fairbairn. (1849). *An Account of the Construction of the Britannia and Conway Tubular Bridges, with a Complete History of their Progress*. John Weale.

Timoshenko, S., & Woinowsky-Krieger, S. (1989). *Theory of Plates and Shells* (Second Edi). McGraw-Hill Book Company.

Troitsky, M. S. (1968). *Orthotropic Bridges : Theory and Design*.

US Department of Transportation. (2012a). Manual for Design, Construction and Maintenance of Orthotropic Steel Deck Bridges.

US Department of Transportation. (2012b). Steel Bridge Design Handbook Structural Behavior of Steel.

Wai-Fah, C., & Lian, D. (2014). *Bridge Engineering Handbook, Construction and Maintenance. CRC Press* (Second Edi). CRC Press.

Waldron, P. (1988). The significance of warping torsion in the design of straight concrete box girder bridges. *Canadian Journal of Civil Engineering*, *15*(5).

Xanthakos, P. P. (1993). *Theory and Design of Bridges* (1st ed.). John Willey & Sons.

Xu, Y. L., & Xia, Y. (2011). *Structural Health Monitoring of Long-Span Suspension Bridges*.

Yilmaz, C., & Wasti, S. T. (1984). *Analysis and Design of Bridges*. NATO ASI Series.

9   Appendix A

Material Properties

$\nu := 0.3$ — Poisson's ratio

$\rho_{S355N} := 7850 \dfrac{kg}{m^3}$ — Density of steel

$E_{S355N} := 210 GPa$ — Modulus of elasticity

$G_c := \dfrac{E_{S355N}}{2 \cdot (1 + \nu)} = 80.769 \cdot GPa$ — Shear modulus of elasticity

$f_y := 355 MPa$ — Yielding strength

$\varepsilon := \sqrt{\dfrac{235 MPa}{f_y}} = 0.814$

$\gamma_{M0} := 1 \qquad \gamma_{M1} := 1$ — Safety factors

$t_{cover} := 50 mm$ — Thickness of the asphalt cover

$a_d := 23 \dfrac{kN}{m^3}$ — Asphalt density, according with Traffikverket_Bro_2011, pg. 45

Höga Kusten Bridge

Parameters need to be inserted - All the dimensions are measured from the centre lines (when this does not happen it is clearly stated)

Whole bridge

$l_{long.stif} := 4m$ — Length of longitudinal stiffeners between vertical stiffeners

$h_{box} := 3.782m$ — Height of the box girder cross section

Top flange

$\alpha_{HK.f.top} := atan\left(\dfrac{2.5}{100}\right) = 1.432 \cdot deg$ — Angle for the slope of the top flange

$t_{HK.f.top} := 12mm$ — Plate thickness in top flange

$l_{HK.f.top.hor} := 18.4m$ — Horizontal length of the top flange

$b_{HK.f.top} := 600mm$ — Distance between top ribs

$y_{HK.f.top} := 3.897m$ — Mean distance between the inclined top and the horizontal bottom flange

Whole box-girder cross-section
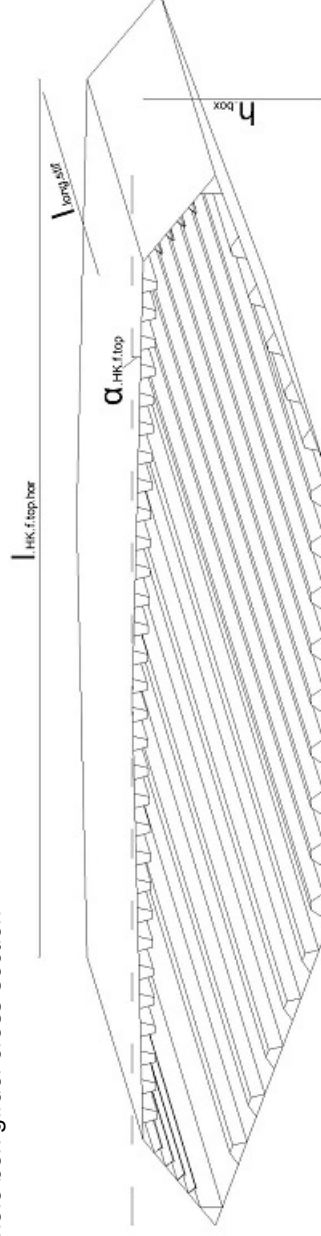
Cross-section of the top ribs
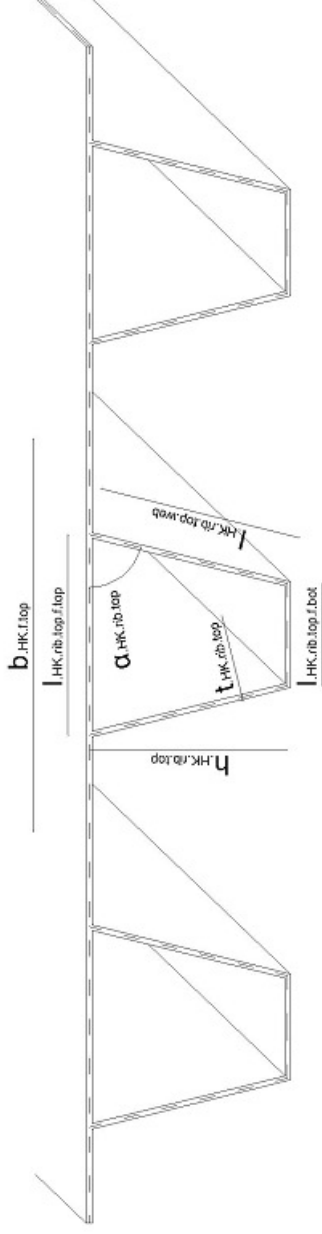
Top ribs

$t_{HK.rib.top} := 8mm$ Thickness of the top ribs

$l_{HK.rib.top.f.top} := 306.2mm$ Distance between rib webs at the top

$l_{HK.rib.top.f.bot} := 156.3mm$ Distance between rib webs at the bottom

$h_{HK.rib.top} := 304mm$ Vertical height of the ribs

$n_{HK.rib.top} := 30$ Number of top ribs

$y_{HK.n.rib.top} := 3.7177m$

Top webs

$t_{HK.web.top} := 12mm$ Plate thickness of the top webs

$l_{HK.web.top.hor} := 1.8m + \dfrac{t_{HK.web.top}}{2} = 1.806\,m$ Horizontal length of the top webs

$h_{HK.web.top} := 1.52m + \dfrac{t_{HK.f.bot}}{2} = 1.526\,m$ Vertical length of the top webs

$y_{HK.web.top} := 3.019m$ Mean distance between the inclined top ribs and the horizontal bottom flange

Side stiffeners

$n_{HK.sid.stif} := 8$

Number of side stiffeners

$A_{HK.sid.stif} := 0.0024m^2$

Area of each side stiffener

$y_{HK.sid.stif} := 3.0913m$

Mean distance between the inclined side stiffeners and the horizontal bottom flange

Side stiffening plate

$t_{HK.sid.pl} := 12mm$

Thickness of side plate

$l_{HK.sid.pl} := 468.4mm$

Length of side plate

$y_{HK.sid.pl} := 2.3461m$

Distance between the side plates and the horizontal bottom flange

Webs of the box-girder cross-section
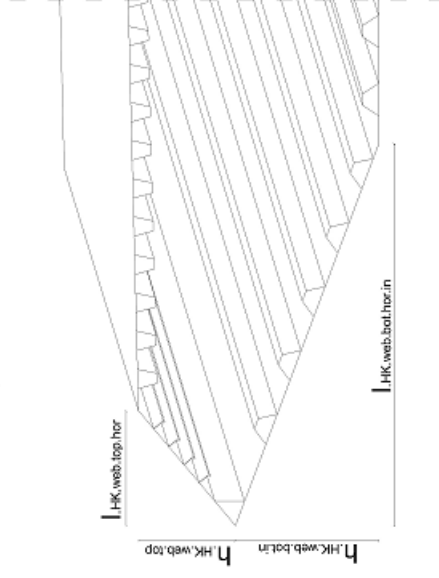
Inclined bottom webs

$t_{HK.web.bot.in} := 12mm$

Thickness of the inclined bottom plates including the webs

$l_{HK.web.bot.hor.in} := 6m + \dfrac{t_{HK.web.bot.in}}{2} = 6.006\,m$

Horizontal length of the inclined bottom plates including the webs

$h_{HK.web.bot.in} := 2250mm + \dfrac{t_{HK.f.bot}}{2} = 2.256\,m$

Vertical length of the inclined bottom plates including the webs

$y_{HK.web.bot.in} := 1.128\,m$

Mean distance between the inclined bottom plates and the horizontal bottom flange

Cross-section of the bottom ribs

Bottom flange

$t_{HK.f.bot} = 12mm$

Plate thickness of the bottom flange

$l_{HK.f.bot} := 10m$

Horizontal length of the bottom flange

Bottom ribs

$t_{HK.rib.bot} := 8mm$ Thickness of the bottom ribs

$l_{HK.rib.bot.f.top} := 174.3mm$ Distance between the rib webs at the top

$l_{HK.rib.bot.f.bot} := 507.4mm$ Distance between rib webs at the bottom

$h_{HK.rib.bot} := 254mm$ Vertical height of the ribs

$n_{HK.rib.bot.in} := 10$ Number of inclined bottom ribs

$b_{HK.f.bot} := 1075mm$ Distance between bottom ribs

$y_{HK.n.rib.bot.in} := 1.0769m$ Mean distance between the inclined bottom ribs and the horizontal bottom flange

$n_{HK.rib.bot} := 9$ Number of horizontal bottom ribs

$y_{HK.n.rib.bot} := 0.155m$ Distance between the horizontal bottom ribs and the horizontal bottom flange

Parameters extracted by themselves

Top flange

$$l_{HK.f.top} := 2\left(\frac{\frac{l_{HK.f.top.hor}}{2}}{\cos(\alpha_{HK.f.top})} \right) = 18.406\,m$$ Inclined length of the compressive flange

$$l_{HK.f.top.end} := \frac{\left(l_{HK.f.top} - n_{HK.rib.top} \cdot b_{HK.f.top}\right)}{2}$$

$l_{HK.f.top.end} = 0.203\,m$ Inclined length of the end parts in the top flanges

Top ribs

$$\alpha_{HK.rib.top} := atan\left[\cfrac{h_{HK.rib.top}}{\left(\cfrac{l_{HK.rib.top.f.top} - l_{HK.rib.top.f.bot}}{2}\right)}\right]$$

Angle of the inclined webs of the top ribs

$$\alpha_{HK.rib.top} = 76.15 \cdot deg$$

$$l_{HK.rib.top.web} := \cfrac{h_{HK.rib.top}}{\sin\left(\alpha_{HK.rib.top}\right)} = 0.313\,m$$

Inclined length of the top rib webs

Top webs

$$\alpha_{HK.web.top} := atan\left(\cfrac{h_{HK.web.top}}{l_{HK.web.top.hor}}\right) = 40.197 \cdot deg$$

Angle of the top inclined webs of the cross section

$$l_{HK.web.top} := \cfrac{h_{HK.web.top}}{\sin\left(\alpha_{HK.web.top}\right)} = 2.364\,m$$

Inclined length of the top webs

Bottom inclined webs

$$\alpha_{HK.web.bot.in} := atan\left(\cfrac{h_{HK.web.bot.in}}{l_{HK.web.bot.hor.in}}\right) = 20.587 \cdot deg$$

Angle of the bottom inclined webs of the cross section

$$l_{HK.web.bot.in} := \cfrac{h_{HK.web.bot.in}}{\sin\left(\alpha_{HK.web.bot.in}\right)} = 6.416\,m$$

Inclined length of the bottom webs

Bottom ribs

$$\alpha_{HK.rib.bot} := atan\left[\cfrac{h_{HK.rib.bot}}{\left(\cfrac{l_{HK.rib.bot.f.bot} - l_{HK.rib.bot.f.top}}{2}\right)}\right]$$

Angle of the inclined webs of the top ribs

$$\alpha_{HK.rib.bot} = 56.747 \cdot deg$$

$$l_{HK.rib.bot.web} := \cfrac{h_{HK.rib.bot}}{\sin\left(\alpha_{HK.rib.bot}\right)} = 0.304\,m$$

Inclined length of the bottom rib webs

Bottom flange

$$l_{HK.f.bot.end} := \frac{\left[l_{HK.f.bot} - \left(n_{HK.rib.bot} - 1 \right) \cdot b_{HK.f.bot} \right]}{2}$$

$$l_{HK.f.bot.end} = 0.7\,m$$

Length of the end parts in the bottom flange

▼ Areas of the cross section

Top flange

$$A_{HK.f.top} := l_{HK.f.top} \cdot t_{HK.f.top} = 0.221 \, m^2$$

Total area of the top plate

Top ribs

$$A_{HK.rib.top} := t_{HK.rib.top} \cdot \left(2 \cdot l_{HK.rib.top.web} + l_{HK.rib.top.f.bot}\right)$$

$$A_{HK.rib.top} = 6.26 \times 10^3 \cdot mm^2$$

Area of each top rib

$$A_{HK.n.rib.top} := n_{HK.rib.top} \cdot A_{HK.rib.top} = 0.188 \, m^2$$

Total area of the top ribs

Top webs

$$A_{HK.web.top} := 2 \cdot t_{HK.web.top} \cdot l_{HK.web.top} = 0.057 \, m^2$$

Total area of the top webs

Side stiffeners

$$A_{HK.n.sid.stif} := n_{HK.sid.stif} \cdot A_{HK.sid.stif} = 0.019 \, m^2$$

Total area of the side stiffeners

Side stiffening plate

$$A_{HK.sid.pl} := 2 \cdot t_{HK.sid.pl} \cdot l_{HK.sid.pl} = 0.011 \, m^2$$

Total area of the side stiffening plates

Inclined bottom webs

$$A_{HK.web.bot.in} := 2 \cdot t_{HK.web.bot.in} \cdot l_{HK.web.bot.in} = 0.154 \, m^2$$

Total area of the inclined bottom webs

Bottom flange

$$A_{HK.f.bot} := l_{HK.f.bot} \cdot t_{HK.f.bot} = 0.12 \, m^2$$

Total area of the bottom flange

Bottom ribs

$$A_{HK.rib.bot} := t_{HK.rib.bot} \cdot \left(2 \cdot l_{HK.rib.bot.web} + l_{HK.rib.bot.f.top}\right)$$

$$A_{HK.rib.bot} = 6.254 \times 10^3 \cdot mm^2$$

Area of each bottom rib

$$A_{HK.n.rib.bot.in} := n_{HK.rib.bot.in} \cdot A_{HK.rib.bot} = 0.063 \, m^2$$

Total area of the inclined bottom ribs

$$A_{HK.n.rib.bot} := n_{HK.rib.bot} \cdot A_{HK.rib.bot} = 0.056 \, m^2$$

Total area of the bottom ribs

Top compression flange

Total area of each unit

$$A_{HK.unit.ortho.x} := b_{HK.f.top} \cdot t_{HK.f.top} + t_{HK.rib.top} \cdot \left(2 \cdot l_{HK.rib.top.web} + l_{HK.rib.top.f.bot}\right)$$

$$A_{HK.unit.ortho.x} = 0.013 \, m^2$$

Total area of each unit

$$A_{HK.ortho.x} := \frac{A_{HK.unit.ortho.x}}{b_{HK.f.top}} = 0.022 \, m$$

Total area of the units per unit width

Bottom compression flange

Total area of each unit

$$A_{HK.unit.ortho.bot.x} := b_{HK.f.bot} \cdot t_{HK.f.bot} + t_{HK.rib.bot} \cdot \left(2 \cdot l_{HK.rib.bot.web} + l_{HK.rib.bot.f.top}\right)$$

$$A_{HK.unit.ortho.bot.x} = 0.019 \, m^2$$

Total area of each unit

$$A_{HK.ortho.bot.x} := \frac{A_{HK.unit.ortho.bot.x}}{b_{HK.f.bot}} = 0.018 \, m$$

Total area of the units per unit width

Total area of the cross-section

$$A_{HK.tot} := A_{HK.f.top} + A_{HK.n.rib.top} + A_{HK.web.top} + A_{HK.n.sid.stif} + A_{HK.sid.pl} + A_{HK.web.bot.in} + A_{HK.f.bot} + A_{HK.n.rib.bot.in} + A_{HK.n.rib.bot}$$

$$A_{HK.tot} = 0.889\,m^2$$

Total area of the cross-section

Gravity centres

Gravity centre of ribs

Top ribs without the top flange (distance from the bottom of the ribs)

$$z_{rib.top} := \frac{2 \cdot I_{HK.rib.top.web} \cdot t_{HK.rib.top} \cdot \dfrac{h_{HK.rib.top}}{2}}{A_{HK.rib.top}} = 0.122\,m$$

Then, y.HK.n.rib.top is added from the drawings due to the inclination in the top flange

Bottom ribs without the bottom flange (distance from the top of the ribs)

$$z_{rib.bot} := \frac{\left(2 \cdot I_{HK.rib.bot.web} \cdot t_{HK.rib.bot} \cdot \dfrac{h_{HK.rib.bot}}{2}\right)}{\left(A_{HK.rib.bot}\right)} = 0.099\,m$$

Then, y.HK.n.rib.bot is added

Gravity centre of the section (distance from the bottom flange)

$$z_{na} := \frac{\begin{aligned}&A_{HK.f.top} \cdot y_{HK.f.top} + A_{HK.n.rib.top} \cdot y_{HK.n.rib.top} + A_{HK.web.top} \cdot y_{HK.web.top} + A_{HK.n.sid.stif} \cdot y_{HK.sid.stif} \cdots\\ &+ A_{HK.sid.pl} \cdot y_{HK.sid.pl} + A_{HK.web.bot.in} \cdot y_{HK.web.bot.in} + A_{HK.n.rib.bot.in} \cdot y_{HK.n.rib.bot.in} + A_{HK.n.rib.bot} \cdot y_{HK.n.rib.bot}\end{aligned}}{A_{HK.tot}} = 2.325\,m$$

Neutral axis of each top rib included the corresponding flange plate (distance from the centre of the bottom flange of the rib)

$$z_c := \frac{2 \cdot \dfrac{h_{HK.rib.top}}{2} \cdot l_{HK.rib.top.web} \cdot t_{HK.rib.top} + b_{HK.f.top} \cdot t_{HK.f.top} \cdot h_{HK.rib.top}}{A_{HK.rib.top} + b_{HK.f.top} \cdot t_{HK.f.top}} = 0.219\,m$$
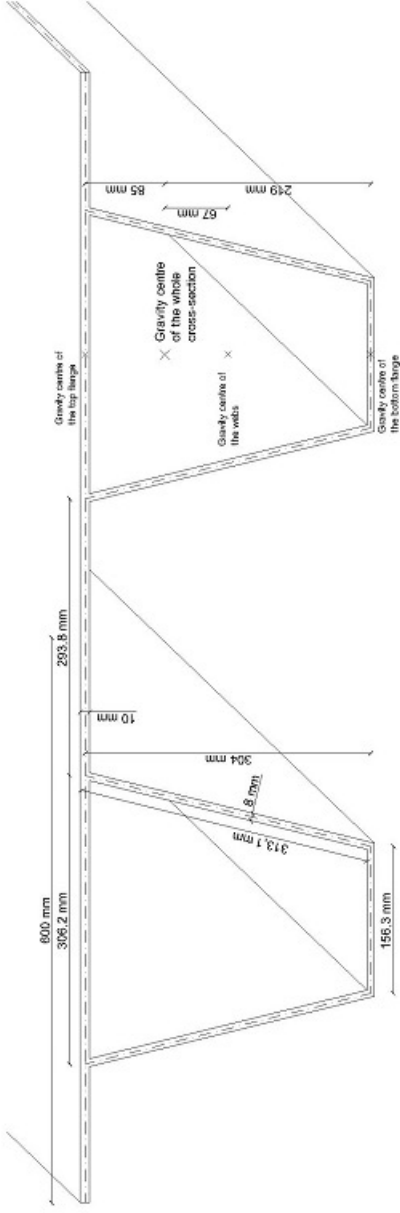
Cross Section of Two Units

Gravity centre of the top flange

× Gravity centre of the whole cross-section

× Gravity centre of the webs

Gravity centre of the bottom flange

85 mm
249 mm
67 mm

293.8 mm

10 mm

304 mm

8 mm

313.1 mm

156.3 mm

600 mm
306.2 mm
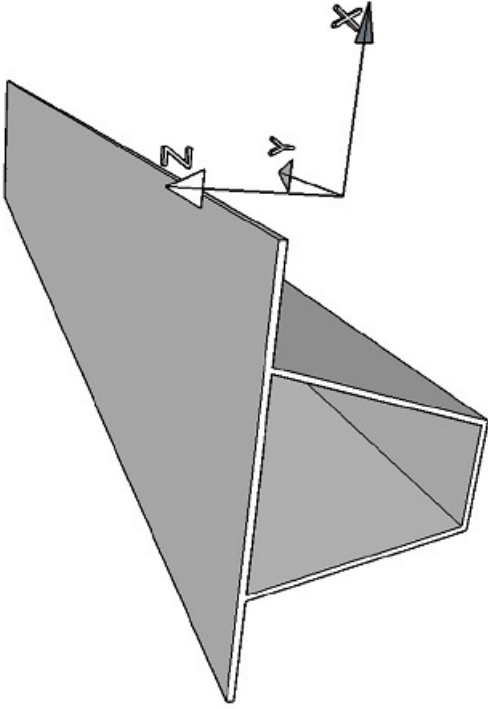
Distance of the upper flange and the webs from the neutral axis

$z_{HK.f.top} := h_{HK.rib.top} - z_c = 0.085\,m$

Distance between upper plate and neutral axis of the rib

$z_{HK.rib.web} := z_c - \dfrac{h_{HK.rib.top}}{2} = 0.067\,m$

Distance between the gravity centre of the webs and neutral axis of the rib

Moment of Inertia in the X direction

$$I_{HK.unit.ortho.x} := \dfrac{b_{HK.f.top} \cdot t_{HK.f.top}^{3}}{12} + b_{HK.f.top} \cdot t_{HK.f.top} \cdot z_{HK.f.top}^{2} + \dfrac{l_{HK.rib.top.f.bot} \cdot t_{HK.rib.top}^{3}}{12} \dots$$

$$+ l_{HK.rib.top.f.bot} \cdot t_{HK.rib.top} \cdot z_c^{2} + 2 \cdot \dfrac{t_{HK.rib.top} \cdot h_{HK.rib.top}}{12} + 2 \cdot t_{HK.rib.top} \cdot h_{HK.rib.top} \cdot z_{HK.rib.web}^{2}$$

Moment of inertia of each top rib around x-x direction

$I_{HK.unit.ortho.x} = 1.714 \times 10^{-4}\,m^{4}$

$I_{HK.ortho.x} := \dfrac{I_{HK.unit.ortho.x}}{b_{HK.f.top}} = 2.856 \times 10^{-4}\,\dfrac{m^{4}}{m}$

Moment of inertia around x-x direction per unit width

Moment of Inertia in the Y direction

$$I_{HK.ortho.y} := \frac{t_{HK.f.top}^{3}}{12}$$

$$I_{HK.ortho.y} = 1.44 \times 10^{-7} \cdot \frac{m^{4}}{m}$$

Moment of inertia around y-y direction per unit width

In the moment of inertia for the Y direction only the top flange is taken only there the units are connected themselves and can transfer the moment.

Total Moment of Inertia in the Z direction

$$I_{HK.unit.ortho.z} := \frac{t_{HK.f.top} b_{HK.f.top}^{3}}{12} + \frac{t_{HK.rib.top} \cdot l_{HK.rib.top.f.bot}^{3}}{12} + 2 \cdot \frac{h_{HK.rib.top} \cdot t_{HK.rib.top}^{3}}{12}$$

$$I_{HK.unit.ortho.z} = 2.186 \times 10^{-4} \ m^{4}$$

Moment of inertia of each top rib around z-z direction

$$I_{HK.ortho.z} := \frac{I_{HK.unit.ortho.z}}{b_{HK.f.top}} = 3.643 \times 10^{-4} \cdot \frac{m^{4}}{m}$$

Moment of inertia around z-z direction per unit width

Product of Inertia

$$I_{HK.unit.ortho.xz} := 2 \left(l_{HK.rib.top.web} \cdot t_{HK.rib.top} \right) z_{HK.rib.web} \cdot \left(\frac{\frac{l_{HK.rib.top.f.top}}{2} + \frac{l_{HK.rib.top.f.bot}}{2}}{2} \right)$$

Product of inertia (the top and bottom flange of the unit do not contribute as their centre of gravity cross-section has the same y coordinate with the centre of gravity of the whole cross-section)

$$I_{HK.unit.ortho.xz} = 3.892 \times 10^{-5} \ m^{4}$$

Bending Stiffness per unit width or length respectively in the plate

X direction

$$D_{HK.ortho.x} := I_{HK.ortho.x} \cdot E_{S355N} = 5.998 \times 10^{7} \cdot N \cdot m$$

Y direction

$$D_{HK.ortho.y} := \frac{I_{HK.ortho.y} \cdot E_{S355N}}{1 - \nu^2 \left(1 - \frac{I_{HK.ortho.y} \cdot E_{S355N}}{D_{HK.ortho.x}}\right)} = 3.323 \times 10^4 \cdot N \cdot m$$

Torsional Rigidity per unit width [Nm]

$$T_{HK.ortho.xy} := \sqrt{D_{HK.ortho.x} \cdot D_{HK.ortho.y}} = 1.412 \times 10^6 \cdot N \cdot m$$

Axial Stiffness per unit width [N/m]

X direction

$$E_{ortho.x} := E_{S355N} \cdot A_{HK.ortho.x} = 4.711 \times 10^9 \cdot \frac{N}{m}$$

Y direction

$$E_{ortho.y} := \frac{E_{S355N} \cdot t_{HK.f.top}}{1 - \nu^2 \left(1 - \frac{E_{S355N} \cdot t_{HK.f.top}}{E_{ortho.x}}\right)} = 2.63 \times 10^9 \cdot \frac{N}{m}$$

$$A_{sl.rib} := t_{HK.rib.top} \cdot \left(2 \cdot l_{HK.rib.top.web} + l_{HK.rib.top.f.bot}\right)$$ Sum of the gross areas of the individual longitudinal stiffeners

$$A_{sl.rib} = 6.26 \times 10^{-3} \, m^2$$

Poisson's ratio

$$\nu_{xy} := \nu = 0.3$$

$$\nu_{yx} := \nu_{xy} \cdot \frac{D_{HK.ortho.y}}{D_{HK.ortho.x}} = 1.662 \times 10^{-4}$$

$$\nu_p := 1 - \nu_{xy}^2 \cdot \frac{D_{HK.ortho.y}}{D_{HK.ortho.x}} = 1$$

Coefficients used in displacment expression

$$D_{HK.ortho.xx} := \frac{D_{HK.ortho.x}}{1 - \nu_{xy} \cdot \nu_{yx}} = 5.998 \times 10^4 \cdot kN \cdot m$$

$$D_{HK.ortho.yy} := \frac{D_{HK.ortho.y}}{1 - \nu_{xy} \cdot \nu_{yx}} = 33.231 \cdot kN \cdot m$$

Transversal shear stiffness

We assume that the shear is taken only by the longitudinal stiffeners in the X direction.

$$D_{HK.ortho.Qx} := \frac{G_c \cdot t_{HK.rib.top}^2}{\dfrac{A_{sl.rib}}{b_{HK.f.top}}} \cdot \left(\frac{h_{HK.rib.top}}{b_{HK.f.top}}\right)^2 = 1.272 \times 10^5 \cdot \frac{kN}{m}$$

$$D_{HK.ortho.Qy} := 0$$

Torsional stiffness

$$J_{HK.ortho.xz} := I_{HK.ortho.x} + I_{HK.ortho.z} = 6.499 \times 10^{-4} \cdot \frac{m^4}{m}$$

$$D_{HK.ortho.xz} := 2 \cdot G_c \cdot J_{HK.ortho.xz} = 1.05 \times 10^5 \cdot kN \cdot m$$

Polar moment of inertia assuming that there is no warping in the plate

Torsional stiffness

▼ Global Deflection of the orthotropic bridge deck

Total area of longitudinal stiffeners

$A_{sl} := A_{HK.unit.ortho.x} = 1.346 \times 10^4 \cdot mm^2$

Loads for each longdiutdinal stiffener with the corresponding plate flange

<u>Self weight of each unit in the compressive flange</u>

$q_{HK.self.unit} := A_{sl} \cdot g \cdot \rho_{S355N} = 1.036 \cdot \dfrac{kN}{m}$ Self weight of the steel per unit length of the construction for each unit

$q_{HK.asp.unit} := a_d \cdot t_{cover} \cdot b_{HK.f.top} = 0.69 \cdot \dfrac{kN}{m}$ Asphalt cover per unit length of the construction for each unit

Total permanent load

$q_{HK.tot.unit} := q_{HK.self.unit} + q_{HK.asp.unit} = 1.726 \cdot \dfrac{kN}{m}$ Total weight per unit length of the construction for each unit

Traffic loads

$\psi_{0.TS} := 0.75$ ψ factor for Tandem System load

$\alpha_{Q1} := 1$ Adjustment factor for Tandem System (TS)

$\psi_{0.UDL} := 0.4$ ψ factor for Uniformly Distributed Load

$\alpha_{q1} := 1$ Adjustment factor for Uniformly Distributed Loads (UDS)

Big Truck

$Q_1 := 300kN$ Load per axle

$Q_{1.wheel} := \dfrac{Q_1}{2} = 150 \cdot kN$ Load per wheel

Medium Truck

$Q_2 := 200kN$ Load per axle

$Q_{2.wheel} := \dfrac{Q_2}{2} = 100 \cdot kN$ Load per wheel

Small Truck

$Q_3 := 100kN$ Load per axle

$Q_{3.wheel} := \dfrac{Q_3}{2} = 50 \cdot kN$ Load per wheel

Main lane

$q_{main} := 9 \, \dfrac{kN}{m^2}$ Load in main lane

$q_{main.unit} := q_{main} \cdot b_{HK.f.top} = 5.4 \cdot \dfrac{kN}{m}$ Total traffic load in the main lane per unit length of the construction for each unit

Traffic Load in Random Lane except from the Main one

$q_{other} := 2.5 \, \dfrac{kN}{m^2}$ Load in other lanes

Global Deflection

For the maximum global deflection, the load combination is performed in Serviceability Limit State (SLS). In this case, just a unit of the plate is going to be studied as a beam. So,

$$q_{comb.loc.SLS} := q_{HK.tot.unit} + \alpha_{q1} \cdot q_{main.unit} = 7.126 \cdot \frac{kN}{m}$$

$$Q_{comb.loc.SLS} := \alpha_{Q1} \cdot Q_{1.wheel} = 150 \cdot kN$$

$$\delta_{allowed} := \frac{l_{long.stif}}{400} = 0.01 \, m \qquad \text{Maximum deflection allowed}$$

$$I_{sl} := I_{HK.unit.ortho.x} = 1.714 \times 10^{-4} \, m^4 \qquad \text{Moment of inertia of each top rib around x-x direction}$$

Input for the programmes to calculate the deflection

$$I_{xx} := I_{sl} = 1.714 \times 10^{-4} \, m^4$$

$$A_{sl} = 1.346 \times 10^4 \cdot mm^2 \qquad \text{Area of the unit used}$$

$$\rho_{S355N} = 7.85 \times 10^3 \, \frac{kg}{m^3} \qquad \text{Density of steel}$$

$$E_{S355N} = 210 \cdot GPa \qquad \text{Modulus of elasticity}$$

The load combination for the global deflection is the one shown below. The unit studied is assumed to be taken from the main lane.

Load Combination
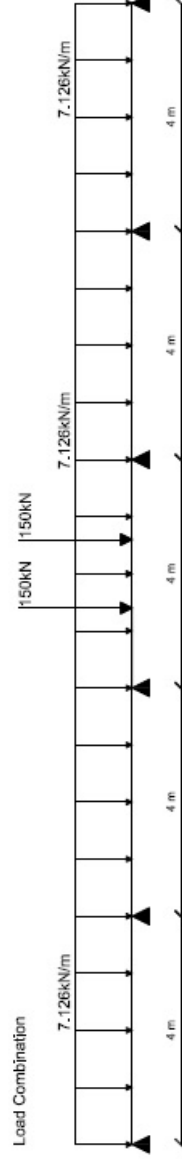
The highest value of the global deflection is going to be appeared in the middle span. For finding the exact value of the deflection, the FEM Software Abaqus was used.

Input for the calculation of the global deflection in Abaqus

$A_{sl} = 0.013 \, m^2$

$I_{HK.unit.ortho.x} = 1.714 \times 10^{-4} \cdot m^4$ Moment of inertia around the x-x axis

$I_{HK.unit.ortho.z} = 2.186 \times 10^{-4} \cdot m^4$ Moment of inertia around the z-z axis

$I_{HK.unit.ortho.xz} = 3.892 \times 10^{-5} \, m^4$ Product of inertia

The results of Abaqus are shown below.

U, Magnitude
+5.261e-03
+4.822e-03
+4.384e-03
+3.945e-03
+3.507e-03
+3.069e-03
+2.630e-03
+2.192e-03
+1.754e-03
+1.315e-03
+8.768e-04
+4.384e-04
+0.000e+00
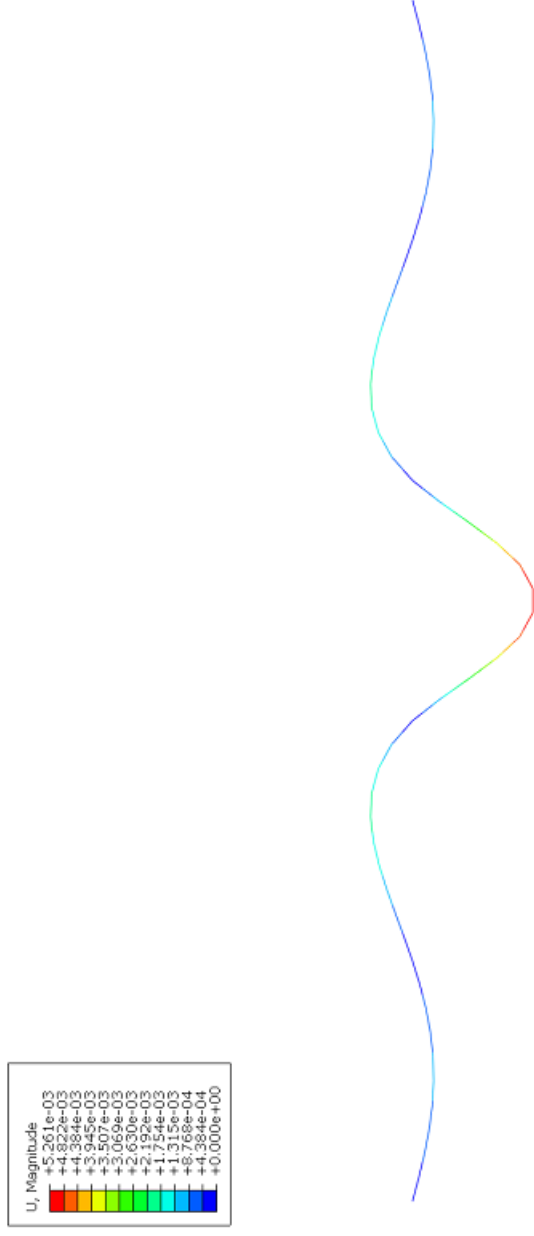
So, the maximum deflection of the unit is concidered to be:

$\delta_{max.ortho} := 5.261 mm$ $\delta_{max.ortho} \leq \delta_{allowed} = 1$

In order to find the maximum deflection, an assumption has been been made that the whole load from the truck wheel is carried by one unit. However, in reality we have a moment distribution in the p so the actuall load carried by each unit is around 90% of what it is calculated for our case. By assuming that the whole wheel track is taken by one unit, the study remains on the safe sife.

Global Deflection of the orthotropic bridge deck

Maximum local deflection allowed

$$\delta_{local.allowed.1} := \frac{l_{HK.rib.top.f.top}}{400} = 7.655 \times 10^{-4} \text{ m}$$ Maximum deflection between the webs of one longitudinal stiffener

$$\delta_{local.allowed.2} := \frac{b_{HK.f.top} - l_{HK.rib.top.f.top}}{400} = 7.345 \times 10^{-4} \text{ m}$$ Maximum deflection between the webs of different longitudinal stiffeners

$$\delta_{local.allowed} := \min\left(\delta_{local.allowed.1}, \delta_{local.allowed.2}\right) = 7.345 \times 10^{-4} \text{ m}$$ Maximum deflection allowed

Permanent loads

For the self-weight, just the top flange is taken into consideration as the investigation of the local deflection is carried out between the longitudinal stiffeners and between the webs of each longidutinal stiffener.

$$q_{HK.f.top} := t_{HK.f.top} \cdot \rho_{S355N} \cdot g = 0.924 \cdot \frac{kN}{m^2}$$ Self-weight of the top flange per square meter of the construction

$$q_{HK.asp} := a_d \cdot t_{cover} = 1.15 \cdot \frac{kN}{m^2}$$ Asphalt cover per square meter of the construction

Load considered for the local deflection

$$q_{comb.local.1} := \left(q_{HK.f.top} + q_{HK.asp} + \alpha_{q1} \cdot q_{main}\right) \cdot 1m$$

$$q_{comb.local.1} = 11.074 \cdot \frac{kN}{m}$$ Uniformly distributed load per unit width for the main lane

$$q_{comb.local.2} := \left(q_{HK.f.top} + q_{HK.asp} + \alpha_{q1} \cdot q_{other}\right) \cdot 1m$$

$$q_{comb.local.2} = 4.574 \cdot \frac{kN}{m}$$ Uniformly distributed load per unit width for the other lanes

$$Q_{comb.local.1} := \alpha_{Q1} Q_{1.wheel} = 150 \cdot kN$$

$$Q_{comb.local.2} := \alpha_{Q1} \cdot Q_{2.wheel} = 100 \cdot kN$$

Pavement

Orthotropic Plate

400 mm

500 mm

45°
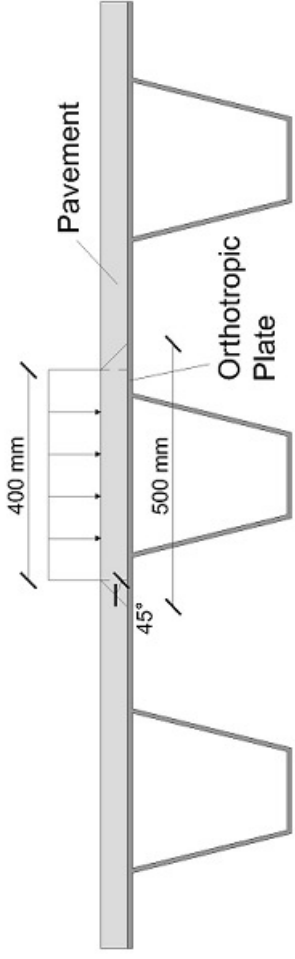
$b_{wheel} := 0.4 \, m$ Width of the wheel

$b_{wheel.pl} := b_{wheel} + 2 \cdot t_{cover} = 0.5 \, m$ Width of the wheel on the top of the plate

$q_{comb.wheel.local.1} := \dfrac{Q_{comb.local.1}}{b_{wheel.pl}} = 300 \cdot \dfrac{kN}{m}$ Distributed loads of the wheels in 0.5m

$q_{comb.wheel.local.2} := \dfrac{Q_{comb.local.2}}{b_{wheel.pl}} = 200 \cdot \dfrac{kN}{m}$

The initial load combination is:
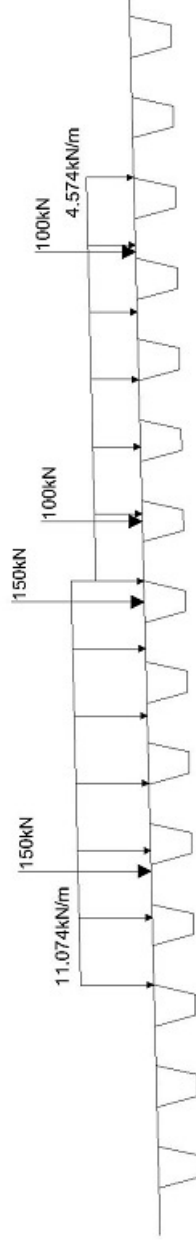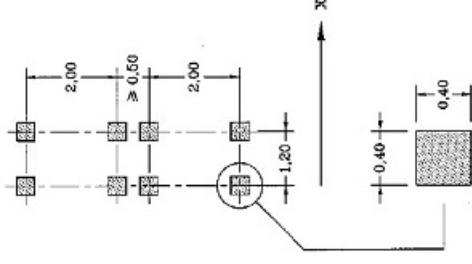
However, for the local buckling, it is going to be assumed that the concentrated load is distributed in an area equal with the width of the wheel on the surface of the top plate. Moreover, the concentrated loads acting not between the webs of one longitudinal stiffener but in the parts of the plate between longitudinal stiffeners have favourite contribution in terms of local buckling; therefore, they can be neglected. So, the final load combination is the one shown below.
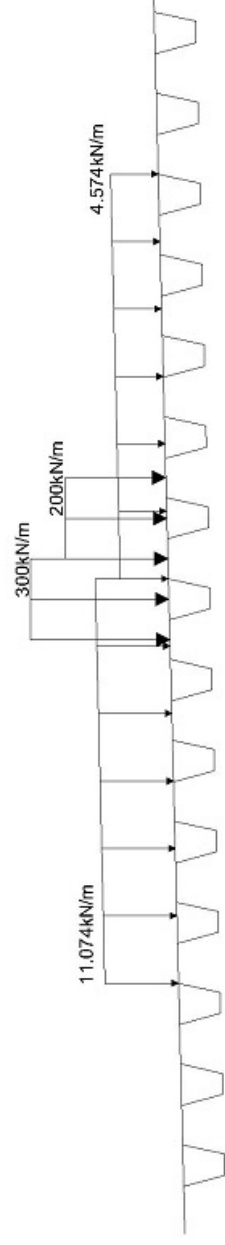
The model in Abaqus is considered to be a simple beam with a width of one meter, while hinges are used in the places where the webs are located, as shown in the picture below. This is not exactly what is happening in reality, as apart from local buckling, the plate will also buckle globally and the webs are going to appear compressive deflection if they do not buckle themselves. However, it is an adequate assumption for studying the local buckling of the different parts of the bridge deck. The beam is loaded as illustrated in the figure above.

U, Magnitude

+3.182e-04
+2.917e-04
+2.652e-04
+2.386e-04
+2.121e-04
+1.856e-04
+1.591e-04
+1.326e-04
+1.061e-04
+7.955e-05
+5.303e-05
+2.652e-05
+0.000e+00
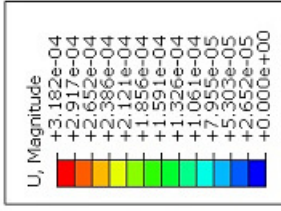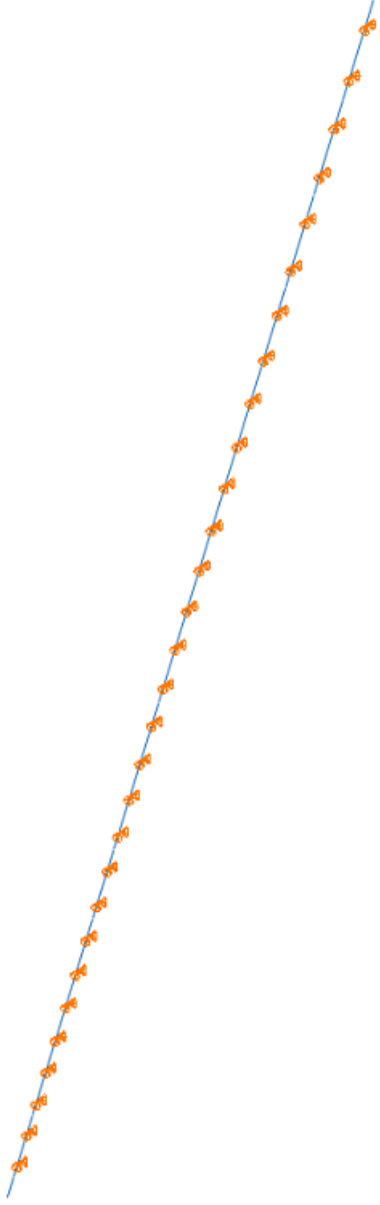
The local deflection of the orthotropic deck in that case is 0.318mm

As the distributed load in the part between the two examined stiffeners causes favourite contribution for the local buckling, the distributed load of the wheels of the trucks has been relocated like below.
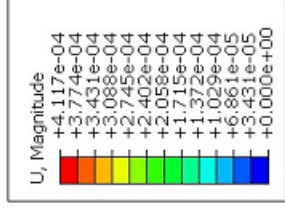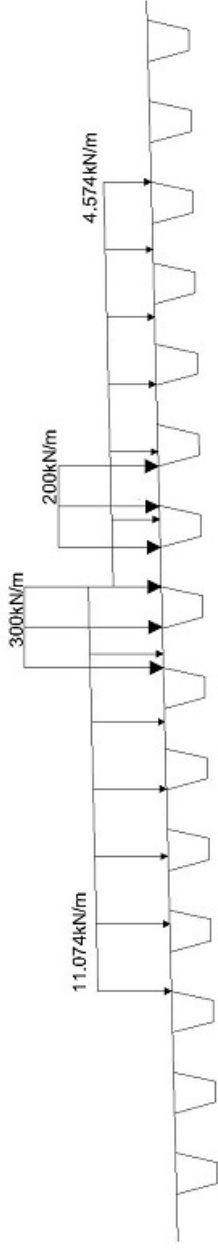
In that case, the local deflection is bigger, as expected, and it has a maximum value equal to 0.412mm.

So, the local deflection is equal with

$\delta_{local.max} := 4.12 \cdot 10^{-4} \text{ m}$

Maximum local deflection in the compression flange

$\delta_{local.max} < \delta_{local.allowed} = 1$

The local deflection is lower than the allowed value

Steel Sandwich Element
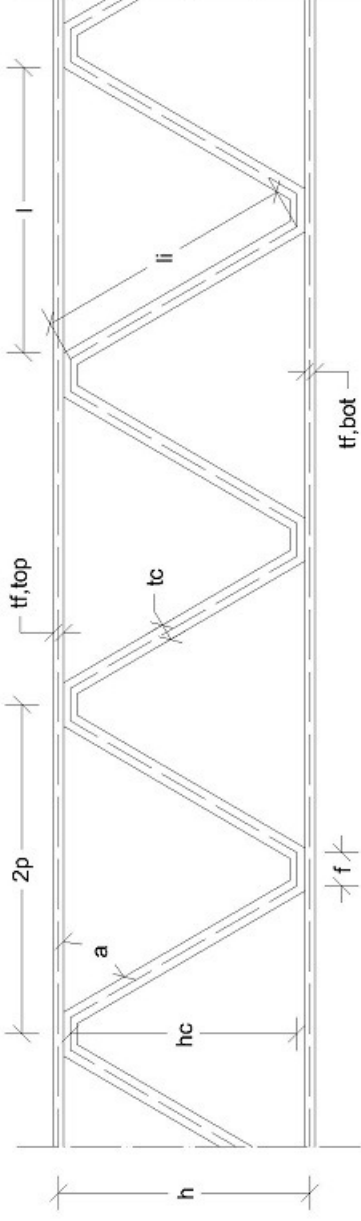
Height of the cross-section

$$h_{ssp}\left(h_{c.ssp}, t_{f.top}, t_{f.bot}, t_{c.ssp}\right) := h_{c.ssp} + \frac{t_{f.top}}{2} + \frac{t_{f.bot}}{2} + 2\frac{t_{c.ssp}}{2}$$

Length of the inclined leg of the core

$$l_{i.ssp}\left(h_{c.ssp}, \alpha_{ssp}\right) := \frac{h_{c.ssp}}{\sin\left(\alpha_{ssp}\right)}$$

Length of corrugation opening

$$l_{buck}\left(h_{c.ssp}, \alpha_{ssp}, f_{ssp}\right) := 2 l_{i.ssp}\left(h_{c.ssp}, \alpha_{ssp}\right) \cdot \cos\left(\alpha_{ssp}\right) + f_{ssp}$$

Half of the corrugation pitch

$$p_{ssp}\left(h_{c.ssp}, \alpha_{ssp}, f_{ssp}\right) := \frac{f_{ssp}}{2} + \frac{l_{buck}\left(h_{c.ssp}, \alpha_{ssp}, f_{ssp}\right)}{2}$$

Length of cross-section

$$l_{ssp}\left(h_{c.ssp}, \alpha_{ssp}, f_{ssp}\right) := 2 \cdot p_{ssp}\left(h_{c.ssp}, \alpha_{ssp}, f_{ssp}\right)$$

Configuration ratios

$$hc\_tc\left(h_{c.ssp}, t_{c.ssp}\right) := \frac{h_{c.ssp}}{t_{c.ssp}}$$

$$p\_hc\left(h_{c.ssp}, \alpha_{ssp}, f_{ssp}\right) := \frac{p_{ssp}\left(h_{c.ssp}, \alpha_{ssp}, f_{ssp}\right)}{h_{c.ssp}}$$

Areas

$$A_{f.top}\left(t_{f.top}, h_{c.ssp}, \alpha_{ssp}, f_{ssp}\right) := t_{f.top} \cdot l_{ssp}\left(h_{c.ssp}, \alpha_{ssp}, f_{ssp}\right) \qquad \text{Area of top flanges}$$

$$A_{f.bot}\left(t_{f.bot}, h_{c.ssp}, \alpha_{ssp}, f_{ssp}\right) := t_{f.bot} \cdot l_{ssp}\left(h_{c.ssp}, \alpha_{ssp}, f_{ssp}\right) \qquad \text{Area of bottom flange}$$

Area of the core

$$A_{c.ssp}\left(t_{c.ssp}, h_{c.ssp}, \alpha_{ssp}, f_{ssp}\right) := 2 \cdot f_{ssp} \cdot t_{c.ssp} + 2 \cdot t_{c.ssp} \cdot l_{i.ssp}\left(h_{c.ssp}, \alpha_{ssp}\right)$$

Area of the core per unit width

$$A_{C.ssp}\left(t_{c.ssp}, h_{c.ssp}, \alpha_{ssp}, f_{ssp}\right) := \frac{A_{c.ssp}\left(t_{c.ssp}, h_{c.ssp}, \alpha_{ssp}, f_{ssp}\right)}{l_{ssp}\left(h_{c.ssp}, \alpha_{ssp}, f_{ssp}\right)}$$

Total Area

$$A_{tot.ssp}\left(h_{c.ssp}, t_{f.top}, t_{f.bot}, t_{c.ssp}, \alpha_{ssp}, f_{ssp}\right) := A_{f.top}\left(t_{f.top}, h_{c.ssp}, \alpha_{ssp}, f_{ssp}\right) + A_{f.bot}\left(t_{f.bot}, h_{c.ssp}, \alpha_{ssp}, f_{ssp}\right) + A_{c.ssp}\left(t_{c.ssp}, h_{c.ssp}, \alpha_{ssp}, f_{ssp}\right)$$

Total area per unit width [m]

$$A_{ssp}\left(h_{c.ssp}, t_{f.top}, t_{f.bot}, t_{c.ssp}, \alpha_{ssp}, f_{ssp}\right) := \frac{A_{tot.ssp}\left(h_{c.ssp}, t_{f.top}, t_{f.bot}, t_{c.ssp}, \alpha_{ssp}, f_{ssp}\right)}{l_{ssp}\left(h_{c.ssp}, \alpha_{ssp}, f_{ssp}\right)}$$

Total weight of the section

$$G_{ssp}\left(h_{c.ssp}, t_{f.top}, t_{f.bot}, t_{c.ssp}, \alpha_{ssp}, f_{ssp}\right) := A_{ssp}\left(h_{c.ssp}, t_{f.top}, t_{f.bot}, t_{c.ssp}, \alpha_{ssp}, f_{ssp}\right) \cdot \rho_{S355N}$$

Neutral Axis of the steel sandwich element (distance from the top)

$$z_{na.ssp}\left(h_{c.ssp}, t_{f.top}, t_{f.bot}, t_{c.ssp}, \alpha_{ssp}, f_{ssp}\right) := \frac{\left[\begin{array}{l} t_{c.ssp} \cdot f_{ssp} \cdot \left(\dfrac{t_{f.top}}{2} + \dfrac{t_{c.ssp}}{2}\right) \dots \\[2mm] + 2 \cdot t_{c.ssp} \cdot l_{i.ssp}\left(h_{c.ssp}, \alpha_{ssp}\right) \cdot \left(\dfrac{h_{c.ssp}}{2} + \dfrac{t_{f.top}}{2} + \dfrac{t_{c.ssp}}{2}\right) \dots \\[2mm] + t_{c.ssp} \cdot f_{ssp} \cdot \left(\dfrac{t_{f.top}}{2} + \dfrac{t_{c.ssp}}{2} + h_{c.ssp}\right) \dots \\[2mm] + A_{f.bot}\left(t_{f.bot}, h_{c.ssp}, \alpha_{ssp}, f_{ssp}\right) \cdot \left(h_{ssp}\left(h_{c.ssp}, t_{f.top}, t_{f.bot}, t_{c.ssp}\right)\right) \end{array}\right]}{A_{tot.ssp}\left(h_{c.ssp}, t_{f.top}, t_{f.bot}, t_{c.ssp}, \alpha_{ssp}, f_{ssp}\right)}$$

Moment of inertia in X- direction

Moment of inertia for the top flange

$$I_{f.top.ssp.x}\left(h_{c.ssp}, t_{f.top}, t_{f.bot}, t_{c.ssp}, \alpha_{ssp}, f_{ssp}\right) := \frac{l_{ssp}\left(h_{c.ssp}, \alpha_{ssp}, f_{ssp}\right) \cdot t_{f.top}^{\,3}}{12} + l_{ssp}\left(h_{c.ssp}, \alpha_{ssp}, f_{ssp}\right) \cdot t_{f.top} \cdot \left(z_{na.ssp}\left(h_{c.ssp}, t_{f.top}, t_{f.bot}, t_{c.ssp}, \alpha_{ssp}, f_{ssp}\right) - \frac{t_{f.top}}{2} - \frac{t_{c.ssp}}{2}\right)^{2}$$

Moment of inertia for the top horisontal part of the core

$$I_{c.top.ssp.x}\left(h_{c.ssp}, t_{f.top}, t_{f.bot}, t_{c.ssp}, \alpha_{ssp}, f_{ssp}\right) := \frac{f_{ssp} \cdot t_{c.ssp}^{\,3}}{12} + f_{ssp} \cdot t_{c.ssp} \cdot \left(z_{na.ssp}\left(h_{c.ssp}, t_{f.top}, t_{f.bot}, t_{c.ssp}, \alpha_{ssp}, f_{ssp}\right) - \frac{t_{f.top}}{2} - \frac{t_{c.ssp}}{2}\right)^{2}$$

Moment of inertia for the inclined part of the core

$$I_{inc.ssp.x}\left(h_{c.ssp}, t_{f.top}, t_{f.bot}, t_{c.ssp}, \alpha_{ssp}, f_{ssp}\right) := 2 \cdot \frac{t_{c.ssp} \cdot l_{i.ssp}\left(h_{c.ssp}, \alpha_{ssp}\right)^{3}}{12} \cdot \sin\left(\alpha_{ssp}\right)^{2} \dots \\ + 2 t_{c.ssp} \cdot l_{i.ssp}\left(h_{c.ssp}, \alpha_{ssp}\right) \cdot \left(\begin{array}{l}\dfrac{t_{f.top}}{2} + \dfrac{t_{c.ssp}}{2} + \dfrac{h_{c.ssp}}{2} \dots \\[2mm] + -z_{na.ssp}\left(h_{c.ssp}, t_{f.top}, t_{f.bot}, t_{c.ssp}, \alpha_{ssp}, f_{ssp}\right)\end{array}\right)^{2}$$

Moment of inertia for the bottom part of the core

$$I_{c.bot.ssp.x}\left(h_{c.ssp}, t_{f.top}, t_{f.bot}, t_{c.ssp}, \alpha_{ssp}, f_{ssp}\right) := \frac{f_{ssp} \cdot t_{c.ssp}^{\ 3}}{12} \dots$$
$$+ f_{ssp} \cdot t_{c.ssp} \cdot \left(\frac{t_{f.top}}{2} + \frac{t_{c.ssp}}{2} + h_{c.ssp} - z_{na.ssp}\left(h_{c.ssp}, t_{f.top}, t_{f.bot}, t_{c.ssp}, \alpha_{ssp}, f_{ssp}\right)\right)^2$$

Moment of inertia for the bottom flange

$$I_{f.bot.ssp.x}\left(h_{c.ssp}, t_{f.top}, t_{f.bot}, t_{c.ssp}, \alpha_{ssp}, f_{ssp}\right) := \frac{l_{ssp}\left(h_{c.ssp}, \alpha_{ssp}, f_{ssp}\right) \cdot t_{f.bot}^{\ 3}}{12} \dots$$
$$+ l_{ssp}\left(h_{c.ssp}, \alpha_{ssp}, f_{ssp}\right) \cdot t_{f.bot} \cdot \left(h_{ssp}\left(h_{c.ssp}, t_{f.top}, t_{f.bot}, t_{c.ssp}\right) \dots + -z_{na.ssp}\left(h_{c.ssp}, t_{f.top}, t_{f.bot}, t_{c.ssp}, \alpha_{ssp}, f_{ssp}\right)\right)^2$$

Total moment of inertia for SSP in X- direction

$$I_{tot.ssp.x}\left(h_{c.ssp}, t_{f.top}, t_{f.bot}, t_{c.ssp}, \alpha_{ssp}, f_{ssp}\right) := I_{f.top.ssp.x}\left(h_{c.ssp}, t_{f.top}, t_{f.bot}, t_{c.ssp}, \alpha_{ssp}, f_{ssp}\right) \dots$$
$$+ I_{c.top.ssp.x}\left(h_{c.ssp}, t_{f.top}, t_{f.bot}, t_{c.ssp}, \alpha_{ssp}, f_{ssp}\right) \dots$$
$$+ I_{inc.ssp.x}\left(h_{c.ssp}, t_{f.top}, t_{f.bot}, t_{c.ssp}, \alpha_{ssp}, f_{ssp}\right) \dots$$
$$+ I_{c.bot.ssp.x}\left(h_{c.ssp}, t_{f.top}, t_{f.bot}, t_{c.ssp}, \alpha_{ssp}, f_{ssp}\right) \dots$$
$$+ I_{f.bot.ssp.x}\left(h_{c.ssp}, t_{f.top}, t_{f.bot}, t_{c.ssp}, \alpha_{ssp}, f_{ssp}\right)$$

Moment of inertia in Y- direction

Moment of inertia for the top flange

$$I_{f.top.ssp.y}\left(h_{c.ssp}, t_{f.top}, t_{f.bot}, t_{c.ssp}, \alpha_{ssp}, f_{ssp}\right) := \frac{l_{ssp}\left(h_{c.ssp}, \alpha_{ssp}, f_{ssp}\right) \cdot t_{f.top}^{\ 3}}{12} \dots$$
$$+ l_{ssp}\left(h_{c.ssp}, \alpha_{ssp}, f_{ssp}\right) \cdot t_{f.top} \cdot \left(z_{na.ssp}\left(h_{c.ssp}, t_{f.top}, t_{f.bot}, t_{c.ssp}, \alpha_{ssp}, f_{ssp}\right)\right)^2$$

Moment of inertia for the bottom flange

$$I_{f.bot.ssp.y}\left(h_{c.ssp}, t_{f.top}, t_{f.bot}, t_{c.ssp}, \alpha_{ssp}, f_{ssp}\right) := \frac{l_{ssp}\left(h_{c.ssp}, \alpha_{ssp}, f_{ssp}\right) \cdot t_{f.bot}^{\ 3}}{12} \dots$$
$$+ l_{ssp}\left(h_{c.ssp}, \alpha_{ssp}, f_{ssp}\right) \cdot t_{f.bot} \cdot \left(h_{ssp}\left(h_{c.ssp}, t_{f.top}, t_{f.bot}, t_{c.ssp}\right) \dots + -z_{na.ssp}\left(h_{c.ssp}, t_{f.top}, t_{f.bot}, t_{c.ssp}, \alpha_{ssp}, f_{ssp}\right)\right)^2$$

Moment of inertia for the top horisontal part of the core

$$I_{c.top.ssp.y}\left(h_{c.ssp}, t_{f.top}, t_{f.bot}, t_{c.ssp}, \alpha_{ssp}, f_{ssp}\right) := \frac{f_{ssp} \cdot t_{c.ssp}^{3}}{12} + f_{ssp} \cdot t_{c.ssp} \cdot \left(z_{na.ssp}\left(h_{c.ssp}, t_{f.top}, t_{f.bot}, t_{c.ssp}, \alpha_{ssp}, f_{ssp}\right) - \frac{t_{f.top}}{2} - \frac{t_{c.ssp}}{2}\right)^{2}$$

Moment of inertia for the bottom part of the core

$$I_{c.bot.ssp.y}\left(h_{c.ssp}, t_{f.top}, t_{f.bot}, t_{c.ssp}, \alpha_{ssp}, f_{ssp}\right) := \frac{f_{ssp} \cdot t_{c.ssp}^{3}}{12} \dots$$
$$+ f_{ssp} \cdot t_{c.ssp} \cdot \left(\frac{t_{f.top}}{2} + \frac{t_{c.ssp}}{2} + h_{c.ssp} - z_{na.ssp}\left(h_{c.ssp}, t_{f.top}, t_{f.bot}, t_{c.ssp}, \alpha_{ssp}, f_{ssp}\right)\right)^{2}$$

Total moment of inertia for SSP in Y- direction

$$I_{tot.ssp.y}\left(h_{c.ssp}, t_{f.top}, t_{f.bot}, t_{c.ssp}, \alpha_{ssp}, f_{ssp}\right) := I_{f.top.ssp.y}\left(h_{c.ssp}, t_{f.top}, t_{f.bot}, t_{c.ssp}, \alpha_{ssp}, f_{ssp}\right) \dots$$
$$+ I_{f.bot.ssp.y}\left(h_{c.ssp}, t_{f.top}, t_{f.bot}, t_{c.ssp}, \alpha_{ssp}, f_{ssp}\right) \dots$$
$$+ I_{c.top.ssp.y}\left(h_{c.ssp}, t_{f.top}, t_{f.bot}, t_{c.ssp}, \alpha_{ssp}, f_{ssp}\right) \dots$$
$$+ I_{c.bot.ssp.y}\left(h_{c.ssp}, t_{f.top}, t_{f.bot}, t_{c.ssp}, \alpha_{ssp}, f_{ssp}\right)$$

Moment of inertia in X and Y direction per unit width [m^3]

$$I_{ssp.x}\left(h_{c.ssp}, t_{f.top}, t_{f.bot}, t_{c.ssp}, \alpha_{ssp}, f_{ssp}\right) := \frac{I_{tot.ssp.x}\left(h_{c.ssp}, t_{f.top}, t_{f.bot}, t_{c.ssp}, \alpha_{ssp}, f_{ssp}\right)}{l_{ssp}\left(h_{c.ssp}, \alpha_{ssp}, f_{ssp}\right)}$$

$$I_{ssp.y}\left(h_{c.ssp}, t_{f.top}, t_{f.bot}, t_{c.ssp}, \alpha_{ssp}, f_{ssp}\right) := \frac{I_{tot.ssp.y}\left(h_{c.ssp}, t_{f.top}, t_{f.bot}, t_{c.ssp}, \alpha_{ssp}, f_{ssp}\right)}{l_{ssp}\left(h_{c.ssp}, \alpha_{ssp}, f_{ssp}\right)}$$

Bending Stiffness per unit width

Bending stiffness in the stiff direction per unit width

$$D_{x.ssp}\left(h_{c.ssp}, t_{f.top}, t_{f.bot}, t_{c.ssp}, \alpha_{ssp}, f_{ssp}\right) := E_{S355N} \cdot I_{ssp.x}\left(h_{c.ssp}, t_{f.top}, t_{f.bot}, t_{c.ssp}, \alpha_{ssp}, f_{ssp}\right)$$

Bending stiffness in the weak direction per unit width

$$D_{y.ssp}\left(h_{c.ssp}, t_{f.top}, t_{f.bot}, t_{c.ssp}, \alpha_{ssp}, f_{ssp}\right) := \frac{E_{S355N} \cdot I_{ssp.y}\left(h_{c.ssp}, t_{f.top}, t_{f.bot}, t_{c.ssp}, \alpha_{ssp}, f_{ssp}\right)}{1 - \nu^2\left(1 - \dfrac{E_{S355N} \cdot I_{ssp.y}\left(h_{c.ssp}, t_{f.top}, t_{f.bot}, t_{c.ssp}, \alpha_{ssp}, f_{ssp}\right)}{D_{x.ssp}\left(h_{c.ssp}, t_{f.top}, t_{f.bot}, t_{c.ssp}, \alpha_{ssp}, f_{ssp}\right)}\right)}$$

Torsional Stiffness per unit width (according to Libova-Hubka)

$$GA\left(h_{c.ssp}, t_{f.top}, t_{f.bot}, t_{c.ssp}, \alpha_{ssp}, f_{ssp}\right) := G_c \cdot t_{f.top} + \frac{G_c \cdot t_{c.ssp}^{2}}{A_{C.ssp}\left(t_{c.ssp}, h_{c.ssp}, \alpha_{ssp}, f_{ssp}\right)} + G_c \cdot t_{f.bot}$$

$$k_c = \frac{1}{2} \cdot \left(1 + \frac{A_1 - A_2}{2 \cdot p \cdot h}\right)$$
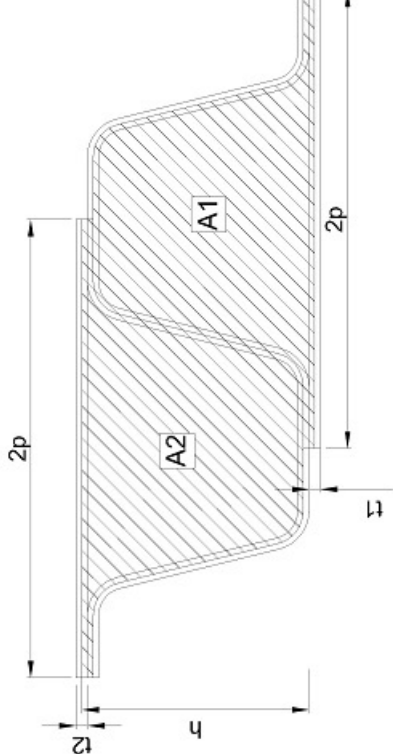
$$k_c\left(h_{c.ssp}, t_{f.top}, t_{f.bot}, t_{c.ssp}\right) := \frac{1}{2}\left(1 + \frac{t_{f.bot} - t_{f.top}}{2 \cdot h_{ssp}\left(h_{c.ssp}, t_{f.top}, t_{f.bot}, t_{c.ssp}\right)}\right)$$

$$k_{GJ}\left(h_{c.ssp}, t_{f.top}, t_{f.bot}, t_{c.ssp}, \alpha_{ssp}, f_{ssp}\right) := \frac{\dfrac{G_c \cdot t_{c.ssp}^{2} \cdot k_c\left(h_{c.ssp}, t_{f.top}, t_{f.bot}, t_{c.ssp}\right)}{A_{C.ssp}\left(t_{c.ssp}, h_{c.ssp}, \alpha_{ssp}, f_{ssp}\right)} + G_c \cdot t_{f.bot}}{GA\left(h_{c.ssp}, t_{f.top}, t_{f.bot}, t_{c.ssp}, \alpha_{ssp}, f_{ssp}\right)}$$

$$GJ\left(h_{c.ssp}, t_{f.top}, t_{f.bot}, t_{c.ssp}, \alpha_{ssp}, f_{ssp}\right) := \left[\frac{G_c \cdot t_{f.top} \cdot k_{GJ}\left(h_{c.ssp}, t_{f.top}, t_{f.bot}, t_{c.ssp}, \alpha_{ssp}, f_{ssp}\right)^2 \cdots}{+ \dfrac{G_c \cdot t_{c.ssp}}{2}} \cdots \right.$$

$$\left. + A_{C.ssp}\left(t_{c.ssp}, h_{c.ssp}, \alpha_{ssp}, f_{ssp}\right) \cdot \left(\begin{array}{c} k_{GJ}\left(h_{c.ssp}, t_{f.top}, t_{f.bot}, t_{c.ssp}, \alpha_{ssp}, f_{ssp}\right) \cdots \\ + -k_c\left(h_{c.ssp}, t_{f.top}, t_{f.bot}, t_{c.ssp}\right) \end{array}\right)^2 \cdots \right.$$

$$\left. + G_c \cdot t_{f.bot} \cdot \left(1 - k_{GJ}\left(h_{c.ssp}, t_{f.top}, t_{f.bot}, t_{c.ssp}, \alpha_{ssp}, f_{ssp}\right)\right)^2 \right] \cdot h_{ssp}\left(h_{c.ssp}, t_{f.top}, t_{f.bot}, t_{c.ssp}\right)^2$$

$$D_{xy.ssp}\left(h_{c.ssp}, t_{f.top}, t_{f.bot}, t_{c.ssp}, \alpha_{ssp}, f_{ssp}\right) := 2 \cdot GJ\left(h_{c.ssp}, t_{f.top}, t_{f.bot}, t_{c.ssp}, \alpha_{ssp}, f_{ssp}\right)$$

Axial Stiffness per unit width

Axial stiffness in the strong direction per unit width

$$E_{x.ssp}\left(h_{c.ssp}, t_{f.top}, t_{f.bot}, t_{c.ssp}, \alpha_{ssp}, f_{ssp}\right) := E_{S355N} \cdot A_{ssp}\left(h_{c.ssp}, t_{f.top}, t_{f.bot}, t_{c.ssp}, \alpha_{ssp}, f_{ssp}\right)$$

Axial stiffness in the weak direction per unit width

$$E_{y.ssp}\left(h_{c.ssp}, t_{f.top}, t_{f.bot}, t_{c.ssp}, \alpha_{ssp}, f_{ssp}\right) := \frac{E_{S355N} \cdot \left(t_{f.top} + t_{f.bot}\right)}{1 - \nu^2 \left[1 - \dfrac{E_{S355N} \cdot \left(t_{f.top} + t_{f.bot}\right)}{E_{x.ssp}\left(h_{c.ssp}, t_{f.top}, t_{f.bot}, t_{c.ssp}, \alpha_{ssp}, f_{ssp}\right)}\right]}$$

Horizontal shear stiffness per unit width

$$G_{xy}\left(h_{c.ssp}, t_{f.top}, t_{f.bot}, t_{c.ssp}, \alpha_{ssp}, f_{ssp}\right) := GA\left(h_{c.ssp}, t_{f.top}, t_{f.bot}, t_{c.ssp}, \alpha_{ssp}, f_{ssp}\right)$$

Dimensions needed for DQx and DQy
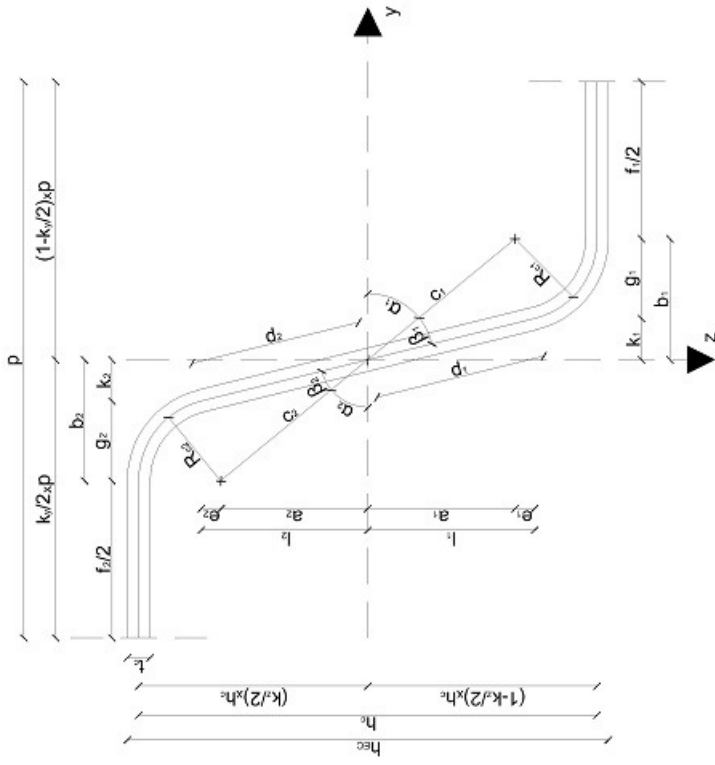
Due to symmetrical corrugation k.y=k.z=1 and K.Ay=K.Az=0. Moreover, we assume that Rc.1=0.

$$k_y := 1 \qquad k_z := 1 \qquad K_{Ay} := 0 \qquad K_{Az} := 0 \qquad R_{C1} := 0mm$$

$$a_1\left(h_{c.ssp}, R_{C1}\right) := \left(1 - \frac{k_z}{2}\right) \cdot h_{c.ssp} - R_{C1}$$

$$b_1\left(h_{c.ssp}, \alpha_{ssp}, f_{ssp}\right) := \left(1 - \frac{k_y}{2}\right) \cdot p_{ssp}\left(h_{c.ssp}, \alpha_{ssp}, f_{ssp}\right) - \frac{f_{ssp}}{2}$$

$$c_1\left(h_{c.ssp}, \alpha_{ssp}, f_{ssp}, R_{C1}\right) := \left(a_1\left(h_{c.ssp}, R_{C1}\right)^2 + b_1\left(h_{c.ssp}, \alpha_{ssp}, f_{ssp}\right)^2\right)^{\frac{1}{2}}$$

$$\alpha_1\left(h_{c.ssp}, \alpha_{ssp}, f_{ssp}, R_{C1}\right) := \operatorname{atan}\left(\frac{a_1\left(h_{c.ssp}, R_{C1}\right)}{b_1\left(h_{c.ssp}, \alpha_{ssp}, f_{ssp}\right)}\right)$$

$$\beta_1\left(h_{c.ssp}, \alpha_{ssp}, f_{ssp}, R_{C1}\right) := \operatorname{asin}\left(\frac{R_{C1}}{c_1\left(h_{c.ssp}, \alpha_{ssp}, f_{ssp}, R_{C1}\right)}\right)$$

$$d_1\left(h_{c.ssp}, \alpha_{ssp}, f_{ssp}, R_{C1}\right) := \left(c_1\left(h_{c.ssp}, \alpha_{ssp}, f_{ssp}, R_{C1}\right)^2 - R_{C1}^{\ 2}\right)^{\frac{1}{2}}$$

$$\theta\left(h_{c.ssp}, \alpha_{ssp}, f_{ssp}, R_{C1}\right) := \alpha_1\left(h_{c.ssp}, \alpha_{ssp}, f_{ssp}, R_{C1}\right) + \beta_1\left(h_{c.ssp}, \alpha_{ssp}, f_{ssp}, R_{C1}\right)$$

$$e_1\left(h_{c.ssp}, \alpha_{ssp}, f_{ssp}, R_{C1}\right) := R_{C1} \cdot \cos\left(\theta\left(h_{c.ssp}, \alpha_{ssp}, f_{ssp}, R_{C1}\right)\right)$$

$$g_1\left(h_{c.ssp}, \alpha_{ssp}, f_{ssp}, R_{C1}\right) := R_{C1} \cdot \sin\left(\theta\left(h_{c.ssp}, \alpha_{ssp}, f_{ssp}, R_{C1}\right)\right)$$

$$l_1\left(h_{c.ssp}, \alpha_{ssp}, f_{ssp}, R_{C1}\right) := a_1\left(h_{c.ssp}, R_{C1}\right) + e_1\left(h_{c.ssp}, \alpha_{ssp}, f_{ssp}, R_{C1}\right)$$

$$k_1\left(h_{c.ssp}, \alpha_{ssp}, f_{ssp}, R_{C1}\right) := b_1\left(h_{c.ssp}, \alpha_{ssp}, f_{ssp}\right) - g_1\left(h_{c.ssp}, \alpha_{ssp}, f_{ssp}, R_{C1}\right)$$

Lenght of one corrugation leg

$$l_s\left(h_{c.ssp}, \alpha_{ssp}, f_{ssp}, R_{C1}\right) := f_{ssp} + 2 \cdot R_{C1} \cdot \theta\left(h_{c.ssp}, \alpha_{ssp}, f_{ssp}, R_{C1}\right) + 2 \cdot d_1\left(h_{c.ssp}, \alpha_{ssp}, f_{ssp}, R_{C1}\right)$$

Transverse shear stiffness parallel to the corrugation per unit width, DQx

The transverse shear stiffness in the strong direction is equal with:

$$D_{Qx} = \frac{G_c \cdot t_{c.ssp}}{A_{c.ssp.x}} \cdot \left(\frac{h_{ssp}}{p_{ssp}}\right)^2$$

So,

$$A_{c.ssp.x}\left(h_{c.ssp}, t_{c.ssp}, \alpha_{ssp}, f_{ssp}, R_{C1}\right) := \frac{l_s\left(h_{c.ssp}, \alpha_{ssp}, f_{ssp}, R_{C1}\right) \cdot t_{c.ssp}}{p_{ssp}\left(h_{c.ssp}, \alpha_{ssp}, f_{ssp}\right)} \qquad \text{Area per unit width of the corrugated core}$$

$$D_{Qx}\left(h_{c.ssp}, t_{f.top}, t_{f.bot}, t_{c.ssp}, \alpha_{ssp}, f_{ssp}\right) := \frac{G_c \cdot t_{c.ssp}}{A_{c.ssp.x}\left(h_{c.ssp}, t_{c.ssp}, \alpha_{ssp}, f_{ssp}, R_{C1}\right)} \cdot \left(\frac{h_{ssp}\left(h_{c.ssp}, t_{f.top}, t_{f.bot}, t_{c.ssp}\right)}{p_{ssp}\left(h_{c.ssp}, \alpha_{ssp}, f_{ssp}\right)}\right)^2$$

Transverse shear stiffness perpendicular to the corrugation per unit width, DQy

The transverse shear stiffness in the weak direction is equal with:

$$D_{Qy} = S \cdot h_{ssp} \left(\frac{E_{S355N}}{1 - \nu_c^2}\right)\left(\frac{t_c}{h_c}\right)^3$$

Non-dimensional coefficient S

The coefficient S is used to take into consideration the core shape in the weak direction. The formulas have been obtained by papers "Elastic Constants for Corrugated-core Sandwich Plates" by Libova and Hubka and "Elasto-plastic Analysis of Corrugated Sandwich Steel Panels" by Chang.

K expressions

$$
K_{Iz}\left(h_{c.ssp},\alpha_{ssp},f_{ssp},R_{C1}\right) := \frac{2}{3}\cdot\left(\frac{k_1\left(h_{c.ssp},\alpha_{ssp},f_{ssp},R_{C1}\right)}{h_{c.ssp}}\right)^2\cdot\frac{d_1\left(h_{c.ssp},\alpha_{ssp},f_{ssp},R_{C1}\right)}{h_{c.ssp}} + \frac{2}{3}\cdot\left[\frac{1}{8}\cdot\left(\frac{p_{ssp}\left(h_{c.ssp},\alpha_{ssp},f_{ssp}\right)}{h_{c.ssp}}\right)^3 - \left(\frac{b_1\left(h_{c.ssp},\alpha_{ssp},f_{ssp}\right)}{h_{c.ssp}}\right)^3 \cdots\right]
$$

$$
\cdots \frac{b_1\left(h_{c.ssp},\alpha_{ssp},f_{ssp},R_{C1}\right)}{h_{c.ssp}}\cdot\left[\frac{\theta\left(h_{c.ssp},\alpha_{ssp},f_{ssp},R_{C1}\right)}{h_{c.ssp}} - 2\cdot\left(\frac{R_{C1}}{h_{c.ssp}} - \frac{e_1\left(h_{c.ssp},\alpha_{ssp},f_{ssp},R_{C1}\right)}{h_{c.ssp}}\right)\right]
$$

$$
+2\cdot\frac{R_{C1}}{h_{c.ssp}}\cdot\frac{g_1\left(h_{c.ssp},\alpha_{ssp},f_{ssp},R_{C1}\right)}{h_{c.ssp}} - \frac{e_1\left(h_{c.ssp},\alpha_{ssp},f_{ssp},R_{C1}\right)}{h_{c.ssp}}
$$

$$
+\frac{1}{2}\cdot\theta\left(h_{c.ssp},\alpha_{ssp},f_{ssp},R_{C1}\right)\cdot\left(\frac{R_{C1}}{h_{c.ssp}}\right)^2
$$

$$
K_{Iyz}\left(h_{c.ssp},\alpha_{ssp},f_{ssp},R_{C1}\right) := \frac{2}{3}\cdot\frac{l_1\left(h_{c.ssp},\alpha_{ssp},f_{ssp},R_{C1}\right)}{h_{c.ssp}}\cdot\frac{k_1\left(h_{c.ssp},\alpha_{ssp},f_{ssp},R_{C1}\right)}{h_{c.ssp}}\cdot\frac{d_1\left(h_{c.ssp},\alpha_{ssp},f_{ssp},R_{C1}\right)}{h_{c.ssp}} \cdots
$$

$$
+\frac{1}{2}\cdot\left[\frac{1}{4}\cdot\left(\frac{p_{ssp}\left(h_{c.ssp},\alpha_{ssp},f_{ssp}\right)}{h_{c.ssp}}\right)^2 - \left(\frac{b_1\left(h_{c.ssp},\alpha_{ssp},f_{ssp}\right)}{h_{c.ssp}}\right)^2 \cdots\right]
$$

$$
+2\cdot\frac{R_{C1}}{h_{c.ssp}}\cdot\left[\frac{a_1\left(h_{c.ssp},R_{C1}\right)}{h_{c.ssp}}\cdot\left(\frac{\theta\left(h_{c.ssp},\alpha_{ssp},f_{ssp},R_{C1}\right)}{h_{c.ssp}} - \frac{b_1\left(h_{c.ssp},\alpha_{ssp},f_{ssp},R_{C1}\right)}{h_{c.ssp}}\right) + \frac{e_1\left(h_{c.ssp},\alpha_{ssp},f_{ssp},R_{C1}\right)}{h_{c.ssp}}\right]
$$

$$
+\frac{g_1\left(h_{c.ssp},\alpha_{ssp},f_{ssp},R_{C1}\right)}{h_{c.ssp}} - \frac{1}{2}\cdot\frac{g_1\left(h_{c.ssp},\alpha_{ssp},f_{ssp},R_{C1}\right)}{h_{c.ssp}}\cdot\left(\frac{R_{C1}}{h_{c.ssp}} - \frac{e_1\left(h_{c.ssp},\alpha_{ssp},f_{ssp},R_{C1}\right)}{h_{c.ssp}}\right)
$$

$$
K_{Iy}\left(h_{c.ssp},\alpha_{ssp},f_{ssp},R_{C1}\right) := \frac{2}{3}\cdot\left(\frac{l_1\left(h_{c.ssp},\alpha_{ssp},f_{ssp},R_{C1}\right)}{h_{c.ssp}}\right)^2\cdot\frac{d_1\left(h_{c.ssp},\alpha_{ssp},f_{ssp},R_{C1}\right)}{h_{c.ssp}} + \frac{1}{4}\cdot\frac{f_{ssp}}{h_{c.ssp}} \cdots
$$

$$
+2\cdot\frac{R_{C1}}{h_{c.ssp}}\cdot\left[\frac{a_1\left(h_{c.ssp},R_{C1}\right)}{h_{c.ssp}}\cdot\left(\frac{\theta\left(h_{c.ssp},\alpha_{ssp},f_{ssp},R_{C1}\right)}{h_{c.ssp}} - \frac{a_1\left(h_{c.ssp},R_{C1}\right)}{h_{c.ssp}}\right) + 2\cdot\frac{g_1\left(h_{c.ssp},\alpha_{ssp},f_{ssp},R_{C1}\right)}{h_{c.ssp}}\right] \cdots
$$

$$
+\frac{g_1\left(h_{c.ssp},\alpha_{ssp},f_{ssp},R_{C1}\right)}{h_{c.ssp}}\cdot\frac{e_1\left(h_{c.ssp},\alpha_{ssp},f_{ssp},R_{C1}\right)}{h_{c.ssp}} + \frac{1}{2}\cdot\theta\left(h_{c.ssp},\alpha_{ssp},f_{ssp},R_{C1}\right)\cdot\left(\frac{R_{C1}}{h_{c.ssp}}\right)^2
$$

$$K_L\big(h_{c.ssp}, \alpha_{ssp}, f_{ssp}, R_{C1}\big) := 2 \cdot \dfrac{d_1\big(h_{c.ssp}, \alpha_{ssp}, f_{ssp}, R_{C1}\big)}{h_{c.ssp}} + 2 \cdot \theta\big(h_{c.ssp}, \alpha_{ssp}, f_{ssp}, R_{C1}\big) \cdot \dfrac{R_{C1}}{h_{c.ssp}} + \dfrac{f_{ssp}}{h_{c.ssp}}$$

$$K_{Ly}\big(h_{c.ssp}, \alpha_{ssp}, f_{ssp}, R_{C1}\big) := \dfrac{f_{ssp}}{h_{c.ssp}} + 2 \cdot \dfrac{d_1\big(h_{c.ssp}, \alpha_{ssp}, f_{ssp}, R_{C1}\big)}{h_{c.ssp}} \cdot \cos\big(\theta\big(h_{c.ssp}, \alpha_{ssp}, f_{ssp}, R_{C1}\big)\big)^2 \dots$$
$$+ \dfrac{R_{C1}}{h_{c.ssp}} \cdot \big(\theta\big(h_{c.ssp}, \alpha_{ssp}, f_{ssp}, R_{C1}\big) + \sin\big(\theta\big(h_{c.ssp}, \alpha_{ssp}, f_{ssp}, R_{C1}\big)\big) \cdot \cos\big(\theta\big(h_{c.ssp}, \alpha_{ssp}, f_{ssp}, R_{C1}\big)\big)\big)$$

$$K_{Lyz}\big(h_{c.ssp}, \alpha_{ssp}, f_{ssp}, R_{C1}\big) := 2 \cdot \dfrac{d_1\big(h_{c.ssp}, \alpha_{ssp}, f_{ssp}, R_{C1}\big)}{h_{c.ssp}} \cdot \sin\big(\theta\big(h_{c.ssp}, \alpha_{ssp}, f_{ssp}, R_{C1}\big)\big) \cdot \cos\big(\theta\big(h_{c.ssp}, \alpha_{ssp}, f_{ssp}, R_{C1}\big)\big) \dots$$
$$+ \dfrac{R_{C1}}{h_{c.ssp}} \cdot \sin\big(\theta\big(h_{c.ssp}, \alpha_{ssp}, f_{ssp}, R_{C1}\big)\big)^2$$

$$K_{Lz}\big(h_{c.ssp}, \alpha_{ssp}, f_{ssp}, R_{C1}\big) := 2 \cdot \dfrac{d_1\big(h_{c.ssp}, \alpha_{ssp}, f_{ssp}, R_{C1}\big)}{h_{c.ssp}} \cdot \sin\big(\theta\big(h_{c.ssp}, \alpha_{ssp}, f_{ssp}, R_{C1}\big)\big)^2 \dots$$
$$+ \dfrac{R_{C1}}{h_{c.ssp}} \cdot \big(\theta\big(h_{c.ssp}, \alpha_{ssp}, f_{ssp}, R_{C1}\big) - \sin\big(\theta\big(h_{c.ssp}, \alpha_{ssp}, f_{ssp}, R_{C1}\big)\big) \cdot \cos\big(\theta\big(h_{c.ssp}, \alpha_{ssp}, f_{ssp}, R_{C1}\big)\big)\big)$$

C expressions

$$C_1\left(h_{c.ssp}, t_{f.top}, t_{c.ssp}, \alpha_{ssp}, f_{ssp}, R_{C1}\right) := K_L\left(h_{c.ssp}, \alpha_{ssp}, f_{ssp}, R_{C1}\right) + \frac{1}{3}\cdot\left(\frac{t_{c.ssp}}{t_{f.top}}\right)^3 \cdot \frac{p_{ssp}\left(h_{c.ssp}, \alpha_{ssp}, f_{ssp}\right)}{h_{c.ssp}}$$

$$C_2\left(h_{c.ssp}, \alpha_{ssp}, f_{ssp}, R_{C1}\right) := \frac{k_y}{2}\cdot\frac{p_{ssp}\left(h_{c.ssp}, \alpha_{ssp}, f_{ssp}\right)}{h_{c.ssp}}\cdot K_L\left(h_{c.ssp}, \alpha_{ssp}, f_{ssp}, R_{C1}\right)$$

$$C_3\left(h_{c.ssp}, t_{c.ssp}, \alpha_{ssp}, f_{ssp}, R_{C1}\right) := K_{Iz}\left(h_{c.ssp}, \alpha_{ssp}, f_{ssp}, R_{C1}\right) + k_y\cdot\frac{p_{ssp}\left(h_{c.ssp}, \alpha_{ssp}, f_{ssp}\right)}{h_{c.ssp}}\cdot\left(\frac{k_y}{4}\cdot\frac{p_{ssp}\left(h_{c.ssp}, \alpha_{ssp}, f_{ssp}\right)}{h_{c.ssp}}\cdot K_L\left(h_{c.ssp}, \alpha_{ssp}, f_{ssp}, R_{C1}\right)\right)\dots$$
$$+ \frac{1}{12}\cdot\left(\frac{t_{c.ssp}}{h_{c.ssp}}\right)^2\cdot K_{Lz}\left(h_{c.ssp}, \alpha_{ssp}, f_{ssp}, R_{C1}\right)$$

$$C_4\left(h_{c.ssp}, t_{f.top}, t_{c.ssp}, \alpha_{ssp}, f_{ssp}, R_{C1}\right) := K_{Iyz}\left(h_{c.ssp}, \alpha_{ssp}, f_{ssp}, R_{C1}\right)\dots$$
$$+ \frac{1}{2}\cdot\left[k_z + \left(1+\frac{t_{f.top}}{t_{c.ssp}}\right)\cdot\frac{t_{c.ssp}}{h_{c.ssp}}\right]\cdot\left(\frac{k_y}{2}\cdot\frac{p_{ssp}\left(h_{c.ssp}, \alpha_{ssp}, f_{ssp}\right)}{h_{c.ssp}}\cdot K_L\left(h_{c.ssp}, \alpha_{ssp}, f_{ssp}, R_{C1}\right)\right)\dots$$
$$+ \frac{1}{12}\cdot\left(\frac{t_{c.ssp}}{h_{c.ssp}}\right)^2\cdot K_{Lyz}\left(h_{c.ssp}, \alpha_{ssp}, f_{ssp}, R_{C1}\right)$$

$$C_5\left(h_{c.ssp}, t_{f.top}, t_{c.ssp}, \alpha_{ssp}, f_{ssp}, R_{C1}\right) := \frac{1}{2}\cdot\left[k_z + \left(1+\frac{t_{f.top}}{t_{c.ssp}}\right)\cdot\frac{t_{c.ssp}}{h_{c.ssp}}\right]\cdot K_L\left(h_{c.ssp}, \alpha_{ssp}, f_{ssp}, R_{C1}\right)$$

$$C_6\left(h_{c.ssp}, t_{f.top}, t_{c.ssp}, \alpha_{ssp}, f_{ssp}, R_{C1}\right) := K_{Iy}\left(h_{c.ssp}, \alpha_{ssp}, f_{ssp}, R_{C1}\right)\dots$$
$$+ \left[k_z + \left(1+\frac{t_{f.top}}{t_{c.ssp}}\right)\cdot\frac{t_{c.ssp}}{h_{c.ssp}}\right]\cdot\left[\frac{1}{4}\cdot k_z + \left(\left(1+\frac{t_{f.top}}{t_{c.ssp}}\right)\cdot\frac{t_{c.ssp}}{h_{c.ssp}}\right)\right]\cdot K_L\left(h_{c.ssp}, \alpha_{ssp}, f_{ssp}, R_{C1}\right)\dots$$
$$+ \frac{1}{12}\cdot\left(\frac{t_{c.ssp}}{h_{c.ssp}}\right)^2\cdot K_{Ly}\left(h_{c.ssp}, \alpha_{ssp}, f_{ssp}, R_{C1}\right)$$

$$C_7\left(t_{f.bot}, t_{c.ssp}\right) := \left(\frac{t_{f.bot}}{t_{c.ssp}}\right)^3$$

$$S_1\left(h_{c.ssp}, t_{f.top}, t_{f.bot}, t_{c.ssp}, \alpha_{ssp}, f_{ssp}, R_{C1}\right) := \frac{p_{ssp}\left(h_{c.ssp}, \alpha_{ssp}, f_{ssp}\right)}{h_{c.ssp}} \cdot \left(\begin{array}{l} C_1\left(h_{c.ssp}, t_{f.top}, t_{c.ssp}, \alpha_{ssp}, f_{ssp}, R_{C1}\right) \cdot C_4\left(h_{c.ssp}, t_{f.top}, t_{c.ssp}, \alpha_{ssp}, f_{ssp}, R_{C1}\right) \cdots \\ +-C_2\left(h_{c.ssp}, \alpha_{ssp}, f_{ssp}, R_{C1}\right) \cdot C_4\left(h_{c.ssp}, t_{f.top}, t_{c.ssp}, \alpha_{ssp}, f_{ssp}, R_{C1}\right) \cdot C_5\left(h_{c.ssp}, t_{f.top}, t_{c.ssp}, \alpha_{ssp}, f_{ssp}, R_{C1}\right) \cdots \\ +-C_3\left(h_{c.ssp}, t_{f.top}, t_{c.ssp}, \alpha_{ssp}, f_{ssp}, R_{C1}\right) \cdot C_5\left(h_{c.ssp}, t_{f.top}, t_{c.ssp}, \alpha_{ssp}, f_{ssp}, R_{C1}\right) \end{array} \right)$$

$$S_2\left(h_{c.ssp}, t_{f.top}, t_{f.bot}, t_{c.ssp}, \alpha_{ssp}, f_{ssp}, R_{C1}\right) := \begin{array}{l} C_1\left(h_{c.ssp}, t_{f.top}, t_{c.ssp}, \alpha_{ssp}, f_{ssp}, R_{C1}\right) \cdot C_4\left(h_{c.ssp}, t_{f.top}, t_{c.ssp}, \alpha_{ssp}, f_{ssp}, R_{C1}\right) \cdots \\ +-2 \cdot C_2\left(h_{c.ssp}, \alpha_{ssp}, f_{ssp}, R_{C1}\right) \cdot C_5\left(h_{c.ssp}, t_{f.top}, t_{c.ssp}, \alpha_{ssp}, f_{ssp}, R_{C1}\right) \end{array}$$

$$S_3\left(h_{c.ssp}, t_{f.top}, t_{f.bot}, t_{c.ssp}, \alpha_{ssp}, f_{ssp}, R_{C1}\right) := \begin{array}{l} C_4\left(h_{c.ssp}, t_{f.top}, t_{c.ssp}, \alpha_{ssp}, f_{ssp}, R_{C1}\right) \cdot S_2\left(h_{c.ssp}, t_{f.top}, t_{f.bot}, t_{c.ssp}, \alpha_{ssp}, f_{ssp}, R_{C1}\right) \cdots \\ +C_3\left(h_{c.ssp}, t_{c.ssp}, \alpha_{ssp}, f_{ssp}, R_{C1}\right) \cdot C_5\left(h_{c.ssp}, t_{f.top}, t_{c.ssp}, \alpha_{ssp}, f_{ssp}, R_{C1}\right)^2 \cdots \\ +-C_6\left(h_{c.ssp}, t_{f.top}, t_{c.ssp}, \alpha_{ssp}, f_{ssp}, R_{C1}\right) \cdot \left(\begin{array}{l} C_1\left(h_{c.ssp}, t_{f.top}, t_{c.ssp}, \alpha_{ssp}, f_{ssp}, R_{C1}\right) \cdot C_3\left(h_{c.ssp}, t_{c.ssp}, \alpha_{ssp}, f_{ssp}, R_{C1}\right) \cdots \\ +-C_2\left(h_{c.ssp}, \alpha_{ssp}, f_{ssp}, R_{C1}\right)^2 \end{array} \right) \end{array}$$

$$S_4\left(h_{c.ssp}, t_{f.top}, t_{f.bot}, t_{c.ssp}, \alpha_{ssp}, f_{ssp}, R_{C1}\right) := 3 \cdot C_7\left(t_{f.bot}, t_{c.ssp}\right) \cdot S_3\left(h_{c.ssp}, t_{f.top}, t_{f.bot}, t_{c.ssp}, \alpha_{ssp}, f_{ssp}, R_{C1}\right) \cdots$$
$$+\frac{p_{ssp}\left(h_{c.ssp}, \alpha_{ssp}, f_{ssp}\right)}{h_{c.ssp}} \cdot \left(\begin{array}{l} C_4\left(h_{c.ssp}, t_{f.top}, t_{c.ssp}, \alpha_{ssp}, f_{ssp}, R_{C1}\right)^2 \cdots \\ +-C_3\left(h_{c.ssp}, t_{c.ssp}, \alpha_{ssp}, f_{ssp}, R_{C1}\right) \cdot C_6\left(h_{c.ssp}, t_{f.top}, t_{c.ssp}, \alpha_{ssp}, f_{ssp}, R_{C1}\right) \end{array} \right) \cdots$$
$$+2 \cdot \left(\frac{p_{ssp}\left(h_{c.ssp}, \alpha_{ssp}, f_{ssp}\right)}{h_{c.ssp}} \right)^2 \cdot \left(\begin{array}{l} C_2\left(h_{c.ssp}, \alpha_{ssp}, f_{ssp}, R_{C1}\right) \cdot C_6\left(h_{c.ssp}, t_{f.top}, t_{c.ssp}, \alpha_{ssp}, f_{ssp}, R_{C1}\right) \cdots \\ +-C_4\left(h_{c.ssp}, t_{f.top}, t_{c.ssp}, \alpha_{ssp}, f_{ssp}, R_{C1}\right) \cdot C_5\left(h_{c.ssp}, t_{f.top}, t_{c.ssp}, \alpha_{ssp}, f_{ssp}, R_{C1}\right) \end{array} \right) \cdots$$
$$+\left(\frac{p_{ssp}\left(h_{c.ssp}, \alpha_{ssp}, f_{ssp}\right)}{h_{c.ssp}} \right)^3 \cdot \left(\begin{array}{l} C_5\left(h_{c.ssp}, t_{f.top}, t_{c.ssp}, \alpha_{ssp}, f_{ssp}, R_{C1}\right)^2 \cdots \\ +-C_1\left(h_{c.ssp}, t_{f.top}, t_{c.ssp}, \alpha_{ssp}, f_{ssp}, R_{C1}\right) \cdot C_6\left(h_{c.ssp}, t_{f.top}, t_{c.ssp}, \alpha_{ssp}, f_{ssp}, R_{C1}\right) \end{array} \right)$$

$$S_5\left(h_{c.ssp}, t_{f.top}, t_{f.bot}, t_{c.ssp}, \alpha_{ssp}, f_{ssp}, R_{C1}\right) := \begin{array}{l} C_2\left(h_{c.ssp}, \alpha_{ssp}, f_{ssp}, R_{C1}\right)^2 \cdots \\ +-C_1\left(h_{c.ssp}, t_{f.top}, t_{c.ssp}, \alpha_{ssp}, f_{ssp}, R_{C1}\right) \cdot C_3\left(h_{c.ssp}, t_{c.ssp}, \alpha_{ssp}, f_{ssp}, R_{C1}\right) \end{array}$$

$$S_6\left(h_{c.ssp}, t_{f.top}, t_{f.bot}, t_{c.ssp}, \alpha_{ssp}, f_{ssp}, R_{C1}\right) := 12 \cdot \left[\frac{\frac{2 p_{ssp}\left(h_{c.ssp}, \alpha_{ssp}, f_{ssp}\right)}{h_{c.ssp}} \cdot S_1\left(h_{c.ssp}, t_{f.top}, t_{f.bot}, t_{c.ssp}, \alpha_{ssp}, f_{ssp}, R_{C1}\right) \cdots}{} + \frac{h_{c.ssp}\left(h_{c.ssp}, t_{f.top}, t_{f.bot}, t_{c.ssp}\right)}{h_{c.ssp}} \cdot S_4\left(h_{c.ssp}, t_{f.top}, t_{f.bot}, t_{c.ssp}, \alpha_{ssp}, f_{ssp}, R_{C1}\right) \cdots + \frac{h_{ssp}\left(h_{c.ssp}, t_{f.top}, t_{f.bot}, t_{c.ssp}\right)}{h_{c.ssp}} \cdot \frac{p_{ssp}\left(h_{c.ssp}, \alpha_{ssp}, f_{ssp}\right)}{h_{c.ssp}} \cdot \left(S_5\left(h_{c.ssp}, t_{f.top}, t_{f.bot}, t_{c.ssp}, \alpha_{ssp}, f_{ssp}, R_{C1}\right)\right) \right]$$

$$
S\left(h_{c.ssp}, t_{f.top}, t_{f.bot}, t_{c.ssp}, \alpha_{ssp}, f_{ssp}, R_{C1}\right) :=
$$

$$
\frac{\dfrac{3 h_{c.ssp} \cdot C_7\!\left(t_{f.bot}, t_{c.ssp}\right)}{p_{ssp}\!\left(h_{c.ssp}, \alpha_{ssp}, f_{ssp}\right)} \cdot \left[\dfrac{C_2\!\left(h_{c.ssp}, \alpha_{ssp}, f_{ssp}, R_{C1}\right)^2 \ldots}{+ -C_1\!\left(h_{c.ssp}, t_{f.top}, t_{c.ssp}, \alpha_{ssp}, f_{ssp}, R_{C1}\right) \ldots} \cdot C_3\!\left(h_{c.ssp}, t_{c.ssp}, \alpha_{ssp}, f_{ssp}, R_{C1}\right) \right] \ldots}{\;}
$$

$$
\frac{+ \dfrac{-C_3\!\left(h_{c.ssp}, t_{c.ssp}, \alpha_{ssp}, f_{ssp}, R_{C1}\right) \ldots}{p_{ssp}\!\left(h_{c.ssp}, \alpha_{ssp}, f_{ssp}\right)} \ldots}{\;}
$$

$$
\frac{+ \dfrac{\dfrac{p_{ssp}\!\left(h_{c.ssp}, \alpha_{ssp}, f_{ssp}\right)}{h_{c.ssp}} \cdot \left[2 \cdot C_2\!\left(h_{c.ssp}, \alpha_{ssp}, f_{ssp}, R_{C1}\right) \ldots + -\dfrac{p_{ssp}\!\left(h_{c.ssp}, \alpha_{ssp}, f_{ssp}\right)}{h_{c.ssp}} \cdot C_1\!\left(h_{c.ssp}, t_{f.top}, t_{c.ssp}, \alpha_{ssp}, f_{ssp}, R_{C1}\right) \right]}{h_{c.ssp}}}{S_6\!\left(h_{c.ssp}, t_{f.top}, t_{f.bot}, t_{c.ssp}, \alpha_{ssp}, f_{ssp}, R_{C1}\right)}
$$

$$
D_{Qy}\left(h_{c.ssp}, t_{f.top}, t_{f.bot}, t_{c.ssp}, \alpha_{ssp}, f_{ssp}\right) := S\left(h_{c.ssp}, t_{f.top}, t_{f.bot}, t_{c.ssp}, \alpha_{ssp}, f_{ssp}, R_{C1}\right) \cdot h_{ssp}\left(h_{c.ssp}, t_{f.top}, t_{f.bot}, t_{c.ssp}\right) \cdot \left(\frac{E_{S355N}}{1 - \nu^2}\right) \cdot \left(\frac{t_{c.ssp}}{h_{c.ssp}}\right)^3
$$

Concentrated load for the main truck

Point load

$Q_{wheel} := Q_{comb.local.1} = 150 \cdot kN$

$q_{wheel} := \dfrac{Q_{wheel}}{b_{wheel.pl}} = 300 \cdot \dfrac{kN}{m}$

Local deflection over the buckling part or the top flange of the SSE

$I_{buck}(t_{f.top}) := \dfrac{b_{wheel.pl} \cdot t_{f.top}^3}{12}$

$\delta_I(h_{c.ssp}, t_{f.top}, \alpha_{ssp}, f_{ssp}) := \dfrac{q_{wheel} \cdot l_{ssp}(h_{c.ssp}, \alpha_{ssp}, f_{ssp})^4}{384 \cdot E_{S355N} \cdot I_{buck}(t_{f.top})}$
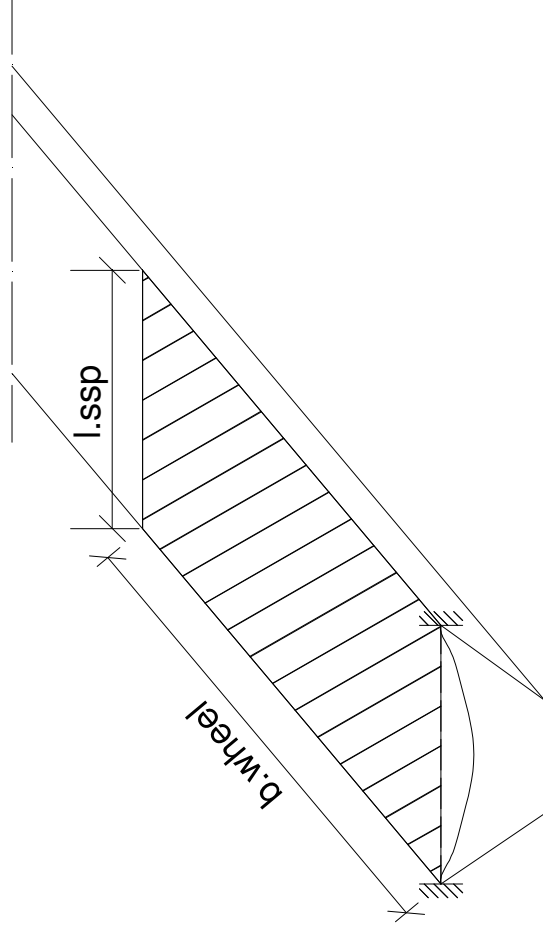
Loads

$q_{comb.gl.pl.1} := q_{main} = 9 \cdot \dfrac{kN}{m^2}$

Total load of the combination for the global deflection of the plate

$q_{comb.gl.pl.2} := q_{other} = 2.5 \cdot \dfrac{kN}{m^2}$

Total load of the combination for the global deflection of the plate

$Q_{comb.gl.pl.1} := Q_{1.wheel} = 150 \cdot kN$

Wheel load of the main truck

$Q_{comb.gl.pl.2} := Q_{2.wheel} = 100 \cdot kN$

Wheel load of the medium truck

$Q_{comb.gl.pl.3} := Q_{3.wheel} = 50 \cdot kN$

Wheel load of the small truck

Values for minimum deflection

Assuming that the crash barrier is 0.406m, the clear distance of half of the plate is:

$l_{HK.half.deck} := \dfrac{l_{HK.f.top} - 0.406m}{2} = 9\,m$

Clear distance for half of the bridge deck

$l_{lane} := 3m$

Length of the each lane

The maximum global deflection of the plate is going to be performed under the below loading condition. The small truck is neglected according to the Swedish legislation but also due to the initial construction of the Höga Kusten Bridge, where just 2 lanes are designed.
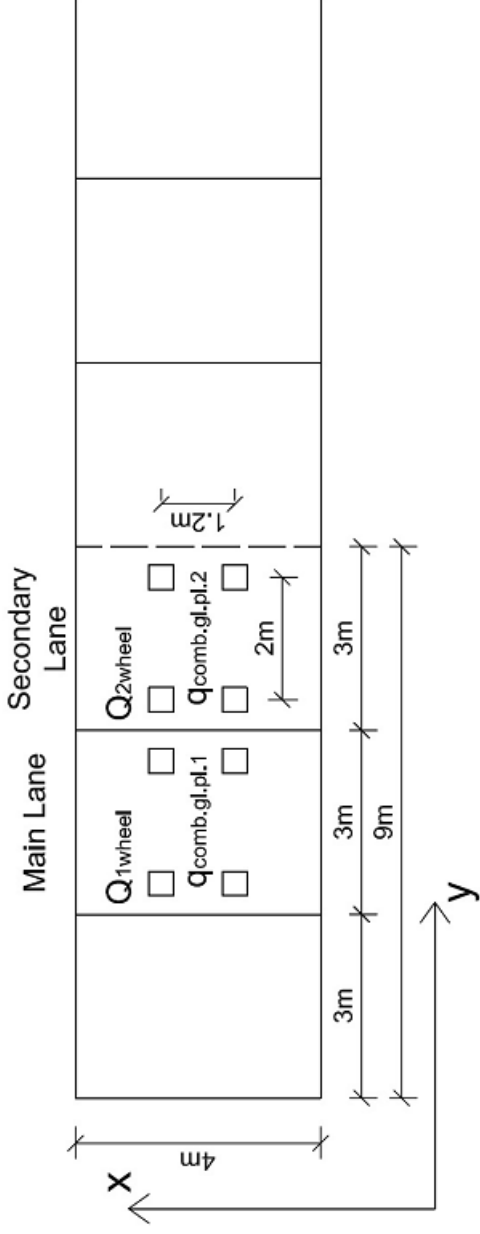
Uniformly distributed load

As there is no possibility of finding with hand calculations the global deflection of a plate, where different uniformly distributed loads are acting with Chang's formulas, an equivalent load is going to be used.

$$q_{eq.d} := \frac{q_{comb.gl.pl.1} \cdot l_{lane} + q_{comb.gl.pl.2} \cdot \left(l_{HK.half.deck} - l_{lane}\right)}{l_{HK.half.deck}} = 4.667 \cdot \frac{kN}{m^2}$$

Equivalent distributed load

Dimensions

$B_{ssp} := l_{HK.half.deck} = 9\,m$

$L_{ssp} := l_{long.stif} = 4\,m$

Loads

$q_{self}\left(h_{c.ssp}, t_{f.top}, t_{f.bot}, t_{c.ssp}, \alpha_{ssp}, f_{ssp}\right) := G_{ssp}\left(h_{c.ssp}, t_{f.top}, t_{f.bot}, t_{c.ssp}, \alpha_{ssp}, f_{ssp}\right) g$

$q_{1d}\left(h_{c.ssp}, t_{f.top}, t_{f.bot}, t_{c.ssp}, \alpha_{ssp}, f_{ssp}\right) := q_{self}\left(h_{c.ssp}, t_{f.top}, t_{f.bot}, t_{c.ssp}, \alpha_{ssp}, f_{ssp}\right) + a_d \cdot t_{cover} + q_{eq.d}$ Distributed load in the bridge deck

Poisson's ratio

$$\nu_{.xy} := \nu = 0.3$$

$$\nu_{.yx}\left(h_{c.ssp}, t_{f.top}, t_{f.bot}, t_{c.ssp}, \alpha_{ssp}, f_{ssp}\right) := \nu_{xy} \cdot \frac{D_{y.ssp}\left(h_{c.ssp}, t_{f.top}, t_{f.bot}, t_{c.ssp}, \alpha_{ssp}, f_{ssp}\right)}{D_{x.ssp}\left(h_{c.ssp}, t_{f.top}, t_{f.bot}, t_{c.ssp}, \alpha_{ssp}, f_{ssp}\right)}$$

$$\nu_{.p}\left(h_{c.ssp}, t_{f.top}, t_{f.bot}, t_{c.ssp}, \alpha_{ssp}, f_{ssp}\right) := 1 - \nu_{xy}^{2} \cdot \frac{D_{y.ssp}\left(h_{c.ssp}, t_{f.top}, t_{f.bot}, t_{c.ssp}, \alpha_{ssp}, f_{ssp}\right)}{D_{x.ssp}\left(h_{c.ssp}, t_{f.top}, t_{f.bot}, t_{c.ssp}, \alpha_{ssp}, f_{ssp}\right)}$$

Coefficients used in displacment expression

$$D_{xx}\left(h_{c.ssp}, t_{f.top}, t_{f.bot}, t_{c.ssp}, \alpha_{ssp}, f_{ssp}\right) := \frac{D_{x.ssp}\left(h_{c.ssp}, t_{f.top}, t_{f.bot}, t_{c.ssp}, \alpha_{ssp}, f_{ssp}\right)}{1 - \nu_{xy} \cdot \nu_{.yx}\left(h_{c.ssp}, t_{f.top}, t_{f.bot}, t_{c.ssp}, \alpha_{ssp}, f_{ssp}\right)}$$

$$D_{yy}\left(h_{c.ssp}, t_{f.top}, t_{f.bot}, t_{c.ssp}, \alpha_{ssp}, f_{ssp}\right) := \frac{D_{y.ssp}\left(h_{c.ssp}, t_{f.top}, t_{f.bot}, t_{c.ssp}, \alpha_{ssp}, f_{ssp}\right)}{1 - \nu_{xy} \cdot \nu_{.yx}\left(h_{c.ssp}, t_{f.top}, t_{f.bot}, t_{c.ssp}, \alpha_{ssp}, f_{ssp}\right)}$$

The critical deflection appears in the middle of the plate

$$X := \frac{L_{ssp}}{2} = 2\,\mathrm{m} \qquad Y := \frac{B_{ssp}}{2} = 4.5\,\mathrm{m}$$

$$i := 1..1 \qquad j := 1..1$$

$$w_{ssp.1.ij}\left(h_{c.ssp}, t_{f.top}, t_{f.bot}, t_{c.ssp}, \alpha_{ssp}, f_{ssp}, i, j\right) := 2 \cdot D_{Qx}\left(h_{c.ssp}, t_{f.top}, t_{f.bot}, t_{c.ssp}, \alpha_{ssp}, f_{ssp}\right) \cdot D_{Qy}\left(h_{c.ssp}, t_{f.top}, t_{f.bot}, t_{c.ssp}, \alpha_{ssp}, f_{ssp}\right) \cdot L_{ssp}^{4} \cdot B_{ssp}^{4} \ldots$$
$$+ D_{xx}\left(h_{c.ssp}, t_{f.top}, t_{f.bot}, t_{c.ssp}, \alpha_{ssp}, f_{ssp}\right) \cdot D_{xy.ssp}\left(h_{c.ssp}, t_{f.top}, t_{f.bot}, t_{c.ssp}, \alpha_{ssp}, f_{ssp}\right) \cdot \pi^{4} \cdot B_{ssp}^{4} \cdot i^{4} \ldots$$
$$+ D_{xy.ssp}\left(h_{c.ssp}, t_{f.top}, t_{f.bot}, t_{c.ssp}, \alpha_{ssp}, f_{ssp}\right) \cdot D_{yy}\left(h_{c.ssp}, t_{f.top}, t_{f.bot}, t_{c.ssp}, \alpha_{ssp}, f_{ssp}\right) \cdot \pi^{4} \cdot L_{ssp}^{4} \cdot j^{4} \ldots$$
$$+ D_{Qx}\left(h_{c.ssp}, t_{f.top}, t_{f.bot}, t_{c.ssp}, \alpha_{ssp}, f_{ssp}\right) \cdot D_{xy.ssp}\left(h_{c.ssp}, t_{f.top}, t_{f.bot}, t_{c.ssp}, \alpha_{ssp}, f_{ssp}\right) \cdot \pi^{2} \cdot L_{ssp}^{2} \cdot B_{ssp}^{4} \cdot i^{2} \ldots$$
$$+ 2 \cdot D_{Qy}\left(h_{c.ssp}, t_{f.top}, t_{f.bot}, t_{c.ssp}, \alpha_{ssp}, f_{ssp}\right) \cdot D_{xx}\left(h_{c.ssp}, t_{f.top}, t_{f.bot}, t_{c.ssp}, \alpha_{ssp}, f_{ssp}\right) \cdot \pi^{2} \cdot L_{ssp}^{2} \cdot B_{ssp}^{4} \cdot i^{2} \ldots$$
$$+ D_{Qy}\left(h_{c.ssp}, t_{f.top}, t_{f.bot}, t_{c.ssp}, \alpha_{ssp}, f_{ssp}\right) \cdot D_{xy.ssp}\left(h_{c.ssp}, t_{f.top}, t_{f.bot}, t_{c.ssp}, \alpha_{ssp}, f_{ssp}\right) \cdot \pi^{2} \cdot L_{ssp}^{4} \cdot B_{ssp}^{2} \cdot j^{2} \ldots$$
$$+ 2 \cdot D_{Qx}\left(h_{c.ssp}, t_{f.top}, t_{f.bot}, t_{c.ssp}, \alpha_{ssp}, f_{ssp}\right) \cdot D_{yy}\left(h_{c.ssp}, t_{f.top}, t_{f.bot}, t_{c.ssp}, \alpha_{ssp}, f_{ssp}\right) \cdot \pi^{2} \cdot L_{ssp}^{4} \cdot B_{ssp}^{2} \cdot j^{2} \ldots$$
$$+ 2 \cdot D_{xx}\left(h_{c.ssp}, t_{f.top}, t_{f.bot}, t_{c.ssp}, \alpha_{ssp}, f_{ssp}\right) \cdot D_{yy}\left(h_{c.ssp}, t_{f.top}, t_{f.bot}, t_{c.ssp}, \alpha_{ssp}, f_{ssp}\right) \cdot \pi^{4} \cdot L_{ssp}^{2} \cdot B_{ssp}^{2} \cdot i^{2} \cdot j^{2} \ldots$$
$$+ -D_{xx}\left(h_{c.ssp}, t_{f.top}, t_{f.bot}, t_{c.ssp}, \alpha_{ssp}, f_{ssp}\right) \cdot D_{yy}\left(h_{c.ssp}, t_{f.top}, t_{f.bot}, t_{c.ssp}, \alpha_{ssp}, f_{ssp}\right) \cdot \pi^{4} \cdot L_{ssp}^{2} \cdot B_{ssp}^{2} \cdot i^{2} \cdot j^{2} \cdot \nu_{xy} \ldots$$
$$+ -D_{xy.ssp}\left(h_{c.ssp}, t_{f.top}, t_{f.bot}, t_{c.ssp}, \alpha_{ssp}, f_{ssp}\right) \cdot D_{yy}\left(h_{c.ssp}, t_{f.top}, t_{f.bot}, t_{c.ssp}, \alpha_{ssp}, f_{ssp}\right) \cdot \pi^{4} \cdot L_{ssp}^{2} \cdot B_{ssp}^{2} \cdot i^{2} \cdot j^{2} \cdot \nu_{xy} \cdot \nu_{.yx}\left(h_{c.ssp}, t_{f.top}, t_{f.bot}, t_{c.ssp}, \alpha_{ssp}, f_{ssp}\right) \ldots$$
$$+ -2 \cdot D_{xx}\left(h_{c.ssp}, t_{f.top}, t_{f.bot}, t_{c.ssp}, \alpha_{ssp}, f_{ssp}\right) \cdot D_{yy}\left(h_{c.ssp}, t_{f.top}, t_{f.bot}, t_{c.ssp}, \alpha_{ssp}, f_{ssp}\right) \cdot \pi^{4} \cdot L_{ssp}^{2} \cdot B_{ssp}^{2} \cdot i^{2} \cdot j^{2} \cdot \nu_{xy} \cdot \nu_{.yx}\left(h_{c.ssp}, t_{f.top}, t_{f.bot}, t_{c.ssp}, \alpha_{ssp}, f_{ssp}\right)$$

$$w_{ssp.2.ij}\left(h_{c.ssp}, t_{f.top}, t_{f.bot}, t_{c.ssp}, \alpha_{ssp}, f_{ssp}, i, j\right) := D_{Qx}\left(h_{c.ssp}, t_{f.top}, t_{f.bot}, t_{c.ssp}, \alpha_{ssp}, f_{ssp}\right) \cdot D_{xx}\left(h_{c.ssp}, t_{f.top}, t_{f.bot}, t_{c.ssp}, \alpha_{ssp}, f_{ssp}\right) \cdot D_{xy.ssp}\left(h_{c.ssp}, t_{f.top}, t_{f.bot}, t_{c.ssp}, \alpha_{ssp}, f_{ssp}\right) \cdot \pi^4 \cdot B_{ssp}^6 \cdot i^6 \; \dots$$

$$+\, D_{Qy}\left(h_{c.ssp}, t_{f.top}, t_{f.bot}, t_{c.ssp}, \alpha_{ssp}, f_{ssp}\right) \cdot D_{xy.ssp}\left(h_{c.ssp}, t_{f.top}, t_{f.bot}, t_{c.ssp}, \alpha_{ssp}, f_{ssp}\right) \cdot D_{yy}\left(h_{c.ssp}, t_{f.top}, t_{f.bot}, t_{c.ssp}, \alpha_{ssp}, f_{ssp}\right) \cdot \pi^4 \cdot L_{ssp}^6 \cdot j^6 \; \dots$$

$$+\, 2 \cdot D_{Qx}\left(h_{c.ssp}, t_{f.top}, t_{f.bot}, t_{c.ssp}, \alpha_{ssp}, f_{ssp}\right) \cdot D_{xx}\left(h_{c.ssp}, t_{f.top}, t_{f.bot}, t_{c.ssp}, \alpha_{ssp}, f_{ssp}\right) \cdot D_{yy}\left(h_{c.ssp}, t_{f.top}, t_{f.bot}, t_{c.ssp}, \alpha_{ssp}, f_{ssp}\right) \cdot \pi^2 \cdot L_{ssp}^2 \cdot B_{ssp}^4 \cdot i^4 \cdot j^2 \; \dots$$

$$+\, 2 \cdot D_{Qx}\left(h_{c.ssp}, t_{f.top}, t_{f.bot}, t_{c.ssp}, \alpha_{ssp}, f_{ssp}\right) \cdot D_{xx}\left(h_{c.ssp}, t_{f.top}, t_{f.bot}, t_{c.ssp}, \alpha_{ssp}, f_{ssp}\right) \cdot D_{yy}\left(h_{c.ssp}, t_{f.top}, t_{f.bot}, t_{c.ssp}, \alpha_{ssp}, f_{ssp}\right) \cdot \pi^2 \cdot L_{ssp}^2 \cdot B_{ssp}^4 \cdot i^4 \cdot j^2 \; \dots$$

$$+\, 4 \cdot D_{Qy}\left(h_{c.ssp}, t_{f.top}, t_{f.bot}, t_{c.ssp}, \alpha_{ssp}, f_{ssp}\right) \cdot D_{xx}\left(h_{c.ssp}, t_{f.top}, t_{f.bot}, t_{c.ssp}, \alpha_{ssp}, f_{ssp}\right) \cdot D_{yy}\left(h_{c.ssp}, t_{f.top}, t_{f.bot}, t_{c.ssp}, \alpha_{ssp}, f_{ssp}\right) \cdot \pi^2 \cdot L_{ssp}^2 \cdot B_{ssp}^4 \cdot i^4 \cdot j^2 \; \dots$$

$$+\, D_{Qy}\left(h_{c.ssp}, t_{f.top}, t_{f.bot}, t_{c.ssp}, \alpha_{ssp}, f_{ssp}\right) \cdot D_{xx}\left(h_{c.ssp}, t_{f.top}, t_{f.bot}, t_{c.ssp}, \alpha_{ssp}, f_{ssp}\right) \cdot D_{xy.ssp}\left(h_{c.ssp}, t_{f.top}, t_{f.bot}, t_{c.ssp}, \alpha_{ssp}, f_{ssp}\right) \cdot \pi^4 \cdot L_{ssp}^2 \cdot B_{ssp}^4 \cdot i^4 \cdot j^2 \; \dots$$

$$+\, 2 \cdot D_{Qx}\left(h_{c.ssp}, t_{f.top}, t_{f.bot}, t_{c.ssp}, \alpha_{ssp}, f_{ssp}\right) \cdot D_{xx}\left(h_{c.ssp}, t_{f.top}, t_{f.bot}, t_{c.ssp}, \alpha_{ssp}, f_{ssp}\right) \cdot D_{xy.ssp}\left(h_{c.ssp}, t_{f.top}, t_{f.bot}, t_{c.ssp}, \alpha_{ssp}, f_{ssp}\right) \cdot \pi^4 \cdot L_{ssp}^2 \cdot B_{ssp}^4 \cdot i^4 \cdot j^2 \; \dots$$

$$+\, D_{Qx}\left(h_{c.ssp}, t_{f.top}, t_{f.bot}, t_{c.ssp}, \alpha_{ssp}, f_{ssp}\right) \cdot D_{xy.ssp}\left(h_{c.ssp}, t_{f.top}, t_{f.bot}, t_{c.ssp}, \alpha_{ssp}, f_{ssp}\right) \cdot D_{yy}\left(h_{c.ssp}, t_{f.top}, t_{f.bot}, t_{c.ssp}, \alpha_{ssp}, f_{ssp}\right) \cdot \pi^4 \cdot L_{ssp}^4 \cdot B_{ssp}^2 \cdot i^2 \cdot j^4 \; \dots$$

$$+\, 2 \cdot D_{Qy}\left(h_{c.ssp}, t_{f.top}, t_{f.bot}, t_{c.ssp}, \alpha_{ssp}, f_{ssp}\right) \cdot D_{xy.ssp}\left(h_{c.ssp}, t_{f.top}, t_{f.bot}, t_{c.ssp}, \alpha_{ssp}, f_{ssp}\right) \cdot D_{yy}\left(h_{c.ssp}, t_{f.top}, t_{f.bot}, t_{c.ssp}, \alpha_{ssp}, f_{ssp}\right) \cdot \pi^4 \cdot L_{ssp}^4 \cdot B_{ssp}^2 \cdot i^2 \cdot j^4 \; \dots$$

$$+\, 2 \cdot D_{Qx}\left(h_{c.ssp}, t_{f.top}, t_{f.bot}, t_{c.ssp}, \alpha_{ssp}, f_{ssp}\right) \cdot D_{yy}\left(h_{c.ssp}, t_{f.top}, t_{f.bot}, t_{c.ssp}, \alpha_{ssp}, f_{ssp}\right) \cdot D_{xx}\left(h_{c.ssp}, t_{f.top}, t_{f.bot}, t_{c.ssp}, \alpha_{ssp}, f_{ssp}\right) \cdot \pi^2 \cdot L_{ssp}^4 \cdot B_{ssp}^2 \cdot i^2 \cdot j^4 \cdot \nu_{yx} \; \dots$$

$$+\, 2 \cdot D_{Qx}\left(h_{c.ssp}, t_{f.top}, t_{f.bot}, t_{c.ssp}, \alpha_{ssp}, f_{ssp}\right) \cdot D_{yy}\left(h_{c.ssp}, t_{f.top}, t_{f.bot}, t_{c.ssp}, \alpha_{ssp}, f_{ssp}\right) \cdot D_{xx}\left(h_{c.ssp}, t_{f.top}, t_{f.bot}, t_{c.ssp}, \alpha_{ssp}, f_{ssp}\right) \cdot \pi^2 \cdot L_{ssp}^4 \cdot B_{ssp}^2 \cdot i^2 \cdot j^4 \cdot \nu_{xy} \; \dots$$

$$+\, -D_{Qx}\left(h_{c.ssp}, t_{f.top}, t_{f.bot}, t_{c.ssp}, \alpha_{ssp}, f_{ssp}\right) \cdot D_{xy.ssp}\left(h_{c.ssp}, t_{f.top}, t_{f.bot}, t_{c.ssp}, \alpha_{ssp}, f_{ssp}\right) \cdot D_{yy}\left(h_{c.ssp}, t_{f.top}, t_{f.bot}, t_{c.ssp}, \alpha_{ssp}, f_{ssp}\right) \cdot \pi^4 \cdot L_{ssp}^2 \cdot B_{ssp}^4 \cdot i^4 \cdot j^2 \cdot \nu_{yx} \; \dots$$

$$+\, -D_{Qy}\left(h_{c.ssp}, t_{f.top}, t_{f.bot}, t_{c.ssp}, \alpha_{ssp}, f_{ssp}\right) \cdot D_{xy.ssp}\left(h_{c.ssp}, t_{f.top}, t_{f.bot}, t_{c.ssp}, \alpha_{ssp}, f_{ssp}\right) \cdot D_{xx}\left(h_{c.ssp}, t_{f.top}, t_{f.bot}, t_{c.ssp}, \alpha_{ssp}, f_{ssp}\right) \cdot \pi^4 \cdot L_{ssp}^2 \cdot B_{ssp}^4 \cdot i^4 \cdot j^2 \cdot \nu_{xy} \; \dots$$

$$+\, -D_{Qy}\left(h_{c.ssp}, t_{f.top}, t_{f.bot}, t_{c.ssp}, \alpha_{ssp}, f_{ssp}\right) \cdot D_{xy.ssp}\left(h_{c.ssp}, t_{f.top}, t_{f.bot}, t_{c.ssp}, \alpha_{ssp}, f_{ssp}\right) \cdot D_{yy}\left(h_{c.ssp}, t_{f.top}, t_{f.bot}, t_{c.ssp}, \alpha_{ssp}, f_{ssp}\right) \cdot \pi^4 \cdot L_{ssp}^4 \cdot B_{ssp}^2 \cdot i^2 \cdot j^4 \cdot \nu_{yx} \; \dots$$

$$+\, -2 \cdot D_{Qx}\left(h_{c.ssp}, t_{f.top}, t_{f.bot}, t_{c.ssp}, \alpha_{ssp}, f_{ssp}\right) \cdot D_{yy}\left(h_{c.ssp}, t_{f.top}, t_{f.bot}, t_{c.ssp}, \alpha_{ssp}, f_{ssp}\right) \cdot D_{xx}\left(h_{c.ssp}, t_{f.top}, t_{f.bot}, t_{c.ssp}, \alpha_{ssp}, f_{ssp}\right) \cdot \pi^2 \cdot L_{ssp}^4 \cdot B_{ssp}^2 \cdot i^2 \cdot j^4 \cdot \nu_{xy} \cdot \nu_{yx} \; \dots$$

$$+\, 2 \cdot D_{Qy}\left(h_{c.ssp}, t_{f.top}, t_{f.bot}, t_{c.ssp}, \alpha_{ssp}, f_{ssp}\right) \cdot D_{xx}\left(h_{c.ssp}, t_{f.top}, t_{f.bot}, t_{c.ssp}, \alpha_{ssp}, f_{ssp}\right) \cdot D_{yy}\left(h_{c.ssp}, t_{f.top}, t_{f.bot}, t_{c.ssp}, \alpha_{ssp}, f_{ssp}\right) \cdot \pi^2 \cdot L_{ssp}^2 \cdot B_{ssp}^4 \cdot i^4 \cdot j^2 \cdot \nu_{xy} \cdot \nu_{yx} \; \dots$$

$$w_{ssp.ij}\left(h_{c.ssp}, t_{f.top}, t_{f.bot}, t_{c.ssp}, \alpha_{ssp}, f_{ssp}, i, j\right) := \frac{L_{ssp}^2 \cdot B_{ssp}^2 \cdot w_{ssp.1.ij}\left(h_{c.ssp}, t_{f.top}, t_{f.bot}, t_{c.ssp}, \alpha_{ssp}, f_{ssp}, i, j\right)}{\pi^2 \cdot w_{ssp.2.ij}\left(h_{c.ssp}, t_{f.top}, t_{f.bot}, t_{c.ssp}, \alpha_{ssp}, f_{ssp}, i, j\right)}$$

$$q_{ssp.C}\left(h_{c.ssp}, t_{f.top}, t_{f.bot}, t_{c.ssp}, \alpha_{ssp}, f_{ssp}, i, j\right) := \frac{4 \cdot q_{1d}\left(h_{c.ssp}, t_{f.top}, t_{f.bot}, t_{c.ssp}, \alpha_{ssp}, f_{ssp}\right)}{i \cdot j \cdot \pi^2} \cdot \left[1 - (-1)^i\right] \cdot \left[1 - (-1)^j\right]$$

Deflection due to each load

Distributed load

$$w_{UDL}\left(h_{c.ssp}, t_{f.top}, t_{f.bot}, t_{c.ssp}, \alpha_{ssp}, f_{ssp}\right) := \sum_j \left[\sum_i \left(w_{ssp.ij}\left(h_{c.ssp}, t_{f.top}, t_{f.bot}, t_{c.ssp}, \alpha_{ssp}, f_{ssp}, i, j\right) \cdot q_{ssp.C}\left(h_{c.ssp}, t_{f.top}, t_{f.bot}, t_{c.ssp}, \alpha_{ssp}, f_{ssp}, i, j\right) \cdot \sin\left(\frac{i \cdot \pi \cdot X}{L_{ssp}}\right) \cdot \sin\left(\frac{j \cdot \pi \cdot Y}{B_{ssp}}\right) \right) \right]$$

Big Truck- Four wheel loads symmetric around the center

Wheel load 1

$$x_{ssp.big.1} := \frac{L_{ssp}}{2} + 0.6\,m = 2.6\,m \qquad y_{ssp.big.1} := \frac{B_{ssp}}{2} - 1\,m = 3.5\,m$$

$$Q_{ssp.big.1}(i,j) := \frac{4 \cdot Q_{comb.gl.pl.1}}{L_{ssp} \cdot B_{ssp}} \cdot \sin\left(\frac{i\,\pi \cdot x_{ssp.big.1}}{L_{ssp}}\right) \cdot \sin\left(\frac{j\,\pi \cdot y_{ssp.big.1}}{B_{ssp}}\right)$$

Wheel load 2

$$x_{ssp.big.2} := \frac{L_{ssp}}{2} + 0.6\,m = 2.6\,m \qquad y_{ssp.big.2} := \frac{B_{ssp}}{2} + 1\,m = 5.5\,m$$

$$Q_{ssp.big.2}(i,j) := \frac{4 \cdot Q_{comb.gl.pl.1}}{L_{ssp} \cdot B_{ssp}} \cdot \sin\left(\frac{i\,\pi \cdot x_{ssp.big.2}}{L_{ssp}}\right) \cdot \sin\left(\frac{j\,\pi \cdot y_{ssp.big.2}}{B_{ssp}}\right)$$

Wheel load 3

$$x_{ssp.big.3} := \frac{L_{ssp}}{2} - 0.6\,m = 1.4\,m \qquad y_{ssp.big.3} := \frac{B_{ssp}}{2} - 1\,m = 3.5\,m$$

$$Q_{ssp.big.3}(i,j) := \frac{4 \cdot Q_{comb.gl.pl.1}}{L_{ssp} \cdot B_{ssp}} \cdot \sin\left(\frac{i\,\pi \cdot x_{ssp.big.3}}{L_{ssp}}\right) \cdot \sin\left(\frac{j\,\pi \cdot y_{ssp.big.3}}{B_{ssp}}\right)$$

Wheel load 4

$$x_{ssp.big.4} := \frac{L_{ssp}}{2} - 0.6\,m = 1.4\,m \qquad y_{ssp.big.4} := \frac{B_{ssp}}{2} + 1\,m = 5.5\,m$$

$$Q_{ssp.big.4}(i,j) := \frac{4 \cdot Q_{comb.gl.pl.1}}{L_{ssp} \cdot B_{ssp}} \cdot \sin\left(\frac{i\,\pi \cdot x_{ssp.big.4}}{L_{ssp}}\right) \cdot \sin\left(\frac{j\,\pi \cdot y_{ssp.big.4}}{B_{ssp}}\right)$$

Wheel load 1

$$w_{ssp.big.1}(h_{c.ssp}, t_{f.top}, t_{f.bot}, t_{c.ssp}, \alpha_{ssp}, f_{ssp}) := \sum_{j}\left[\sum_{i}\left[w_{ssp.ij}(h_{c.ssp}, t_{f.top}, t_{f.bot}, t_{c.ssp}, \alpha_{ssp}, f_{ssp}, i, j) \cdot Q_{ssp.big.1}(i,j) \cdot \sin\left(\frac{i\,\pi \cdot X}{L_{ssp}}\right) \cdot \sin\left(\frac{j\,\pi \cdot Y}{B_{ssp}}\right)\right]\right]$$

Wheel load 2

$$w_{ssp.big.2}\left(h_{c.ssp}, t_{f.top}, t_{f.bot}, t_{c.ssp}, \alpha_{ssp}, f_{ssp}\right) := \sum_j \left[\sum_i \left(w_{ssp.ij}\left(h_{c.ssp}, t_{f.top}, t_{f.bot}, t_{c.ssp}, \alpha_{ssp}, f_{ssp}, i, j\right) \cdot Q_{ssp.big.2}(i,j) \cdot \sin\left(\frac{i \pi \cdot X}{L_{ssp}}\right) \cdot \sin\left(\frac{j \pi \cdot Y}{B_{ssp}}\right) \right) \right]$$

Wheel load 3

$$w_{ssp.big.3}\left(h_{c.ssp}, t_{f.top}, t_{f.bot}, t_{c.ssp}, \alpha_{ssp}, f_{ssp}\right) := \sum_j \left[\sum_i \left(w_{ssp.ij}\left(h_{c.ssp}, t_{f.top}, t_{f.bot}, t_{c.ssp}, \alpha_{ssp}, f_{ssp}, i, j\right) \cdot Q_{ssp.big.3}(i,j) \cdot \sin\left(\frac{i \pi \cdot X}{L_{ssp}}\right) \cdot \sin\left(\frac{j \pi \cdot Y}{B_{ssp}}\right) \right) \right]$$

Wheel load 4

$$w_{ssp.big.4}\left(h_{c.ssp}, t_{f.top}, t_{f.bot}, t_{c.ssp}, \alpha_{ssp}, f_{ssp}\right) := \sum_j \left[\sum_i \left(w_{ssp.ij}\left(h_{c.ssp}, t_{f.top}, t_{f.bot}, t_{c.ssp}, \alpha_{ssp}, f_{ssp}, i, j\right) \cdot Q_{ssp.big.4}(i,j) \cdot \sin\left(\frac{i \pi \cdot X}{L_{ssp}}\right) \cdot \sin\left(\frac{j \pi \cdot Y}{B_{ssp}}\right) \right) \right]$$

Medium Truck - Four wheel loads symmetric around the centre of the secondary lane on the right hand side

Wheel load 1

$$x_{ssp.med.1} := \frac{L_{ssp}}{2} + 0.6m = 2.6m \qquad y_{ssp.med.1} := \frac{B_{ssp}}{2} + l_{lane} - 1m = 6.5m$$

$$Q_{ssp.med.1}(i,j) := \frac{4 \cdot Q_{comb.gl.pl.2}}{L_{ssp} \cdot B_{ssp}} \cdot \sin\left(\frac{i \pi \cdot x_{ssp.med.1}}{L_{ssp}}\right) \cdot \sin\left(\frac{j \pi \cdot y_{ssp.med.1}}{B_{ssp}}\right)$$

Wheel load 2

$$x_{ssp.med.2} := \frac{L_{ssp}}{2} + 0.6m = 2.6m \qquad y_{ssp.med.2} := \frac{B_{ssp}}{2} + l_{lane} + 1m = 8.5m$$

$$Q_{ssp.med.2}(i,j) := \frac{4 \cdot Q_{comb.gl.pl.2}}{L_{ssp} \cdot B_{ssp}} \cdot \sin\left(\frac{i \pi \cdot x_{ssp.med.2}}{L_{ssp}}\right) \cdot \sin\left(\frac{j \pi \cdot y_{ssp.med.2}}{B_{ssp}}\right)$$

Wheel load 3

$$x_{ssp.med.3} := \frac{L_{ssp}}{2} - 0.6m = 1.4m \qquad y_{ssp.med.3} := \frac{B_{ssp}}{2} + l_{lane} - 1m = 6.5m$$

$$Q_{ssp.med.3}(i,j) := \frac{4 \cdot Q_{comb.gl.pl.2}}{L_{ssp} \cdot B_{ssp}} \cdot \sin\left(\frac{i \pi \cdot x_{ssp.med.3}}{L_{ssp}}\right) \cdot \sin\left(\frac{j \pi \cdot y_{ssp.med.3}}{B_{ssp}}\right)$$

Wheel load 4

$$x_{ssp.med.4} := \frac{L_{ssp}}{2} - 0.6m = 1.4m \qquad y_{ssp.med4} := \frac{B_{ssp}}{2} + l_{lane} + 1m = 8.5m$$

$$Q_{ssp.med.4}(i,j) := \frac{4 \cdot Q_{comb.gl.pl.2}}{L_{ssp} \cdot B_{ssp}} \cdot \sin\left(\frac{i\pi \cdot x_{ssp.med4}}{L_{ssp}}\right) \cdot \sin\left(\frac{j\pi \cdot y_{ssp.med4}}{B_{ssp}}\right)$$

Wheel load 1

$$w_{ssp.med.1}(h_{c.ssp}, t_{f.top}, t_{f.bot}, t_{c.ssp}, \alpha_{ssp}, f_{ssp}) := \sum_j \left[\sum_i \left(w_{ssp.ij}(h_{c.ssp}, t_{f.top}, t_{f.bot}, t_{c.ssp}, \alpha_{ssp}, f_{ssp}, i,j) \cdot Q_{ssp.med.1}(i,j) \cdot \sin\left(\frac{i\pi \cdot X}{L_{ssp}}\right) \cdot \sin\left(\frac{j\pi \cdot Y}{B_{ssp}}\right) \right) \right]$$

Wheel load 2

$$w_{ssp.med.2}(h_{c.ssp}, t_{f.top}, t_{f.bot}, t_{c.ssp}, \alpha_{ssp}, f_{ssp}) := \sum_j \left[\sum_i \left(w_{ssp.ij}(h_{c.ssp}, t_{f.top}, t_{f.bot}, t_{c.ssp}, \alpha_{ssp}, f_{ssp}, i,j) \cdot Q_{ssp.med.2}(i,j) \cdot \sin\left(\frac{i\pi \cdot X}{L_{ssp}}\right) \cdot \sin\left(\frac{j\pi \cdot Y}{B_{ssp}}\right) \right) \right]$$

Wheel load 3

$$w_{ssp.med.3}(h_{c.ssp}, t_{f.top}, t_{f.bot}, t_{c.ssp}, \alpha_{ssp}, f_{ssp}) := \sum_j \left[\sum_i \left(w_{ssp.ij}(h_{c.ssp}, t_{f.top}, t_{f.bot}, t_{c.ssp}, \alpha_{ssp}, f_{ssp}, i,j) \cdot Q_{ssp.med.3}(i,j) \cdot \sin\left(\frac{i\pi \cdot X}{L_{ssp}}\right) \cdot \sin\left(\frac{j\pi \cdot Y}{B_{ssp}}\right) \right) \right]$$

Wheel load 4

$$w_{ssp.med.4}(h_{c.ssp}, t_{f.top}, t_{f.bot}, t_{c.ssp}, \alpha_{ssp}, f_{ssp}) := \sum_j \left[\sum_i \left(w_{ssp.ij}(h_{c.ssp}, t_{f.top}, t_{f.bot}, t_{c.ssp}, \alpha_{ssp}, f_{ssp}, i,j) \cdot Q_{ssp.med.4}(i,j) \cdot \sin\left(\frac{i\pi \cdot X}{L_{ssp}}\right) \cdot \sin\left(\frac{j\pi \cdot Y}{B_{ssp}}\right) \right) \right]$$

The small truck according to Eurocodes is neglected due to Swedish limitations.

Total deflection in the middle of the plate

$$w_{tot}(h_{c.ssp}, t_{f.top}, t_{f.bot}, t_{c.ssp}, \alpha_{ssp}, f_{ssp}) := w_{UDL}(h_{c.ssp}, t_{f.top}, t_{f.bot}, t_{c.ssp}, \alpha_{ssp}, f_{ssp}) + w_{ssp.big.1}(h_{c.ssp}, t_{f.top}, t_{f.bot}, t_{c.ssp}, \alpha_{ssp}, f_{ssp}) + w_{ssp.big.2}(h_{c.ssp}, t_{f.top}, t_{f.bot}, t_{c.ssp}, \alpha_{ssp}, f_{ssp}) \cdots$$
$$+ w_{ssp.big.3}(h_{c.ssp}, t_{f.top}, t_{f.bot}, t_{c.ssp}, \alpha_{ssp}, f_{ssp}) + w_{ssp.big.4}(h_{c.ssp}, t_{f.top}, t_{f.bot}, t_{c.ssp}, \alpha_{ssp}, f_{ssp}) \cdots$$
$$+ w_{ssp.med.1}(h_{c.ssp}, t_{f.top}, t_{f.bot}, t_{c.ssp}, \alpha_{ssp}, f_{ssp}) + w_{ssp.med.2}(h_{c.ssp}, t_{f.top}, t_{f.bot}, t_{c.ssp}, \alpha_{ssp}, f_{ssp}) \cdots$$
$$+ w_{ssp.med.3}(h_{c.ssp}, t_{f.top}, t_{f.bot}, t_{c.ssp}, \alpha_{ssp}, f_{ssp}) + w_{ssp.med.4}(h_{c.ssp}, t_{f.top}, t_{f.bot}, t_{c.ssp}, \alpha_{ssp}, f_{ssp})$$

◄ Global deflection

Tolerance (margin of error)

$\underline{CTOL} := 10^{-6}$

The cross-section dimensions of the steel sandwich element are optimized with the below constraints.

Definition of constraints

$\dfrac{l_{i.ssp}}{t_{c.ssp}} \leq 42 \cdot \varepsilon_3$

$\dfrac{b_{buck}}{t_{f.top}} \leq 42 \cdot \varepsilon_3$ Maximum width to thickness ratios for compression parts, in order the cross-section to be in class 3

$\dfrac{b_{buck}}{t_{f.bot}} \leq 42\varepsilon_3$

$A_{ssp} = \dfrac{A_{sl}}{b_{HK.f.top}}$ The steel sandwich element should have at least equal material area per square meter compared with the orthotropic deck.

$w \leq \min\left(\dfrac{L_{ssp}}{400}, \dfrac{B_{ssp}}{400}\right)$ The global deflection in the midspan should be limited to the shortest span divided by 400.

$40\deg \leq \alpha_{ssp} \leq 70\deg$ The angle of corrugation should be between 40 and 70 degrees according to several studies. When the angle increases more than 70 degrees , the shear stiffness both directions could be decreased while the cross-section would be more dense, so more material would be used. On the other hand, if the angle is less than 40 degrees bending stiffness decreases rapidly.

$20\text{mm} \leq f_{ssp} \leq 40\text{mm}$ The length of the horizontal corrugated segment has to be as small as possible to minimize local moments.

$\delta_I \leq \dfrac{l_{ssp}}{400}$ The local deflection on the top plate needs to fulfill the required control l.ssp/400 according to Swedish National Annex.

Optimization Analysis

For starting the optimization analysis, some predefined values should be inserted.

Predefined values

$h_{c.ssp} := 125mm$ $\qquad t_{f.top} := 5.5mm$ $\qquad \alpha_{ssp} := 70 \cdot deg$

$t_{c.ssp} := 4mm$ $\qquad t_{f.bot} := 4mm$ $\qquad f_{ssp} := 20mm$

Constrains

Given

$$0 \leq \frac{l_{buck}(h_{c.ssp}, \alpha_{ssp}, f_{ssp})}{t_{f.bot}} \leq 42\varepsilon \qquad 0 \leq \frac{l_{buck}(h_{c.ssp}, \alpha_{ssp}, f_{ssp})}{t_{f.top}} \leq 42\varepsilon \qquad 0 \leq \frac{l_{i.ssp}(h_{c.ssp}, \alpha_{ssp})}{t_{c.ssp}} \leq 42 \cdot \varepsilon$$

$$40deg \leq \alpha_{ssp} \leq 70deg \qquad 20mm \leq f_{ssp} \leq 40mm$$

$$A_{ssp}(h_{c.ssp}, t_{f.top}, t_{f.bot}, t_{c.ssp}, \alpha_{ssp}, f_{ssp}) = \frac{A_{sl}}{b_{HK.f.top}}$$

$$\delta_I(h_{c.ssp}, t_{f.top}, \alpha_{ssp}, f_{ssp}) \leq \frac{l_{ssp}(h_{c.ssp}, \alpha_{ssp}, f_{ssp})}{400}$$

$$w_{tot}(h_{c.ssp}, t_{f.top}, t_{f.bot}, t_{c.ssp}, \alpha_{ssp}, f_{ssp}) \leq min\left(\frac{L_{ssp}}{400}, \frac{B_{ssp}}{400}\right)$$

Maximizing the length of the steel sandwich element keeping the same amount of material per square meter of the construction.

$$\begin{pmatrix} h_{c.sspA} \\ t_{f.topA} \\ t_{f.botA} \\ t_{c.sspA} \\ \alpha_{sspA} \\ f_{sspA} \end{pmatrix} := Minimize\left(w_{tot}, h_{c.ssp}, t_{f.top}, t_{f.bot}, t_{c.ssp}, \alpha_{ssp}, f_{ssp}\right)$$

Results after optimization of the steel sandwich element

$h_{c.sspA}$ = 162.958·mm   Height of the core of the SSE

$t_{f.topA}$ = 6.498·mm   Thickness of the top flange of the SSE

$t_{f.botA}$ = 5.143·mm   Thickness of the bottom flange of the SSE

$t_{c.sspA}$ = 5.275·mm   Thickness of the core of the SSE

α_{sspA} = 64.69·deg   Angle of the corrugated core of the SSE

f_{sspA} = 21.581·mm   Length of the horizontal part of the core of the SSE

▶ Area, stiffness and engineering constants with optimised dimensions

Dimensions

$h := h_{ssp}(h_{c.sspA}, t_{f.topA}, t_{f.botA}, t_{c.sspA}) = 174.054 \cdot mm$

$l_{sspA} := l_{ssp}(h_{c.sspA}, \alpha_{sspA}, f_{sspA}) = 0.197\,m$

Area

$A_{sspA} := A_{ssp}(h_{c.sspA}, t_{f.topA}, t_{f.botA}, t_{c.sspA}, \alpha_{sspA}, f_{sspA}) = 22.434 \cdot mm$

Stiffness

$I_x := I_{ssp.x}(h_{c.sspA}, t_{f.topA}, t_{f.botA}, t_{c.sspA}, \alpha_{sspA}, f_{sspA}) = 1.166 \times 10^{-4} \cdot \dfrac{m^4}{m}$

$I_y := I_{ssp.y}(h_{c.sspA}, t_{f.topA}, t_{f.botA}, t_{c.sspA}, \alpha_{sspA}, f_{sspA}) = 9.499 \times 10^{-5} \cdot \dfrac{m^4}{m}$

$E_x := E_{x.ssp}(h_{c.sspA}, t_{f.topA}, t_{f.botA}, t_{c.sspA}, \alpha_{sspA}, f_{sspA}) = 4.711 \times 10^{9} \cdot \dfrac{N}{m}$

$E_y := E_{y.ssp}(h_{c.sspA}, t_{f.topA}, t_{f.botA}, t_{c.sspA}, \alpha_{sspA}, f_{sspA}) = 2.555 \times 10^{9} \cdot \dfrac{N}{m}$

$G_{xy.h} := G_{xy}(h_{c.sspA}, t_{f.topA}, t_{f.botA}, t_{c.sspA}, \alpha_{sspA}, f_{sspA}) = 1.148 \times 10^{9} \cdot \dfrac{N}{m}$

$D_x := D_{x.ssp}(h_{c.sspA}, t_{f.topA}, t_{f.botA}, t_{c.sspA}, \alpha_{sspA}, f_{sspA}) = 2.449 \times 10^{7} \cdot N \cdot m$

$D_y := D_{y.ssp}(h_{c.sspA}, t_{f.topA}, t_{f.botA}, t_{c.sspA}, \alpha_{sspA}, f_{sspA}) = 2.029 \times 10^{7} \cdot N \cdot m$

$D_{xy} := D_{xy.ssp}(h_{c.sspA}, t_{f.topA}, t_{f.botA}, t_{c.sspA}, \alpha_{sspA}, f_{sspA}) = 1.408 \times 10^{7} \cdot N \cdot m$

$D_{Qx1} := D_{Qx}(h_{c.sspA}, t_{f.topA}, t_{f.botA}, t_{c.sspA}, \alpha_{sspA}, f_{sspA}) = 6.483 \times 10^{8} \cdot \dfrac{N}{m}$

$D_{Qy1} := D_{Qy}(h_{c.sspA}, t_{f.topA}, t_{f.botA}, t_{c.sspA}, \alpha_{sspA}, f_{sspA}) = 9.321 \times 10^{7} \cdot \dfrac{N}{m}$

Engineering constants for Abaqus

$$E_{xe} := \frac{E_{x.ssp}(h_{c.sspA}, t_{f.topA}, t_{f.botA}, t_{c.sspA}, \alpha_{sspA}, f_{sspA})}{h} = 27.067 \cdot GPa$$

$$E_{ye} := \frac{E_{y.ssp}(h_{c.sspA}, t_{f.topA}, t_{f.botA}, t_{c.sspA}, \alpha_{sspA}, f_{sspA})}{h} = 14.68 \cdot GPa$$

$$E_{xb} := \frac{12 \cdot D_x}{h^3} = 5.573 \times 10^4 \cdot \frac{N}{mm^2}$$

$$E_{yb} := \frac{12 \cdot D_y}{h^3} = 4.617 \times 10^4 \cdot \frac{N}{mm^2}$$

$$G_{xy.1} := \frac{6 \cdot D_{xy}}{h^3} = 1.602 \times 10^4 \cdot \frac{N}{mm^2}$$

$$G_{xz} := \frac{D_{Qx1}}{\left(\frac{5}{6}\right) \cdot h} = 4.469 \times 10^3 \cdot \frac{N}{mm^2}$$

$$G_{yz} := \frac{D_{Qy1}}{\left(\frac{5}{6}\right) \cdot h} = 642.604 \cdot \frac{N}{mm^2}$$

Deflections

$$w_{tot1} := w_{tot}(h_{c.sspA}, t_{f.topA}, t_{f.botA}, t_{c.sspA}, \alpha_{sspA}, f_{sspA}) = 6.7218 \cdot mm$$

$$\delta_{I.1} := \delta_I(h_{c.sspA}, t_{f.topA}, \alpha_{sspA}, f_{sspA}) = 4.931 \times 10^{-4} \, m$$

◀ Area, stiffness and engineering constants with optimised dimensions

Area per unit width

$$\frac{A_{sspA} - \dfrac{A_{sl}}{b_{HK.f.top}}}{\dfrac{A_{sl}}{b_{HK.f.top}}} = 3.736 \times 10^{-3} \cdot \%$$

Moment of inertia per unit width

$$\frac{I_x - I_{HK.ortho.x}}{I_{HK.ortho.x}} = -59.173 \cdot \%$$

$$\frac{I_y - I_{HK.ortho.y}}{I_{HK.ortho.y}} = 6.587 \times 10^{4} \cdot \%$$

Axial Stiffness

$$\frac{E_x - E_{ortho.x}}{E_{ortho.x}} = 3.736 \times 10^{-3} \cdot \%$$

$$\frac{E_y - E_{ortho.y}}{E_{ortho.y}} = -2.85 \cdot \%$$

Bending Stiffness

$$\frac{D_x - D_{HK.ortho.x}}{D_{HK.ortho.x}} = -59.173 \cdot \%$$

$$\frac{D_y - D_{HK.ortho.y}}{D_{HK.ortho.y}} = 6.095 \times 10^{4} \cdot \%$$

Torsional Stiffness

$$\frac{D_{xy} - T_{HK.ortho.xy}}{T_{HK.ortho.xy}} = 897.395 \cdot \%$$

Transversal shear stiffness

$$\frac{D_{Qx1} - D_{HK.ortho.Qx}}{D_{HK.ortho.Qx}} = 409.7 \cdot \%$$

Global deflection

$$\frac{w_{tot1} - \delta_{max.ortho}}{\delta_{max.ortho}} = 27.767 \cdot \%$$

Local deflection

$$\frac{\delta_{I.1} - \delta_{local.max}}{\delta_{local.max}} = 40.084 \cdot \%$$

By calculating the deflection in Abaqus for a simple supported equivalent lamina plate with the same constants:

$\delta_{simple.sup} := 6.71mm$

Deflection in the simple supported plate

U, U3

+0.000e+00
-6.122e-01
-1.224e+00
-1.836e+00
-2.449e+00
-3.061e+00
-3.673e+00
-4.285e+00
-4.897e+00
-5.509e+00
-6.122e+00
-6.734e+00
-7.346e+00

6.71 mm
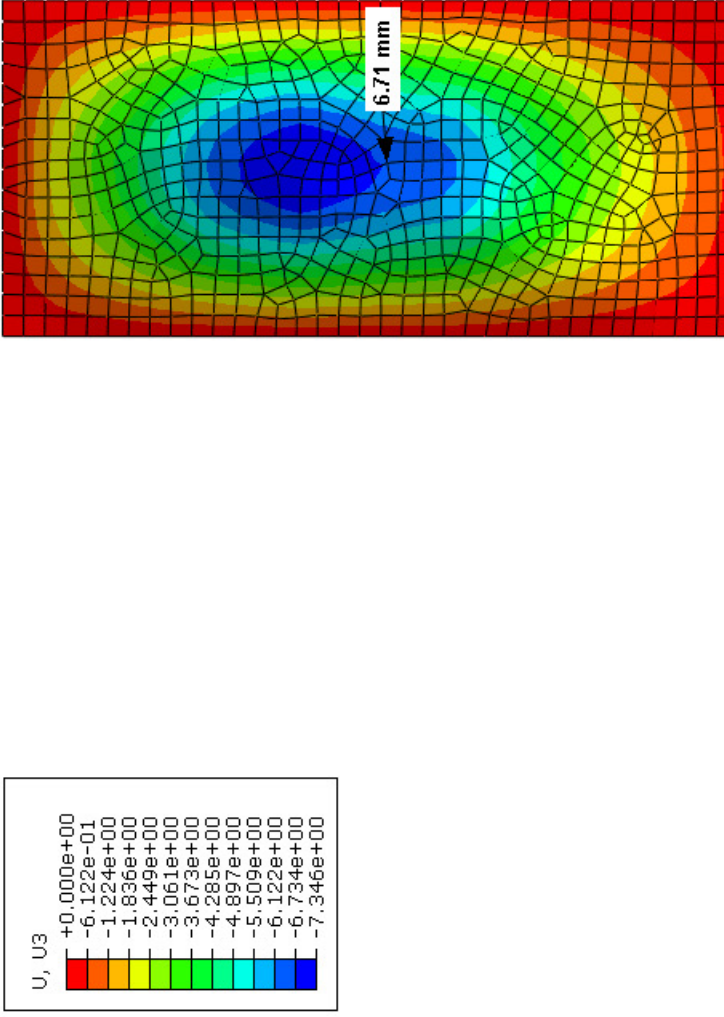
$\dfrac{\delta_{simple.sup} - w_{tot1}}{w_{tot1}} = -0.176 \cdot \%$

So, it is clear that the optimization routine corresponds really well with the FEM model.

However, it is visible that the maximum deflection is displayed in a different position and not in the middle of the plate. That is due to the second truck added. That point has coordinates (2m,5.4m) with a maximum deflection 7.35mm and it is going to be used for the following analyses.

U, U3

+0.000e+00
-6.122e-01
-1.224e+00
-1.836e+00
-2.449e+00
-3.061e+00
-3.673e+00
-4.285e+00
-4.897e+00
-5.509e+00
-6.122e+00
-6.734e+00
-7.346e+00

X=2000, Y=5400
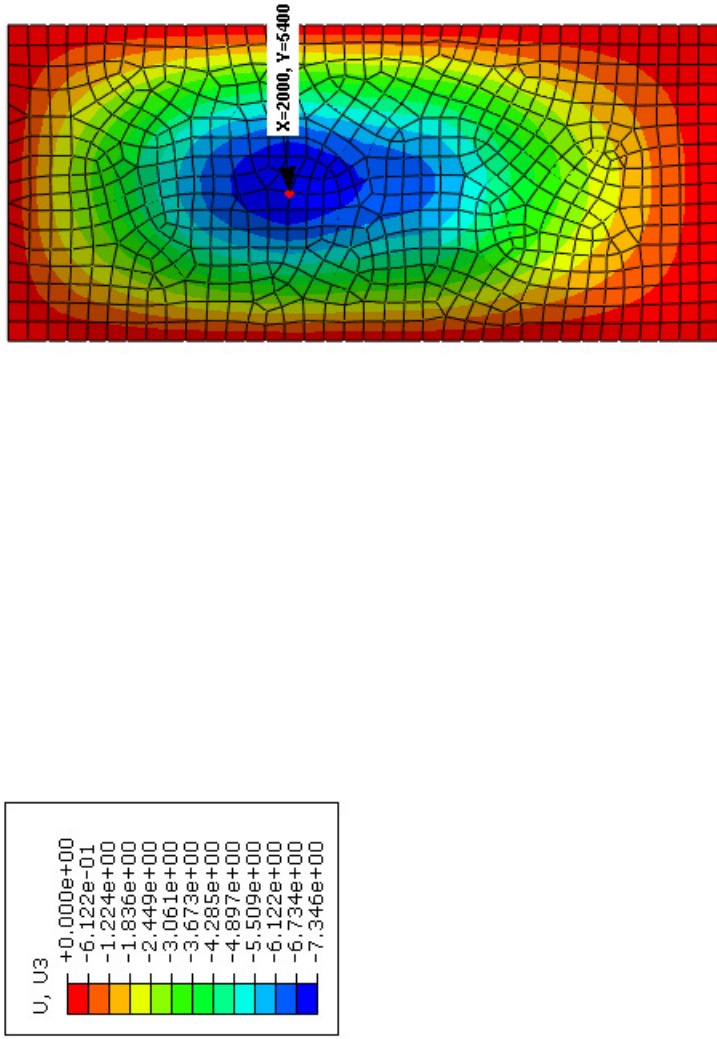
10 Appendix B

Part of the compression flange between the webs of the rib

$$\frac{l_{HK.rib.top.f.top} - 2 \cdot \dfrac{t_{HK.rib.top}}{2}}{t_{HK.f.top}} = 24.85$$

$$\frac{l_{HK.rib.top.f.top} - 2 \cdot \dfrac{t_{HK.rib.top}}{2}}{t_{HK.f.top}} < 33 \cdot \varepsilon = 1$$

Plate in Class 1

Part of the compression flange outside the webs of the rib

$$\frac{b_{HK.f.top} - l_{HK.rib.top.f.top} - 2 \cdot \dfrac{t_{HK.rib.top}}{2}}{t_{HK.f.top}} = 23.817$$

$$\frac{b_{HK.f.top} - l_{HK.rib.top.f.top} - 2 \cdot \dfrac{t_{HK.rib.top}}{2}}{t_{HK.f.top}} < 33 \cdot \varepsilon = 1$$

Plate in Class 1

Part of the compression flange in the end of the plates

$$\frac{l_{HK.f.top.end} - \dfrac{t_{HK.rib.bot}}{2}}{t_{HK.f.top}} = 16.573$$

$$\frac{l_{HK.f.top.end}}{t_{HK.f.top}} < 33\varepsilon = 1$$

Part in class 1

Bottom flange of rib

$$\frac{l_{HK.rib.top.f.bot} - 2 \cdot \dfrac{t_{HK.rib.top}}{2}}{t_{HK.rib.top}} = 18.538$$

$$\frac{l_{HK.rib.top.f.bot} - 2 \cdot \dfrac{t_{HK.rib.top}}{2}}{t_{HK.rib.top}} < 33 \cdot \epsilon = 1 \qquad \text{Part in class 1}$$

Webs of the top ribs

$$\frac{l_{HK.rib.top.web} - \dfrac{t_{HK.f.top}}{2} - \dfrac{t_{HK.rib.top}}{2}}{t_{HK.rib.top}} = 37.888$$

$$\frac{l_{HK.rib.top.web} - \dfrac{t_{HK.f.top}}{2} - \dfrac{t_{HK.rib.top}}{2}}{t_{HK.rib.top}} < 42 \cdot \epsilon = 0 \qquad \text{Part in class 4}$$

◄ Cross - Section Classification of the top plate of Hoga Kusten Bridge

The solution is according to Eurocode EN_1993-1-5
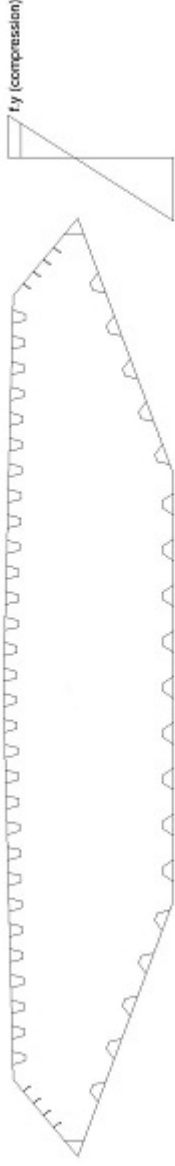
t y (compression)

$$\sigma_{HK.rib.top.f.bot} := \frac{h_{box} - z_{na} - h_{HK.rib.top}}{h_{box} - z_{na}} \cdot f_y$$

Stresses in the bottom flange of the top ribs

$$\sigma_{HK.rib.top.f.bot} = 280.954 \cdot MPa$$

$$\psi_1 := \frac{\sigma_{HK.rib.top.f.bot}}{f_y} = 0.791 \qquad 0 \le \psi_1 \le 1 = 1$$

$$\kappa_\sigma := \frac{8.2}{(1.05 + \psi_1)} = 4.453$$

Buckling factor κ.σ for uniform compression

The webs of the longitudinal stiffeners are in class 4

$$\sigma_{cr} := \kappa_\sigma \cdot \frac{E_{S355N} \cdot \pi^2}{12 \cdot \left(1 - \nu^2\right) \cdot \left(\frac{l_{HK.rib.top.web}}{t_{HK.rib.top}}\right)^2} = 551.776 \cdot MPa$$

Elastic critical plate buckling stress of the equivalent orthotropic plate for the webs of the top ribs

$$\lambda_p := \sqrt{\frac{f_y}{\sigma_{cr}}} = 0.802 \qquad \lambda_p > 0.673 = 1 \qquad \text{Plate slenderness}$$

$$\rho := \frac{\lambda_p - 0.055 \cdot (3 + \psi_1)}{\lambda_p^2} = 0.923 \qquad \text{Reduction factor } \rho$$

$$l_{HK.rib.top.web.eff} := \rho \cdot \left(l_{HK.rib.top.web} - \frac{t_{HK.f.top}}{2} - \frac{t_{HK.rib.top}}{2} \right) = 0.28 \, m \qquad \text{Effective length of the webs in top ribs}$$

$$h_{HK.rib.top.eff} := \rho \cdot \left(h_{HK.rib.top} - \frac{t_{HK.f.top}}{2} - \frac{t_{HK.rib.top}}{2} \right) = 0.271 \, m \qquad \text{Effective vertical height of the webs in top ribs}$$

$$l_{HK.rib.top.web.eff1} := \frac{2}{5 - \psi_1} \cdot l_{HK.rib.top.web.eff} = 0.133 \, m \qquad \text{Length of the top effective part of the webs}$$

$$l_{HK.rib.top.web.eff2} := l_{HK.rib.top.web.eff} - l_{HK.rib.top.web.eff1} = 0.147 \cdot m \qquad \text{Length of the bottom effective part of the webs}$$

$$l_{HK.rib.top.web.eff.no} := l_{HK.rib.top.web} - l_{HK.rib.top.web.eff1} - l_{HK.rib.top.web.eff2} - \frac{t_{HK.f.top}}{2} - \frac{t_{HK.rib.top}}{2} \qquad \text{Length of the non effective part of the webs}$$

$$l_{HK.rib.top.web.eff.no} = 0.023 \, m$$

$$h_{HK.rib.top.eff1} := \frac{2}{5 - \psi_1} \cdot h_{HK.rib.top.eff} = 0.129 \, m \qquad \text{Height of the top effective part of the webs}$$

$$h_{HK.rib.top.eff2} := h_{HK.rib.top.eff} - h_{HK.rib.top.eff1} = 0.142 \, m \qquad \text{Height of the bottom effective part of the webs}$$

$$h_{HK.rib.top.eff.no} := h_{HK.rib.top} - h_{HK.rib.top.eff1} - h_{HK.rib.top.eff2} - \frac{t_{HK.f.top}}{2} - \frac{t_{HK.rib.top}}{2} \qquad \text{Height of the non effective part of the webs}$$

$$h_{HK.rib.top.eff.no} = 0.023 \, m$$

Total and effective area of longitudinal stiffeners

$A_{sl} := A_{HK.unit.ortho.x} = 1.346 \times 10^4 \cdot mm^2$

$A_{sl.eff} := b_{HK.f.top} \cdot t_{HK.f.top} + t_{HK.rib.top} \cdot \left(2 \cdot l_{HK.rib.top.web.eff} + l_{HK.rib.top.f.bot} \right) = 1.292 \times 10^4 \cdot mm^2$

◀ Calculation of effective area of the top plate of Hoga Kusten Bridge
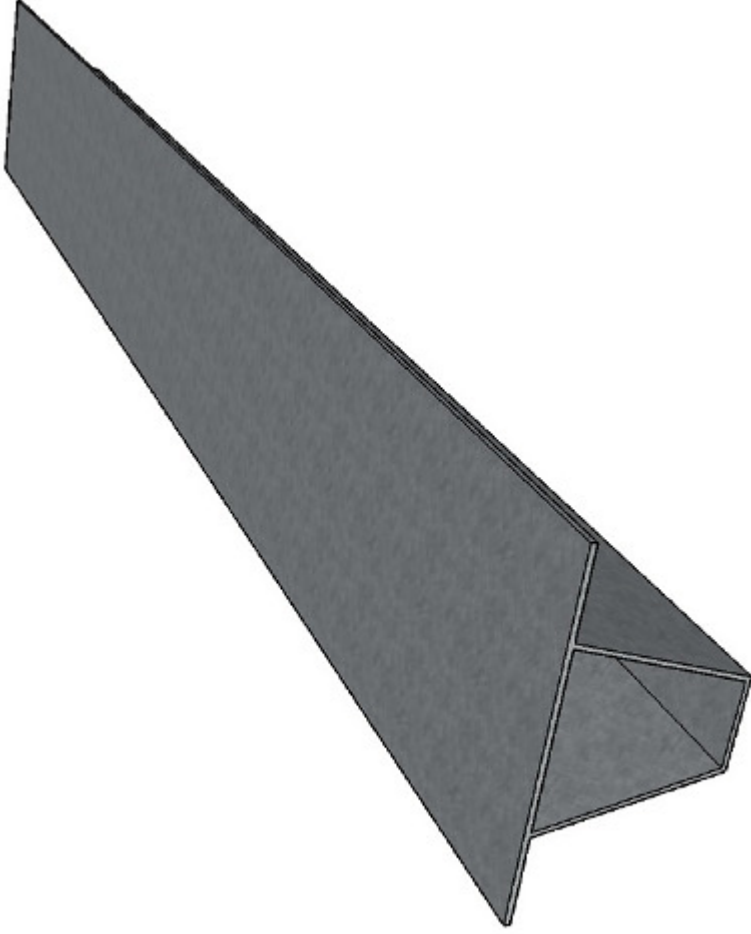
Column-like buckling behaviour

$I_{sl} := I_{HK.unit.ortho.x} = 1.714 \times 10^{-4} \ m^4$ Moment of inertia of each top rib

$\beta_{Ac} := \dfrac{A_{sl.eff}}{A_{sl}} = 0.96$

$\sigma_{cr.sl} := \dfrac{\pi^2 \cdot E_{S355N} \cdot I_{sl}}{A_{sl} \cdot l_{long.stif}^2} = 1.649 \times 10^3 \cdot MPa$ Elastic critical column buckling stress for a stiffened plate

$\lambda_c := \sqrt{\dfrac{\beta_{Ac} \cdot f_y}{\sigma_{cr.sl}}} = 0.455$ Relative column slenderness

$$i := \sqrt{\frac{I_{sl}}{A_{sl}}} = 112.836 \cdot mm$$

$$e := \max\left(z_{HK.f.top}, z_c, z_{HK.rib.web}\right) = 219.187 \cdot mm$$

Largest distance from the respective centroids of the plate from the NA

$$\alpha := 0.34$$

For closed stiffeners

$$\alpha_e := \alpha + \frac{0.09}{\dfrac{i}{e}} = 0.515$$

Column type behaviour

$$\Phi := 0.5 \cdot \left[1 + \alpha_e \cdot \left(\lambda_c - 0.2 \right) + \lambda_c^2 \right] = 0.669$$

$$\chi_c := \frac{1}{\Phi + \sqrt{\Phi^2 - \lambda_c^2}} = 0.862$$

$$\rho_c := \chi_c = 0.862$$

Reduction factor ρ for the column-like buckling

Plate-like buckling using equivalent orthotropic plate (half of the top plate is used for the calculations)

$$\alpha_2 := \frac{l_{long.stif}}{\dfrac{l_{HK.f.top}}{2}} = 0.435 \qquad \alpha_2 > 0.5 = 0$$

Length to width ratio of the top plate

Although α.2 is not bigger than 0.5 which is the limit value, hand calculations according to Annex A are going to be done, and then are compared with EBPlate program results, in order to provi a more accurate value.

$$\psi_{pl} := \psi_1 \qquad \psi_{pl} > 0.5 = 1$$

$$I_p := \frac{b_{HK.f.top} \cdot t_{HK.f.top}^3}{12 \cdot \left(1 - \nu^2\right)} = 9.495 \times 10^4 \cdot mm^4$$

Second moment of area for bending of the plate

Area of the plate

$$A_p := b_{HK.f.top} \cdot t_{HK.f.top} = 7.2 \times 10^{-3} \, m^2$$

$$\gamma_2 := \frac{I_{sl}}{I_p} = 1.805 \times 10^3$$

Sum of the gross areas of the individual longitudinal stiffeners

$$A_{sl.rib} = 6.26 \times 10^{-3} \, m^2$$

$$\delta_2 := \frac{A_{sl.rib}}{A_p} = 0.869$$

According to Annex A, Eurocodes 1993-1-5

$$\kappa_{\sigma\rho} := \begin{cases} \sqrt{\dfrac{2\left[\left(1+\alpha_2^2\right)^2 + \gamma_2 - 1\right]}{\alpha_2^2 \cdot (\psi_{pl}+1) \cdot (1+\delta_2)}} & \text{if } \alpha_2 \le \sqrt[4]{\gamma_2} \\[2em] \dfrac{4 \cdot \left(1 + \sqrt{\gamma_2}\right)}{(\psi_{pl}+1)(1+\delta_2)} & \text{if } \alpha_2 > \sqrt[4]{\gamma_2} \end{cases}$$

$$\kappa_{\sigma\rho} = 5.707 \times 10^3$$

As the Annex A for Eurocode can not be applied, EBPlate programme is going to be used for the calculation of the elastic critical stress.
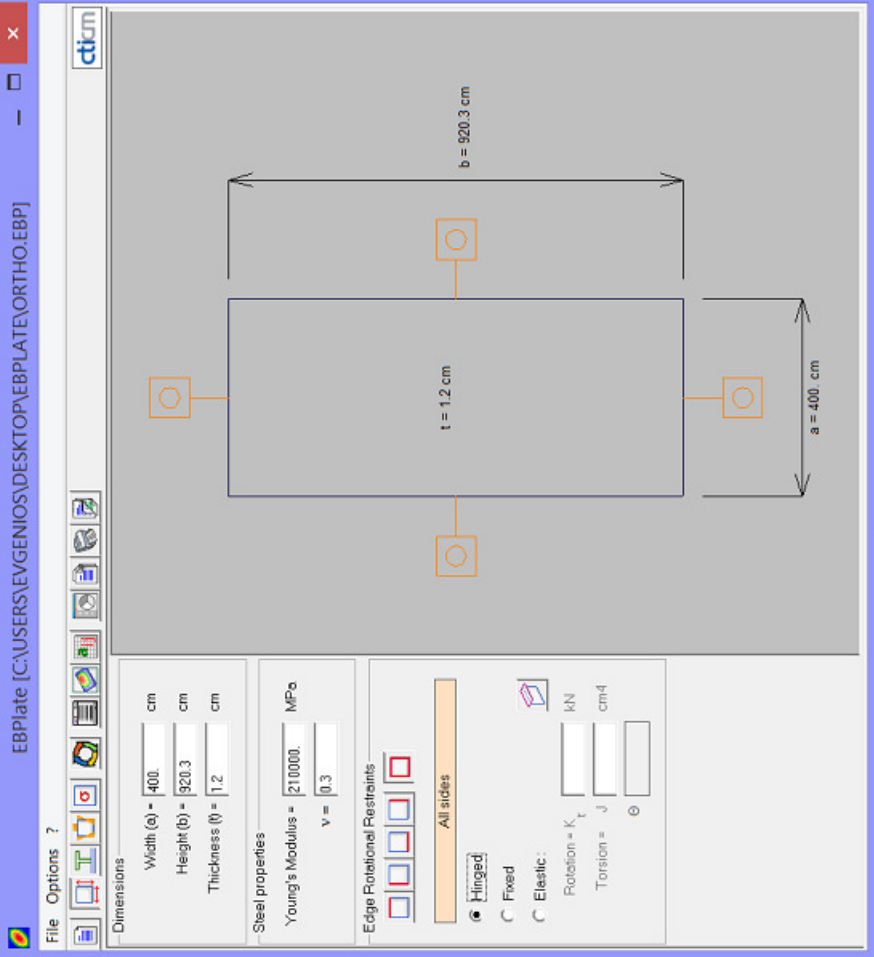
EBPlate

File   Options   ?

cticm

σ_{xtr} σ_{xbr}

σ_{xtl} σ_{xbl}

Analytical longitudinal stresses

Zero

σ_{xtl} 355.   MPa
σ_{xbl} 355.   MPa
Ψ_l 1.   Signe

RHS = LHS

σ_{xtr} 355.   MPa
σ_{xbr} 355.   MPa
Ψ_r 1.

Imposed longitudinal stresses

Meshed longitudinal stresses

Meshed stresses
Imposed values

EBPlate

File Options ?

Results

Euler's Stress σ_E = 0.32 **MPa**

Critical factor ϕ_{cr} = 5.0569

Buckling factors

$k_{\sigma xtl}$ =	5563.015	
$k_{\sigma xbl}$ =	5563.015	
$k_{\sigma xtr}$ =	5563.015	
$k_{\sigma xbr}$ =	5563.015	
$k_{\sigma yut}$ =		
$k_{\sigma yub}$ =		
$k_{\sigma ypt}$ =		
$k_{\sigma ypb}$ =		
k_{τ} =		

Critical stresses

$\sigma_{xtl.cr}$ =	1795.19	MPa
$\sigma_{xbl.cr}$ =	1795.19	MPa
$\sigma_{xtr.cr}$ =	1795.19	MPa
$\sigma_{xbr.cr}$ =	1795.19	MPa
$\sigma_{yut.cr}$ =		MPa
$\sigma_{yub.cr}$ =		MPa
$\sigma_{ypt.cr}$ =		MPa
$\sigma_{ypb.cr}$ =		MPa
τ_{cr} =		MPa

Calculation's options

Deformed shape parameters

Eigenmode complexity :
( ) Automatic   1 2 3

( ) User defined
7 × 16

Number of modes
1 20 N

Contour lines
[ ] To be calculated

Plate behaviour

[ ] Prevention of local buckling

Calculation

Calculations times
Preparation of the matrices   0.19 s
Resolution   0.03 s
Contour lines   0.00 s

Calculation OK.
Number of calculated modes   1

Go
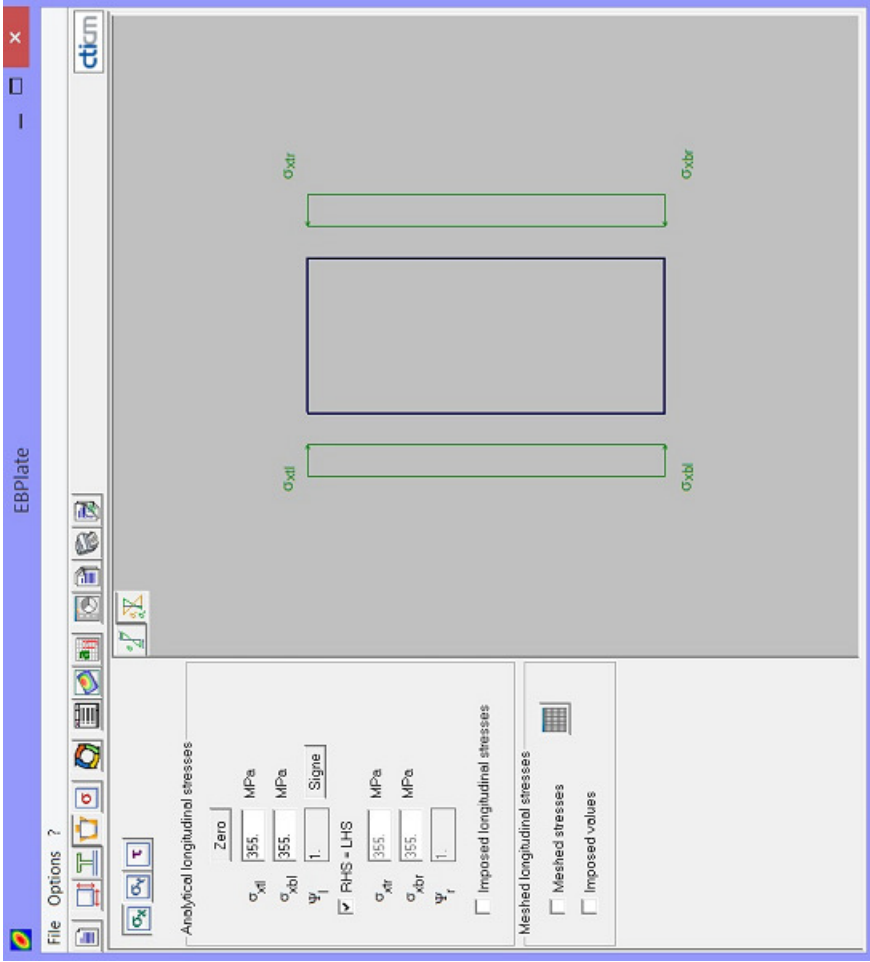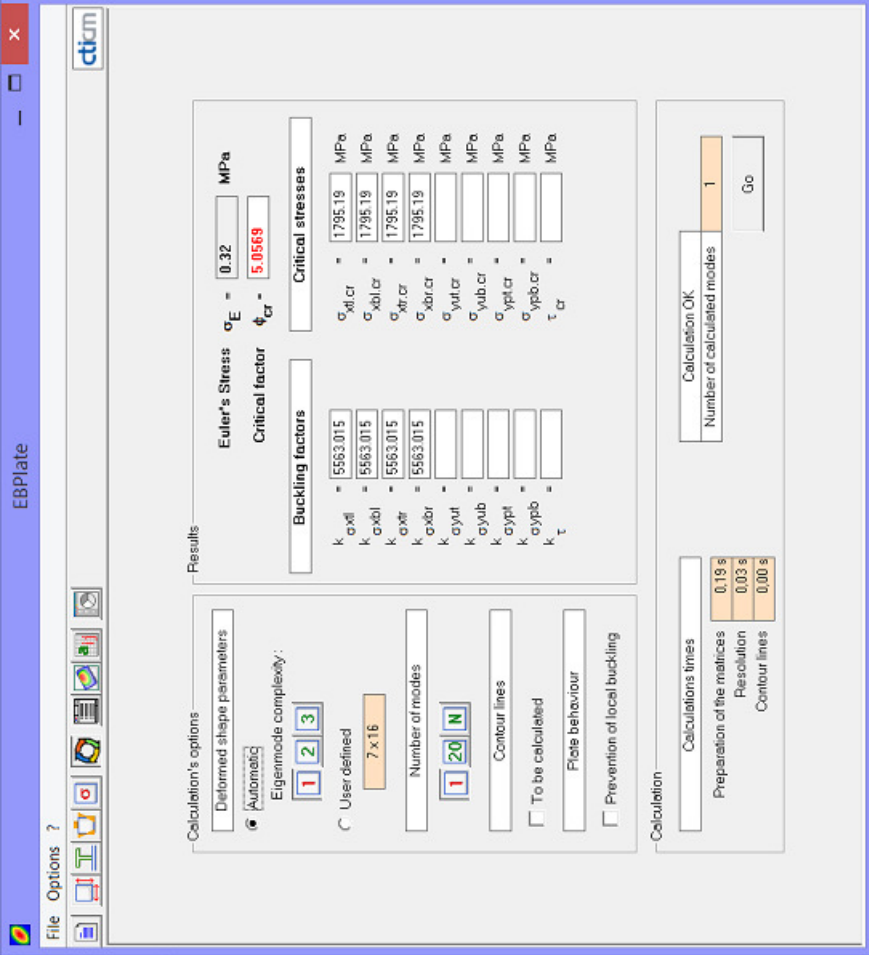
$\sigma_{cr.p} := 1795.19\,MPa$ — Elastic critical stress for the plate-like buckling

$A_{HK.comp.f} := A_{HK.f.top} + A_{HK.n.rib.top} = 0.409\,m^2$ — Total area of the compressive flange

$A_{HK.rib.top.eff} := t_{HK.rib.top} \cdot \left(2 \cdot I_{HK.rib.top.web.eff} + I_{HK.rib.top.f.bot}\right)$

$A_{HK.rib.top.eff} = 5.725 \times 10^3 \cdot mm^2$ — Effective area of each top rib

$A_{HK.n.rib.top.eff} := n_{HK.rib.top} \cdot A_{HK.rib.top.eff} = 0.172\,m^2$ — Total effective area of the top ribs

$A_{HK.comp.f.eff} := A_{HK.f.top} + A_{HK.n.rib.top.eff} = 0.393\,m^2$ — Total effective area of the compressive flange

$\beta_{Apl} := \dfrac{A_{HK.comp.f.eff}}{A_{HK.comp.f}} = 0.961$

$\lambda_{pl} := \sqrt{\dfrac{\beta_{Apl} \cdot f_y}{\sigma_{cr.p}}} = 0.436$ — Relative plate slenderness

$\rho_{pl} := \begin{cases} \dfrac{\left(\lambda_{pl} - 0.055\left(3 + \psi_{pl}\right)\right)}{\lambda_{pl}^2} & \text{if } \lambda_{pl} \geq 0.673 \\ 1 & \text{otherwise} \end{cases}$

$\rho_{pl} = 1 \qquad \rho_{pl} \leq 1 = 1$ — Reduction factor ρ for the plate-like buckling

0

$$\xi := \frac{\sigma_{cr.p}}{\sigma_{cr.sl}} - 1 = 0.088$$

$$\rho_{c.new} := \left(\rho_{pl} - \chi_c\right) \cdot \xi \cdot (2 - \xi) + \chi_c$$

New reduction factor ρ.c after the interaction between column-like and plate-like buckling

$$\rho_{c.new} = 0.886$$

Moment Capacity of the Compressive Flange
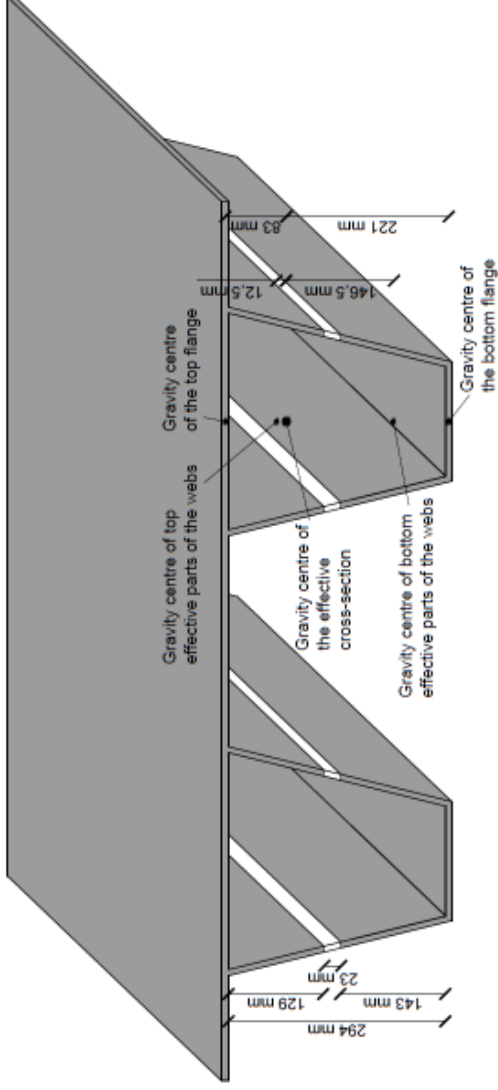
New neutral axis of each top rib (distance from the centre of the bottom flange of the rib)

$$z_{c.new} := \frac{2 \left[l_{HK.rib.top.web.eff1} \cdot t_{HK.rib.top} \cdot \left(h_{HK.rib.top} - \dfrac{t_{HK.f.top}}{2} - \dfrac{h_{HK.rib.top.eff1}}{2} \right) \dots \right. }{A_{sl.eff}}$$
$$\left. + l_{HK.rib.top.web.eff2} \cdot t_{HK.rib.top} \cdot \left(\dfrac{t_{HK.rib.top}}{2} + \dfrac{h_{HK.rib.top.eff2}}{2} \right) + b_{HK.f.top} \cdot t_{HK.f.top} \cdot h_{HK.rib.top} \right]$$

$$z_{c.new} = 0.221\,m$$

$$z_{HK.f.top.new} := h_{HK.rib.top} - z_{c.new} = 0.083\,m$$

Distance between the upper plate and the neutral axis of the rib

Moment of Inertia

$$I_{eff1} := \frac{b_{HK.f.top} \cdot t_{HK.f.top}^3}{12} + b_{HK.f.top} \cdot t_{HK.f.top} \cdot z_{HK.f.top.new}^2 \ldots$$
$$+ 2 \cdot \left[\frac{t_{HK.rib.top} \cdot h_{HK.rib.top.eff1}^3}{12} \ldots \right.$$
$$\left. + t_{HK.rib.top} \cdot h_{HK.rib.top.eff1} \cdot \left(z_{HK.f.top.new} - \frac{h_{HK.rib.top.eff1}}{2} - \frac{t_{HK.f.top}}{2} \right)^2 \right]$$

$$I_{eff1} = 5.234 \times 10^7 \cdot mm^4$$

$$I_{eff2} := \frac{l_{HK.rib.top.f.bot} \cdot t_{HK.rib.top}^3}{12} + l_{HK.rib.top.f.bot} \cdot t_{HK.rib.top} \cdot z_{c.new}^2 \ldots$$
$$+ 2 \cdot \left[\frac{t_{HK.rib.top} \cdot h_{HK.rib.top.eff2}^3}{12} \ldots \right.$$
$$\left. + t_{HK.rib.top} \cdot h_{HK.rib.top.eff2} \cdot \left(z_{c.new} - \frac{h_{HK.rib.top.eff2}}{2} - \frac{t_{HK.rib.top}}{2} \right)^2 \right]$$

$$I_{eff2} = 1.139 \times 10^8 \cdot mm^4$$

$$I_{eff} := I_{eff1} + I_{eff2} = 1.662 \times 10^8 \cdot mm^4$$

First moment of area

$$W_{over} := \frac{I_{eff}}{z_{HK.f.top.new}} = 2.013 \times 10^6 \cdot mm^3$$

$$W_{under} := \frac{I_{eff}}{z_{c.new}} = 7.506 \times 10^5 \cdot mm^3$$

Effective moment of inertia

Due to the position of the neutral axis or each rib, yielding will probably take place at the bottom flange of the ribs and therefore the bending moment capacity is defined by the corresponding fi moment of area and stresses at that depth. However, the moment capacity of the top part will be also found to verify it.

Design moment capacity

$$M_{Rd.unit.1} := W_{over} \cdot \frac{f_y}{\gamma_{M1}} = 714.601 \cdot kN \cdot m$$

$$M_{Rd.unit.2} := W_{under} \cdot \frac{f_y}{\gamma_{M1}} = 266.477 \cdot kN \cdot m$$

$$M_{Rd.unit} := min(M_{Rd.unit.1}, M_{Rd.unit.2}) = 266.477 \cdot kN \cdot m$$

Design moment capacity per unit length

$$M_{Rd} := \frac{M_{Rd.unit}}{b_{HK.f.top}} = 444.129 \cdot \frac{kN \cdot m}{m}$$

In defining the design moment capacity the end parts in edges are neglected.

Axial load carrying capacity

For a stiffened plate panel the effective area of the compression zone is:
$A_{c,eff} = \rho_c A_{c,eff,loc} t + \Sigma b_{edge,eff} t$, where $A_{c,eff,loc} = A_{sl,eff} + \Sigma \rho_{loc} b_{c,loc} t$

$$A_{c.eff} := \rho_{c.new} \cdot n_{HK.rib.top} \cdot A_{sl.eff} + 2l_{HK.f.top.end} \cdot t_{HK.f.top} = 0.348 \, m^2$$

Effective area per unit width

$$A_{c.eff.unit} := \frac{A_{c.eff}}{l_{HK.f.top}}$$

$$A_{c.eff.unit} = 0.019 \cdot m$$

Total load carrying capacity of the top plate

$$N_{Rd.tot} := A_{c.eff} \cdot \frac{f_y}{\gamma_{M1}} = 1.236 \times 10^5 \cdot kN$$

Load carrying capacity per unit length

$$N_{Rd} := \frac{N_{Rd.tot}}{l_{HK.f.top}} = 6.718 \times 10^3 \cdot \frac{kN}{m}$$

◄ Moment and axial load carrying capacity of the top plate of Höga Kusten Bridge

SM, SM1
(Avg: 75%)

+7.958e+01
+6.219e+01
+4.481e+01
+2.743e+01
+1.005e+01
-7.327e+00
-2.471e+01
-4.209e+01
-5.947e+01
-7.685e+01
-9.423e+01
-1.116e+02
-1.290e+02
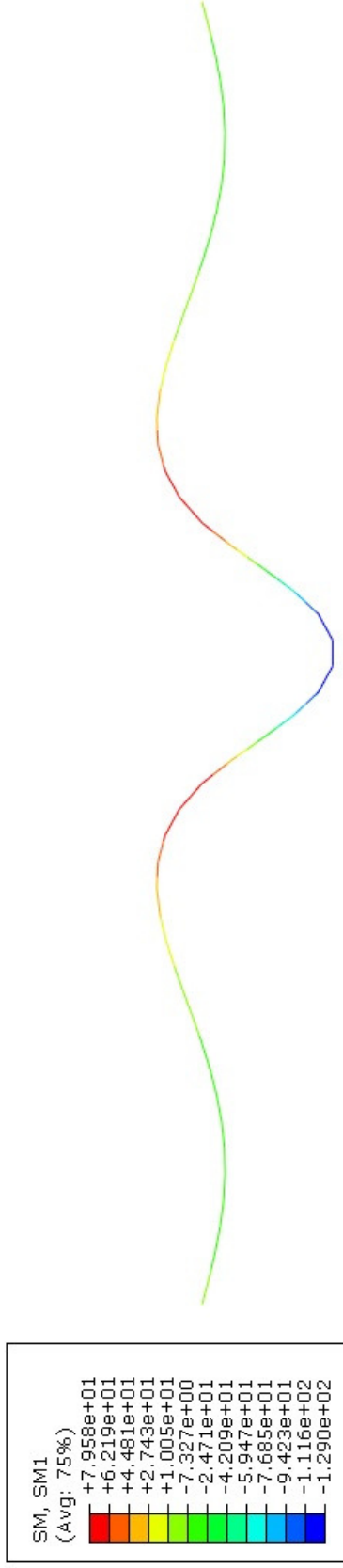
$$M_{Ed} := 129 kN \cdot \frac{m}{m}$$

$$u_M := \frac{M_{Ed}}{M_{Rd}} = 0.29$$

Areas of the top SSE

$A_{tot.sspA} := A_{tot.ssp} \left(h_{c.sspA}, t_{f.topA}, t_{f.botA}, t_{c.sspA}, \alpha_{sspA}, f_{sspA} \right) = 3.653 \times 10^3 \cdot mm^2$

Area of the repeated part of the SSE

$A_{sspA} = 0.02\,m$

Area of the top SSE per unit width

$A_{f.top.sspA} := A_{sspA} \cdot l_{HK.f.top} = 0.374\,m^2$

Total area of the top SSE

New total area of the cross-section

$A_{HK.tot.ssp} := A_{f.top.sspA} + A_{HK.web.top} + A_{HK.n.sid.stif} + A_{HK.sid.pl} + A_{HK.web.bot.in} + A_{HK.f.bot} + A_{HK.n.rib.bot.in} + A_{HK.n.rib.bot}$

$A_{HK.tot.ssp} = 0.854\,m^2$

Total area of the box cross-section with the new SSE

Gravity centres of SSE

Gravity centre of the top SSE (distance from the centreline of the top flange)

$z_{na.sspA} := z_{na.ssp} \left(h_{c.sspA}, t_{f.topA}, t_{f.botA}, t_{c.sspA}, \alpha_{sspA}, f_{sspA} \right) = 0.074\,m$

$y_{f.top.sspA} := 3.815\,m$

Counted from the Autocad due to inclination

Gravity centre of the section (distance from the bottom flange)

$z_{na.new} := \dfrac{\begin{array}{l} A_{f.top.sspA} \cdot y_{f.top.sspA} + A_{HK.web.top} \cdot y_{HK.web.top} + A_{HK.n.sid.stif} \cdot y_{HK.sid.stif} \cdots \\ + A_{HK.sid.pl} \cdot y_{HK.sid.pl} + A_{HK.web.bot.in} \cdot y_{HK.web.bot.in} + A_{HK.n.rib.bot.in} \cdot y_{HK.n.rib.bot.in} + A_{HK.n.rib.bot} \cdot y_{HK.n.rib.bot} \end{array}}{A_{HK.tot.ssp}} = 2.264\,m$

With the same way as done for the orthotropic deck, the stresses in the bottom flange of the SSE are found:

Stresses in the bottom flange of the SSE

$$\sigma_{HK.ssp.f.bot} := \frac{h_{box} - z_{na.new} - h_{sspA}}{h_{box} - z_{na.new}} \cdot f_y$$

$$\sigma_{HK.ssp.f.bot} = 318.127 \cdot MPa$$

$$\psi_{1.ssp} := \frac{\sigma_{HK.ssp.f.bot}}{f_y} = 0.896 \qquad 0 \le \psi_{1.ssp} \le 1 = 1$$

The whole cross-section of the steel sandwich element is in class 3. So, the whole area is effective. For finding the reduction factor due to buckling one of the repeated parts of the steel sandwich element is going to be used.

Column-like buckling behaviour
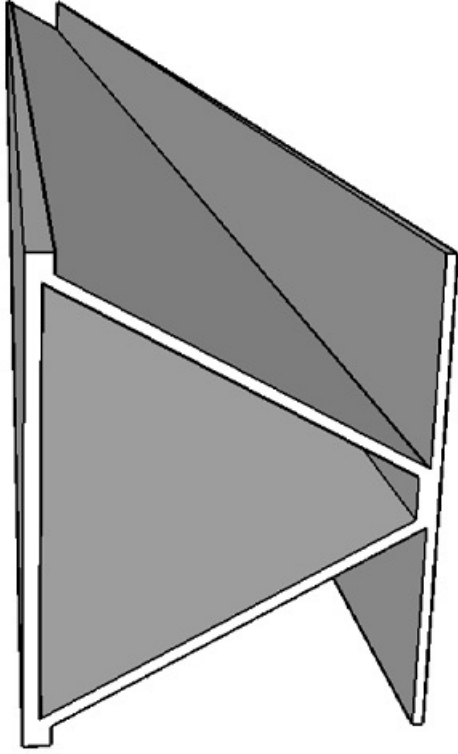
$$I_{sl.ssp} := I_{tot.ssp.x}\left(h_{c.sspA}, t_{f.topA}, t_{f.botA}, t_{c.sspA}, \alpha_{sspA}, f_{sspA}\right) = 1.565 \times 10^{-5} \ m^4$$

Moment of inertia of each top rib

$$A_{sl.ssp} := A_{tot.ssp}\left(h_{c.sspA}, t_{f.topA}, t_{f.botA}, t_{c.sspA}, \alpha_{sspA}, f_{sspA}\right) = 3.653 \times 10^{-3} \ m^2$$

$$\beta_{Ac.ssp} := 1$$

The whole cross-section is in class 3 or higher

$$\sigma_{cr.sl.ssp} := \frac{\pi^2 \cdot E_{S355N} \cdot I_{sl.ssp}}{A_{sl.ssp} \cdot l_{long.stif}^2} = 555.063 \cdot MPa$$

Elastic critical column buckling stress for a stiffened plate

$$\lambda_{c.ssp} := \sqrt{\frac{\beta_{Ac.ssp} \cdot f_y}{\sigma_{cr.sl.ssp}}} = 0.8$$

Relative column slenderness

$$i_{ssp} := \sqrt{\frac{I_{sl.ssp}}{A_{sl.ssp}}} = 65.459 \cdot mm$$

$$e_{ssp} := \max\left(z_{na.sspA}, h_{sspA} - z_{na.sspA}\right) = 83.699 \cdot mm$$

Largest distance from the respective centroids of the plate from the NA

$$\alpha_{ssp.} := 0.34$$

For closed stiffeners

$$\alpha_{e.ssp} := \alpha_{ssp.} + \frac{0.09}{\frac{i_{ssp}}{e_{ssp}}} = 0.455$$

Column type behaviour

$$\Phi_{spp} := 0.5 \cdot \left[1 + \alpha_{e.ssp} \cdot \left(\lambda_{c.ssp} - 0.2\right) + \lambda_{c.ssp}^2\right] = 0.956$$

$$\chi_{c.ssp} := \frac{1}{\Phi_{spp} + \sqrt{\Phi_{spp}^2 - \lambda_{c.ssp}^2}} = 0.675$$

$$\rho_{c.ssp} := \chi_{c.ssp} = 0.675$$

Reduction factor ρ for the column-like buckling

Plate-like buckling using equivalent orthotropic plate (half of the top plate is used for the calculations)

$$\psi_{pl.ssp} := \psi_{1.ssp} = 0.896$$

For the steel sandwich element, neither the Eurocode nor the EBPlate software could be applied directly. Following Jón Pétur Indriðason's and Vésteinn Sigmundsson's Master Thesis 'Bucklin analysis of orthotropic plates', an equivalent plate could be created that gives quite close results to the steel sandwich elements. For deciding the thickness of the equivalent plate, it is assumed that the total bending stiffness of the new plate is equal with the bending stiffness of the steel sandwich element in the y direction.

$$D_x = 1.828 \times 10^4 \cdot kN \cdot m$$

$$D_y = 1.519 \times 10^4 \cdot kN \cdot m$$

$$D_{eq} := D_y = 1.519 \times 10^7 \cdot N \cdot m$$

$$t_{eq} := \sqrt[3]{\frac{D_{eq} \cdot 12 \cdot \left(1 - \nu^2\right)}{E_{S355N}}} = 0.092\,m$$

$$\beta_x := \frac{D_x}{D_{eq}} - 1 = 0.203$$

$$\eta_x := \frac{A_{f.top.sspA}}{t_{eq} \cdot l_{HK.f.top}} - 1 = -0.78$$

The, the software EBplate is used for the new equivalent plate.

EBPlate [C:\USERS\EVGENIOS\DESKTOP\EBPLATE4 EPI 9.EBP]

File Options ?

Results

Euler's Stress   σ_E = 18.97   MPa

Critical factor   Φ_cr = 2.0782

Buckling factors

k_σxl	=	38.895
k_σxbl	=	38.895
k_σxr	=	38.895
k_σxbr	=	38.895
k_σyut	=	
k_σyub	=	
k_σypt	=	
k_σypb	=	
k_τ	=	

Critical stresses

σ_xll.cr	=	737.75	MPa
σ_xbl.cr	=	737.75	MPa
σ_xlr.cr	=	737.75	MPa
σ_xbr.cr	=	737.75	MPa
σ_yut.cr	=		MPa
σ_yub.cr	=		MPa
σ_ypt.cr	=		MPa
σ_ypb.cr	=		MPa
τ_cr	=		MPa

Calculation's options

Deformed shape parameters

Eigenmode complexity :
● Automatic   [1] [2] [3]
○ User defined   [7 x 16]

Number of modes   [1] [20] [N]

Contour lines
☐ To be calculated

Plate behaviour
☐ Prevention of local buckling

Calculation

Calculations times
Preparation of the matrices   0.01 s
Resolution   0.01 s
Contour lines   0.00 s

Calculation OK
Number of calculated modes   1

[Go]

Elastic critical stress for the plate-like buckling

$$\sigma_{cr.p.ssp} := 737.75\text{MPa}$$

$$\beta_{Apl.ssp} := \beta_{Ac.ssp} = 1$$

Relative plate slenderness

$$\lambda_{pl.ssp} := \sqrt{\frac{\beta_{Apl.ssp} \cdot f_y}{\sigma_{cr.p.ssp}}} = 0.694$$

Reduction factor ρ for the plate-like buckling

$$\rho_{pl.ssp} := \begin{vmatrix} \dfrac{\lambda_{pl.ssp} - 0.055(3 + \psi_{pl.ssp})}{\lambda_{pl.ssp}^2} & \text{if } \lambda_{pl.ssp} \geq 0.673 \\ 1 & \text{otherwise} \end{vmatrix}$$

$$\rho_{pl.ssp} = 0.996 \qquad \rho_{pl.ssp} \leq 1 = 1$$

$$\xi_{ssp} := \frac{\sigma_{cr.p.ssp}}{\sigma_{cr.sl.ssp}} - 1 = 0.329$$

New reduction factor ρ.c after the interaction between column-like and plate-like buckling

$$\rho_{c.new.ssp} := (\rho_{pl.ssp} - \chi_{c.ssp}) \cdot \xi_{ssp} \cdot (2 - \xi_{ssp}) + \chi_{c.ssp}$$

$$\rho_{c.new.ssp} = 0.852$$

Moment Capacity of the Compressive Flange

First moment of area

$$W_{over.ssp} := \frac{I_{sl.ssp}}{z_{na.sspA}} = 2.116 \times 10^5 \cdot \text{mm}^3$$

$$W_{under.ssp} := \frac{I_{sl.ssp}}{h_{sspA} - z_{na.sspA}} = 1.87 \times 10^5 \cdot \text{mm}^3$$

Due to the position of the neutral axis or each rib, yielding will probably take place at the bottom flange of the ribs and therefore the bending moment capacity is defined by the corresponding first moment of area and stresses at that depth. However, the moment capacity of the top part will be also found to verify it.

Design moment capacity

$$M_{Rd.ssp.1} := W_{over.ssp} \cdot \frac{f_y}{\gamma_{M1}} = 75.108 \cdot kN \cdot m$$

$$M_{Rd.ssp.2} := W_{under.ssp} \cdot \frac{f_y}{\gamma_{M1}} = 66.388 \cdot kN \cdot m$$

$$M_{Rd.ssp.unit} := min\left(M_{Rd.ssp.1}, M_{Rd.ssp.2}\right) = 66.388 \cdot kN \cdot m$$

Design moment capacity per unit length

$$M_{Rd.ssp} := \frac{M_{Rd.ssp.unit}}{l_{sspA}} = 369.125 \cdot \frac{kN \cdot m}{m}$$

In defining the design moment capacity the end parts in edges are neglected.

Axial load carrying capacity

Effective area per unit width

$$A_{c.eff.ssp} := \rho_{c.new.ssp} \cdot A_{sspA} = 0.017 \, m$$

Load carrying capacity per unit length

$$N_{Rd.ssp} := A_{c.eff.ssp} \cdot \frac{f_y}{\gamma_{M1}} = 6.142 \times 10^3 \cdot \frac{kN}{m}$$

◀ Moment and axial load carrying capacity of the top SSE

$$\frac{M_{Rd.ssp} - M_{Rd}}{M_{Rd}} = -16.888 \cdot \%$$

$$\frac{N_{Rd.ssp} - N_{Rd}}{N_{Rd}} = -8.564 \cdot \%$$

$A_{tot.sspA} := A_{tot.ssp}(h_{c.sspA}, t_{f.topA}, t_{f.botA}, t_{c.sspA}, \alpha_{sspA}, f_{sspA}) = 2.769 \times 10^3 \cdot mm^2$ Area of the repeated part of the SSE

$A_{sspA} = 0.017\,m$ Area of the top SSE per unit width

$A_{f.top.sspA} := A_{sspA} \cdot l_{HK.f.top} = 0.315\,m^2$ Total area of the top SSE

New total area of the cross-section

$A_{HK.tot.ssp} := A_{f.top.sspA} + A_{HK.web.top} + A_{HK.n.sid.stif} + A_{HK.sid.pl} + A_{HK.n.sid.stif} + A_{HK.web.bot.in} + A_{HK.f.bot} + A_{HK.n.rib.bot.in} + A_{HK.n.rib.bot}$

Total area of the box cross-section with the new SSE

$A_{HK.tot.ssp} = 0.795\,m^2$

Gravity centre of the top SSE (distance from the centreline of the top flange)

$z_{na.sspA} := z_{na.ssp}(h_{c.sspA}, t_{f.topA}, t_{f.botA}, t_{c.sspA}, \alpha_{sspA}, f_{sspA}) = 0.061\,m$

$y_{f.top.sspA} := 3.815\,m$ Counted from the Autocad due to inclination

Gravity centre of the section (distance from the bottom flange)

$$z_{na.new} := \frac{\begin{array}{l} A_{f.top.sspA} \cdot y_{f.top.sspA} + A_{HK.web.top} \cdot y_{HK.web.top} + A_{HK.n.sid.stif} \cdot y_{HK.sid.stif} \cdots \\ + A_{HK.sid.pl} \cdot y_{HK.sid.pl} + A_{HK.web.bot.in} \cdot y_{HK.web.bot.in} + A_{HK.n.rib.bot.in} \cdot y_{HK.n.rib.bot.in} + A_{HK.n.rib.bot} \cdot y_{HK.n.rib.bot} \end{array}}{A_{HK.tot.ssp}} = 2.149\,m$$

With the same way as done for the orthotropic deck, the stresses in the bottom flange of the SSE are found:

Stresses in the bottom flange of the SSE

$$\sigma_{HK.ssp.f.bot} := \frac{h_{box} - z_{na.new} - h_{sspA}}{h_{box} - z_{na.new}} \cdot f_y$$

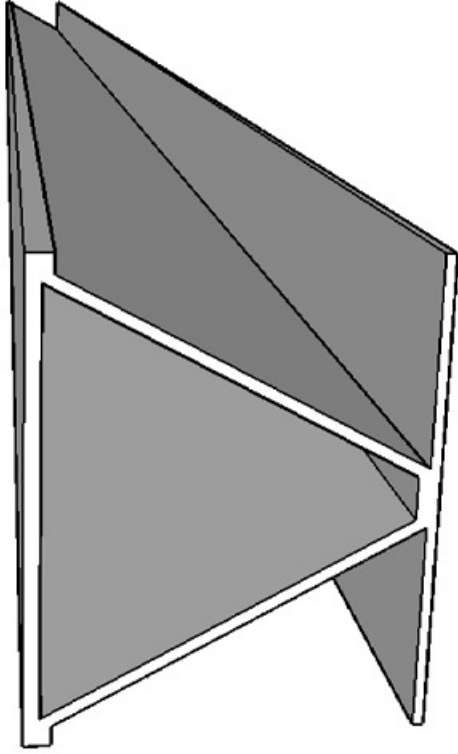$$\sigma_{HK.ssp.f.bot} = 326.739 \cdot MPa$$

$$\psi_{1.ssp} := \frac{\sigma_{HK.ssp.f.bot}}{f_y} = 0.92 \qquad 0 \le \psi_{1.ssp} \le 1 = 1$$

The whole cross-section of the steel sandwich element is in class 3. So, the whole area is effective. For finding the reduction factor due to buckling one of the repeated parts of the steel sandwich element is going to be used.

Column-like buckling behaviour

$$I_{sl.ssp} := I_{tot.ssp.x}\left(h_{c.sspA}, t_{f.topA}, t_{f.botA}, t_{c.sspA}, \alpha_{sspA}, f_{sspA}\right) = 8.33 \times 10^{-6} \ m^4$$

Moment of inertia of each top rib

$$A_{sl.ssp} := A_{tot.ssp}\left(h_{c.sspA}, t_{f.topA}, t_{f.botA}, t_{c.sspA}, \alpha_{sspA}, f_{sspA}\right) = 2.769 \times 10^{-3} \ m^2$$

$$\beta_{Ac.ssp} := 1$$

The whole cross-section is in class 3 or higher

$$\sigma_{cr.sl.ssp} := \frac{\pi^2 \cdot E_{S355N} \cdot I_{sl.ssp}}{A_{sl.ssp} \cdot l_{long.stif}^2} = 389.624 \cdot MPa$$

Elastic critical column buckling stress for a stiffened plate

$$\lambda_{c.ssp} := \sqrt{\frac{\beta_{Ac.ssp} \cdot f_y}{\sigma_{cr.sl.ssp}}} = 0.955$$

Relative column slenderness

$$i_{ssp} := \sqrt{\frac{I_{sl.ssp}}{A_{sl.ssp}}} = 54.843 \cdot mm$$

$$e_{ssp} := \max\left(z_{na.sspA}, h_{sspA} - z_{na.sspA}\right) = 69.33 \cdot mm$$

Largest distance from the respective centroids of the plate from the NA

$$\alpha_{ssp.} := 0.34$$

For closed stiffeners

$$\alpha_{e.ssp} := \alpha_{ssp.} + \frac{0.09}{\dfrac{i_{ssp}}{e_{ssp}}} = 0.454$$

Column type behaviour

$$\Phi_{spp} := 0.5 \cdot \left[1 + \alpha_{e.ssp} \cdot \left(\lambda_{c.ssp} - 0.2\right) + \lambda_{c.ssp}^2\right] = 1.127$$

$$\chi_{c.ssp} := \frac{1}{\Phi_{spp} + \sqrt{\Phi_{spp}^2 - \lambda_{c.ssp}^2}} = 0.58$$

$$\rho_{c.ssp} := \chi_{c.ssp} = 0.58$$

Reduction factor ρ for the column-like buckling

Plate-like buckling using equivalent orthotropic plate (half of the top plate is used for the calculations)

$$\psi_{pl.ssp} := \psi_{1.ssp} = 0.92$$

For the steel sandwich element, neither the Eurocode nor the EBPlate software could be applied directly. Following Jón Pétur Indriðason's and Vésteinn Sigmundsson's Master Thesis 'Buckling analysis of orthotropic plates', an equivalent plate could be created that gives quite close results to the steel sandwich elements. For deciding the thickness of the equivalent plate, it is assumed that the total bending stiffness of the new plate is equal with the bending stiffness of the steel sandwich element in the y direction.

$$D_x = 1.081 \times 10^4 \cdot kN \cdot m$$

$$D_y = 9.202 \times 10^3 \cdot kN \cdot m$$

$$D_{eq} := D_y = 9.202 \times 10^6 \cdot N \cdot m$$

$$t_{eq} := \sqrt[3]{\dfrac{D_{eq} \cdot 12 \cdot \left(1 - \nu^2\right)}{E_{S355N}}} = 0.078\,m$$

$$\beta_x := \dfrac{D_x}{D_{eq}} - 1 = 0.175$$

$$\eta_x := \dfrac{A_{f.top.sspA}}{t_{eq} \cdot l_{HK.f.top}} - 1 = -0.781$$

The, the software EBplate is used for the new equivalent plate.

File   Options   ?

Calculation's options

Deformed shape parameters

● Automatic

Eigenmode complexity : 1 2 3

○ User defined   10×11

Number of modes   1 20 N

Contour lines

☐ To be calculated

Plate behaviour

☐ Prevention of local buckling

Calculation

Calculation OK.

Number of calculated modes   1

Go

Calculations times

Preparation of the matrices   0.02 s

Resolution   0.01 s

Contour lines   0.00 s

Results

Euler's Stress σ_E = 54.54   MPa

Critical factor ϕ_{cr} = 3.0230

Buckling factors

$k_{\sigma xtl}$ = 19.683

$k_{\sigma xbl}$ = 19.683

$k_{\sigma xtr}$ = 19.683

$k_{\sigma xbr}$ = 19.683

$k_{\sigma yut}$ =

$k_{\sigma yub}$ =

$k_{\sigma ypt}$ =

$k_{\sigma ypb}$ =

k_{τ} =

Critical stresses

$\sigma_{xtl.cr}$ = 1073.45   MPa

$\sigma_{xbl.cr}$ = 1073.45   MPa

$\sigma_{xtr.cr}$ = 1073.45   MPa

$\sigma_{xbr.cr}$ = 1073.45   MPa

$\sigma_{yut.cr}$ =   MPa

$\sigma_{yub.cr}$ =   MPa

$\sigma_{ypt.cr}$ =   MPa

$\sigma_{ypb.cr}$ =   MPa

τ_{cr} =   MPa

cticm

Elastic critical stress for the plate-like buckling

$$\sigma_{cr.p.ssp} := 1073.45 \text{MPa}$$

$$\beta_{Apl.ssp} := \beta_{Ac.ssp} = 1$$

Relative plate slenderness

$$\lambda_{pl.ssp} := \sqrt{\frac{\beta_{Apl.ssp} \cdot f_y}{\sigma_{cr.p.ssp}}} = 0.575$$

Reduction factor ρ for the plate-like buckling

$$\rho_{pl.ssp} := \begin{vmatrix} \dfrac{\lambda_{pl.ssp} - 0.055\left(3 + \psi_{pl.ssp}\right)}{\lambda_{pl.ssp}^2} & \text{if } \lambda_{pl.ssp} \geq 0.673 \\ 1 & \text{otherwise} \end{vmatrix}$$

$$\rho_{pl.ssp} = 1 \qquad\qquad \rho_{pl.ssp} \leq 1 = 1$$

$$\xi_{ssp} := \frac{\sigma_{cr.p.ssp}}{\sigma_{cr.sl.ssp}} - 1 = 1.755$$

$$\rho_{c.new.ssp} := \left(\rho_{pl.ssp} - \chi_{c.ssp}\right) \cdot \xi_{ssp} \cdot \left(2 - \xi_{ssp}\right) + \chi_{c.ssp}$$

New reduction factor ρ.c after the interaction between column-like and plate-like buckling

$$\rho_{c.new.ssp} = 0.76$$

Moment Capacity of the Compressive Flange

First moment of area

$$W_{over.ssp} := \frac{I_{sl.ssp}}{z_{na.sspA}} = 1.373 \times 10^5 \cdot \text{mm}^3$$

$$W_{under.ssp} := \frac{I_{sl.ssp}}{h_{sspA} - z_{na.sspA}} = 1.201 \times 10^5 \cdot \text{mm}^3$$

Due to the position of the neutral axis or each rib, yielding will probably take place at the bottom flange of the ribs and therefore the bending moment capacity is defined by the corresponding first moment of area and stresses at that depth. However, the moment capacity of the top part will be also found to verify it.

Design moment capacity

$$M_{Rd.ssp.1} := W_{over.ssp} \cdot \frac{f_y}{\gamma_{M1}} = 48.759 \cdot kN \cdot m$$

$$M_{Rd.ssp.2} := W_{under.ssp} \cdot \frac{f_y}{\gamma_{M1}} = 42.651 \cdot kN \cdot m$$

$$M_{Rd.ssp.unit} := min(M_{Rd.ssp.1}, M_{Rd.ssp.2}) = 42.651 \cdot kN \cdot m$$

Design moment capacity per unit length

$$M_{Rd.ssp} := \frac{M_{Rd.ssp.unit}}{l_{sspA}} = 263.657 \cdot \frac{kN \cdot m}{m}$$

In defining the design moment capacity the end parts in edges are neglected.

Axial load carrying capacity

Effective area per unit width

$$A_{c.eff.ssp} := \rho_{c.new.ssp} \cdot A_{sspA} = 0.013 \, m$$

Load carrying capacity per unit length

$$N_{Rd.ssp} := A_{c.eff.ssp} \cdot \frac{f_y}{\gamma_{M1}} = 4.62 \times 10^3 \cdot \frac{kN}{m}$$

◀ Moment and axial load carrying capacity of the top SSE

$$\frac{M_{Rd.ssp} - M_{Rd}}{M_{Rd}} = -40.635 \cdot \%$$

$$\frac{N_{Rd.ssp} - N_{Rd}}{N_{Rd}} = -31.222 \cdot \%$$

$A_{tot.sspA} := A_{tot.ssp}\left(h_{c.sspA}, t_{f.topA}, t_{f.botA}, t_{c.sspA}, \alpha_{sspA}, f_{sspA}\right) = 4.588 \times 10^3 \cdot mm^2$ — Area of the repeated part of the SSE

$A_{sspA} = 0.022\,m$ — Area of the top SSE per unit width

$A_{f.top.sspA} := A_{sspA} \cdot l_{HK.f.top} = 0.413\,m^2$ — Total area of the top SSE

New total area of the cross-section

$A_{HK.tot.ssp} := A_{f.top.sspA} + A_{HK.web.top} + A_{HK.n.sid.stif} + A_{HK.sid.pl} + A_{HK.n.rib.bot.in} + A_{HK.f.bot} + A_{HK.n.rib.bot.in} + A_{HK.n.rib.bot}$

$A_{HK.tot.ssp} = 0.893\,m^2$ — Total area of the box cross-section with the new SSE

Gravity centre of the top SSE (distance from the centreline of the top flange)

$z_{na.sspA} := z_{na.ssp}\left(h_{c.sspA}, t_{f.topA}, t_{f.botA}, t_{c.sspA}, \alpha_{sspA}, f_{sspA}\right) = 0.081\,m$

$y_{f.top.sspA} := 3.815\,m$

Gravity centre of the section (distance from the bottom flange)

$z_{na.new} := \dfrac{\begin{array}{l} A_{f.top.sspA} \cdot y_{f.top.sspA} + A_{HK.web.top} \cdot y_{HK.web.top} + A_{HK.n.sid.stif} \cdot y_{HK.sid.stif} \cdots \\ + A_{HK.sid.pl} \cdot y_{HK.sid.pl} + A_{HK.web.bot.in} \cdot y_{HK.web.bot.in} + A_{HK.n.rib.bot.in} \cdot y_{HK.n.rib.bot.in} + A_{HK.n.rib.bot} \cdot y_{HK.n.rib.bot} \end{array}}{A_{HK.tot.ssp}} = 2.332\,m$

— Counted from the Autocad due to inclination

With the same way as done for the orthotropic deck, the stresses in the bottom flange of the SSE are found:

$$\sigma_{HK.ssp.f.bot} := \frac{h_{box} - z_{na.new} - h_{sspA}}{h_{box} - z_{na.new}} \cdot f_y$$
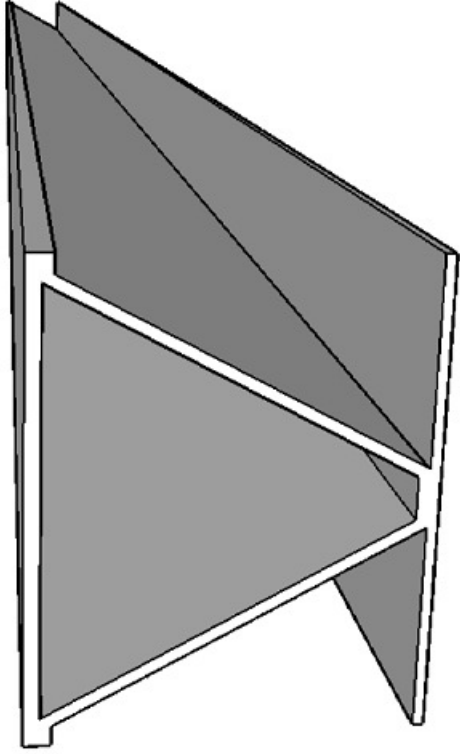
Stresses in the bottom flange of the SSE

$$\sigma_{HK.ssp.f.bot} = 312.985 \cdot MPa$$

$$\psi_{1.ssp} := \frac{\sigma_{HK.ssp.f.bot}}{f_y} = 0.882 \qquad 0 \le \psi_{1.ssp} \le 1 = 1$$

The whole cross-section of the steel sandwich element is in class 3. So, the whole area is effective. For finding the reduction factor due to buckling one of the repeated parts of the steel sandwich element is going to be used.

Column-like buckling behaviour

$$I_{sl.ssp} := I_{tot.ssp.x}\left(h_{c.sspA}, t_{f.topA}, t_{f.botA}, t_{c.sspA}, \alpha_{sspA}, f_{sspA}\right) = 2.36 \times 10^{-5} \ m^4$$

Moment of inertia of each top rib

$$A_{sl.ssp} := A_{tot.ssp}\left(h_{c.sspA}, t_{f.topA}, t_{f.botA}, t_{c.sspA}, \alpha_{sspA}, f_{sspA}\right) = 4.588 \times 10^{-3} \ m^2$$

$$\beta_{Ac.ssp} := 1$$

The whole cross-section is in class 3 or higher

$$\sigma_{cr.sl.ssp} := \frac{\pi^2 \cdot E_{S355N} \cdot I_{sl.ssp}}{A_{sl.ssp} \cdot l_{long.stif}^2} = 666.185 \cdot MPa$$

Elastic critical column buckling stress for a stiffened plate

$$\lambda_{c.ssp} := \sqrt{\frac{\beta_{Ac.ssp} \cdot f_y}{\sigma_{cr.sl.ssp}}} = 0.73$$

Relative column slenderness

$$i_{ssp} := \sqrt{\frac{I_{sl.ssp}}{A_{sl.ssp}}} = 71.713 \cdot mm$$

$$e_{ssp} := \max\left(z_{na.sspA}, h_{sspA} - z_{na.sspA}\right) = 90.875 \cdot mm$$

Largest distance from the respective centroids of the plate from the NA

$$\alpha_{ssp.} := 0.34$$

For closed stiffeners

$$\alpha_{e.ssp} := \alpha_{ssp.} + \frac{0.09}{\frac{i_{ssp}}{e_{ssp}}} = 0.454$$

Column type behaviour

$$\Phi_{spp} := 0.5 \cdot \left[1 + \alpha_{e.ssp} \cdot \left(\lambda_{c.ssp} - 0.2\right) + \lambda_{c.ssp}^2\right] = 0.887$$

$$\chi_{c.ssp} := \frac{1}{\Phi_{spp} + \sqrt{\Phi_{spp}^2 - \lambda_{c.ssp}^2}} = 0.719$$

$$\rho_{c.ssp} := \chi_{c.ssp} = 0.719$$

Reduction factor ρ for the column-like buckling

Plate-like buckling using equivalent orthotropic plate (half of the top plate is used for the calculations)

$$\psi_{pl.ssp} := \psi_{1.ssp} = 0.882$$

For the steel sandwich element, neither the Eurocode nor the EBPlate software could be applied directly. Following Jón Pétur Indriðason's and Vésteinn Sigmundsson's Master Thesis 'Buckling analysis of orthotropic plates', an equivalent plate could be created that gives quite close results to the steel sandwich elements. For deciding the thickness of the equivalent plate, it is assumed that the total bending stiffness of the new plate is equal with the bending stiffness of the steel sandwich element in the y direction.

$$D_x = 2.423 \times 10^4 \cdot kN \cdot m$$
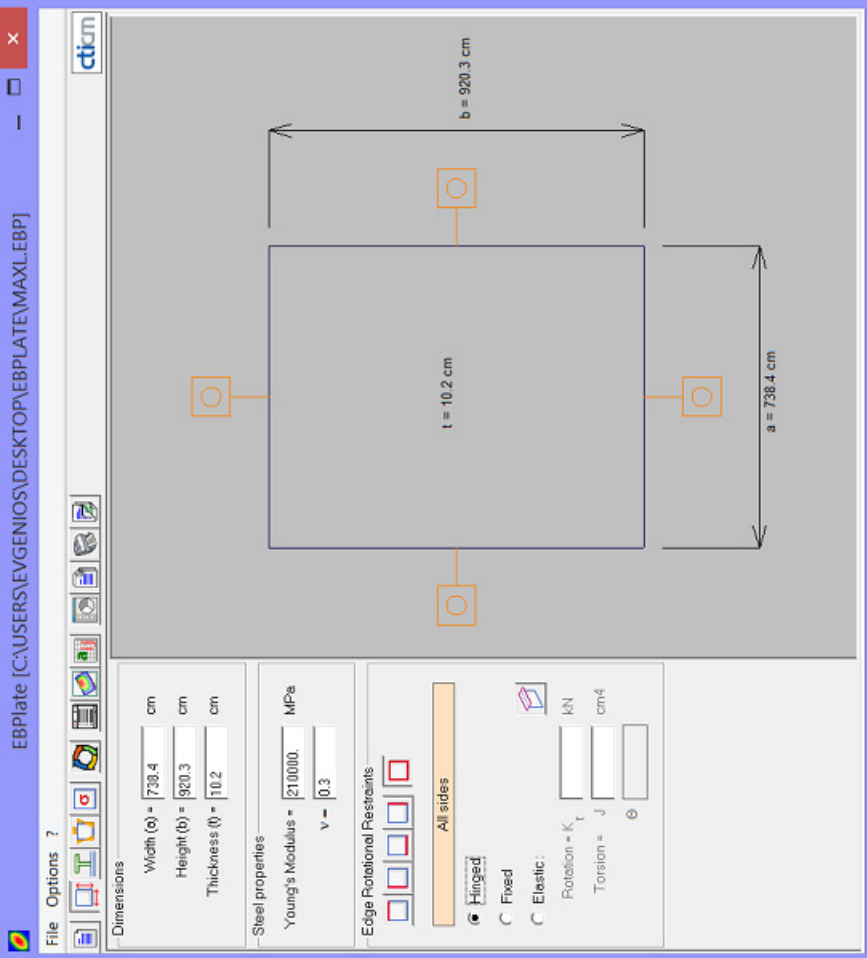
$$D_y = 2.033 \times 10^4 \cdot kN \cdot m$$

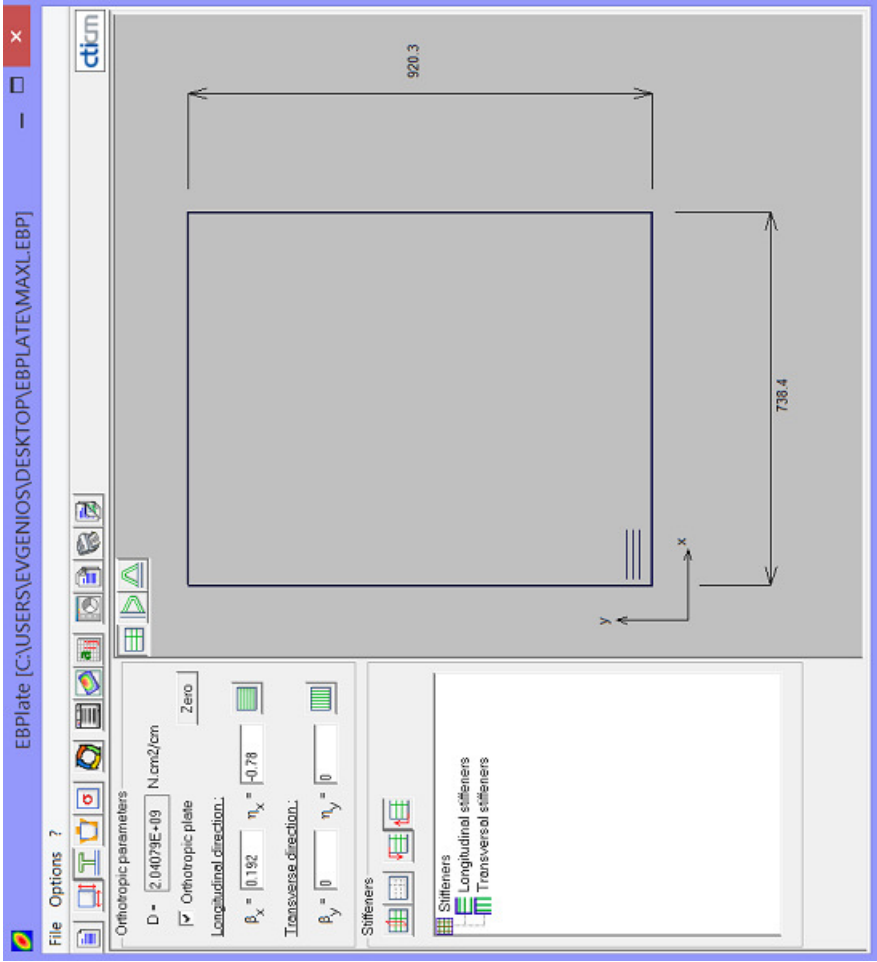$$D_{eq} := D_y = 2.033 \times 10^7 \cdot N \cdot m$$

$$t_{eq} := \sqrt[3]{\frac{D_{eq} \cdot 12 \cdot \left(1 - \nu^2\right)}{E_{S355N}}} = 0.102\,m$$
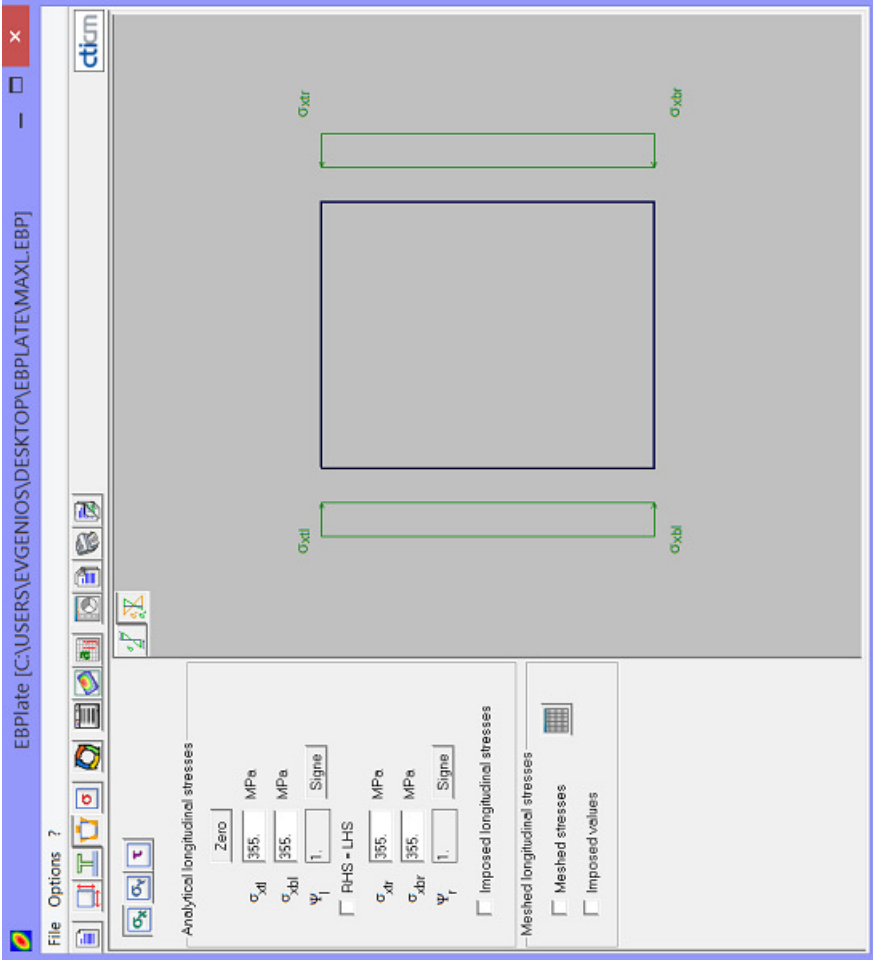
$$\beta_x := \frac{D_x}{D_{eq}} - 1 = 0.192$$

$$\eta_x := \frac{A_{f.top.sspA}}{t_{eq} \cdot l_{HK.f.top}} - 1 = -0.78$$

The, the software EBplate is used for the new equivalent plate.

EBPlate [C:\USERS\EVGENIOS\DESKTOP\EBPLATE\MAXL.EBP]

File   Options   ?

ctim

Calculation's options

Deformed shape parameters

● Automatic

Eigenmode complexity :   1   2   3

○ User defined   10 x 12

Number of modes

1   20 N

Contour lines

☐ To be calculated

Plate behaviour

☐ Prevention of local buckling

Calculation

Calculations times

Preparation of the matrices   0.01 s
Resolution   0.01 s
Contour lines   0.00 s

Results

Euler's Stress   σ_E = 23.32   MPa

Critical factor   φ_cr = 1.3420

Buckling factors

k_σxl = 20.434
k_σxbl = 20.434
k_σxr = 20.434
k_σxbr = 20.434
k_σyut =
k_σyub =
k_σypt =
k_σypb =
k_τ   =

Critical stresses

σ_xtl.cr = 476.41   MPa
σ_xbl.cr = 476.41   MPa
σ_xtr.cr = 476.41   MPa
σ_xbr.cr = 476.41   MPa
σ_yut.cr =   MPa
σ_yub.cr =   MPa
σ_ypt.cr =   MPa
σ_ypb.cr =   MPa
τ_cr   =   MPa

Calculation OK

Number of calculated modes   1

Go

Elastic critical stress for the plate-like buckling

$$\sigma_{cr.p.ssp} := 476.41 MPa$$

$$\beta_{Apl.ssp} := \beta_{Ac.ssp} = 1$$

Relative plate slenderness

$$\lambda_{pl.ssp} := \sqrt{\frac{\beta_{Apl.ssp} \cdot f_y}{\sigma_{cr.p.ssp}}} = 0.863$$

Reduction factor ρ for the plate-like buckling

$$\rho_{pl.ssp} := \begin{vmatrix} \dfrac{\lambda_{pl.ssp} - 0.055(3 + \psi_{pl.ssp})}{\lambda_{pl.ssp}^2} & \text{if } \lambda_{pl.ssp} \geq 0.673 \\ 1 & \text{otherwise} \end{vmatrix}$$

$$\rho_{pl.ssp} = 0.872 \qquad \rho_{pl.ssp} \leq 1 = 1$$

$$\xi_{ssp} := \frac{\sigma_{cr.p.ssp}}{\sigma_{cr.sl.ssp}} - 1 = -0.285$$

New reduction factor ρ.c after the interaction between column-like and plate-like buckling

$$\rho_{c.new.ssp} := (\rho_{pl.ssp} - \chi_{c.ssp}) \cdot \xi_{ssp} \cdot (2 - \xi_{ssp}) + \chi_{c.ssp}$$

$$\rho_{c.new.ssp} = 0.62$$

Moment Capacity of the Compressive Flange

First moment of area

$$W_{over.ssp} := \frac{I_{sl.ssp}}{z_{na.sspA}} = 2.922 \times 10^5 \cdot mm^3$$

$$W_{under.ssp} := \frac{I_{sl.ssp}}{h_{sspA} - z_{na.sspA}} = 2.597 \times 10^5 \cdot mm^3$$

Due to the position of the neutral axis or each rib, yielding will probably take place at the bottom flange of the ribs and therefore the bending moment capacity is defined by the corresponding first moment of area and stresses at that depth. However, the moment capacity of the top part will be also found to verify it.

Design moment capacity

$$M_{Rd.ssp.1} := W_{over.ssp} \cdot \frac{f_y}{\gamma_{M1}} = 103.724 \cdot kN \cdot m$$

$$M_{Rd.ssp.2} := W_{under.ssp} \cdot \frac{f_y}{\gamma_{M1}} = 92.18 \cdot kN \cdot m$$

$$M_{Rd.ssp.unit} := \min\left(M_{Rd.ssp.1}, M_{Rd.ssp.2}\right) = 92.18 \cdot kN \cdot m$$

Design moment capacity per unit length

$$M_{Rd.ssp} := \frac{M_{Rd.ssp.unit}}{l_{sspA}} = 450.696 \cdot \frac{kN \cdot m}{m}$$

In defining the design moment capacity the end parts in edges are neglected.

Axial load carrying capacity

Effective area per unit width

$$A_{c.eff.ssp} := \rho_{c.new.ssp} \cdot A_{sspA} = 0.014 \, m$$

Load carrying capacity per unit length

$$N_{Rd.ssp} := A_{c.eff.ssp} \cdot \frac{f_y}{\gamma_{M1}} = 4.937 \times 10^3 \cdot \frac{kN}{m}$$

◄ Moment and axial load carrying capacity of the top SSE

$$\frac{M_{Rd.ssp} - M_{Rd}}{M_{Rd}} = 1.479 \cdot \%$$

$$\frac{N_{Rd.ssp} - N_{Rd}}{N_{Rd}} = -26.504 \cdot \%$$